Exploring the roles of chloroplast envelope proteins in plant acclimation processes

Dissertation

zur Erlangung des naturwissenschaftlichen Doktorgrades "Doctor rerum naturalium"

(Dr. rer. nat.)

an der Fakultät für Biologie der Ludwig-Maximilians-Universität München

Vorgelegt von

Wing Tung Lo

München, 04.06.2025

Die Dissertation wurde angefertigt unter der Leitung von PD Dr. Serena Schwenkert im Bereich Molekularbiologie der Pflanzen an der Fakultät für Biologie der Ludwig-Maximilians-Universität München (LMU)

Erstgutachter:	PD Dr. Serena Schwenkert
Zweitgutachter:	Prof. Dr. Gudrun Kadereit
Tag der Abgabe:	04.06.2025
Tag der mündlichen Prüfung:	06.08.2025

Erklärung
Declaration

Hiermit erkläre ich,
Hereby I declare,

dass die Dissertation nicht ganz oder in wesentlichen Teilen einer anderen Prüfungskommission vorgelegt worden ist.
that this work, complete or in parts, has not yet been submitted to another examination institution

dass ich mich anderweitig einer Doktorprüfung ohne Erfolg **nicht** unterzogen habe.
*that I did **not** undergo another doctoral examination without success*

_____

München, Deutschland, 04.06.2025

WING TUNG LO

Eigenständigkeitserklärung

Hiermit versichere ich an Eides statt, dass die vorliegende schriftliche Dissertation mit dem Titel "Exploring the roles of chloroplast envelope proteins in plant acclimation processes" von mir selbstständig verfasst wurde und dass keine anderen als die angegebenen Quellen und Hilfsmittel benutzt wurden. Die Stellen der Arbeit, die anderen Werken dem Wortlaut oder dem Sinne nach entnommen sind, wurden in jedem Fall unter Angabe der Quellen (einschließlich des World Wide Web und anderer elektronischer Text- und Datensammlungen) kenntlich gemacht. Weiterhin wurden alle Teile der Arbeit, die mit Hilfe von Werkzeugen der künstlichen Intelligenz de novo generiert wurden, durch Fußnote/Anmerkung an den entsprechenden Stellen kenntlich gemacht und die verwendeten Werkzeuge der künstlichen Intelligenz gelistet. Die genutzten Prompts befinden sich im Anhang. Diese Erklärung gilt für alle in der Arbeit enthaltenen Texte, Graphiken, Zeichnungen, Kartenskizzen und bildliche Darstellungen.

_____

München, Deutschland, 04.06.2025

WING TUNG LO

Affidavit

Herewith I certify under oath that I wrote the accompanying Dissertation myself.

Title: Exploring the roles of chloroplast envelope proteins in plant acclimation processes

In the thesis no other sources and aids have been used than those indicated. The passages of the thesis that are taken in wording or meaning from other sources have been marked with an indication of the sources (including the World Wide Web and other electronic text and data collections). Furthermore, all parts of the thesis that were de novo generated with the help of artificial intelligence tools were identified by footnotes/annotations at the appropriate places and the artificial intelligence tools used were listed. The prompts used were listed in the appendix. This statement applies to all text, graphics, drawings, sketch maps, and pictorial representations contained in the work.

_____

Munich, Germany, 04.06.2025

WING TUNG LO

Table of Contents

Summary

In vascular plants, the chloroplast not only serves as the cellular site of photosynthesis but also houses the enzymatic machinery essential for numerous interwoven biochemical pathways central to plant metabolism. As the interface between plastid and cytosol, the chloroplast envelopes perform a range of critical functions including the facilitation of ionic and metabolic exchange and acting as a major site for lipid metabolism in plants. Changes in chloroplast metabolism is instrumental in plant acclimation to adverse environmental conditions. Correspondingly, proteins of the chloroplast envelope have been increasingly recognised for their roles in such processes, particularly cold acclimation.

While extensive efforts have illuminated the multifaceted nature of the chloroplast envelope and its potential role in cold acclimation, many of its constituent proteins remain to be characterised on the molecular level. In this work, artificial microRNA-based screens were conducted to probe the chloroplast outer envelope landscape, which led us to investigate the Chloroplast Lipid Remodelling Protein 23 (CLRP23) in more detail. Formerly known in published literature as Outer Envelope Protein 23 (OEP23), CLRP23 was originally identified in the chloroplast envelopes of Pea and assumed to localise to the outer envelope due to the absence of a predicted transit peptide. While subfractionation analysis and protease protection assays suggest an alternative localisation of CLRP23 to the chloroplast inner envelope, characterisation of mutants deficient in CLRP23 reveal significant impairments in photosynthesis and altered galactolipid responses under cold treatment.

This work predominantly explores the alternative function of CLRP23 as component of the chloroplast inner envelope and investigates its role in lipid remodelling processes during cold acclimation. Finally, eight envelope transporter candidates with as yet unknown molecular functions were identified from proteomic analysis of chloroplast envelopes and subjected to preliminary characterisation to provide a basis for future research.

Zusammenfassung

In Gefäßpflanzen fungiert der Chloroplast nicht nur als zellulärer Ort der Photosynthese, sondern beherbergt auch die enzymatische Maschinerie, die zahlreiche für den Pflanzenstoffwechsel zentrale biochemische Prozesse ermöglicht. Als Schnittstelle zwischen Plastid und Cytosol übernehmen die Chloroplastenhüllmembranen vielfältige Aufgaben, darunter den Austausch von Ionen und Metaboliten sowie eine zentrale Rolle im Lipidstoffwechsel. Veränderungen im Chloroplastenstoffwechsel sind entscheidend für die Anpassungsfähigkeit von Pflanzen an ungünstige Umweltbedingungen. Entsprechend rückt die Bedeutung der Proteine der Chloroplastenhüllmembran, insbesondere im Kontext der Kälteakklimatisierung, zunehmend in den Fokus der Forschung.

Obwohl die komplexe Beteiligung der Hüllmembranen an der Kälteanpassung bereits Gegenstand früherer Untersuchungen war, sind viele der beteiligten Proteine auf molekularer Ebene noch unzureichend charakterisiert. Im Rahmen dieser Arbeit wurden mikroRNA-basierte Screens eingesetzt, um die Proteinzusammensetzung der äußeren Chloroplastenhülle zu analysieren. Dabei rückte das Chloroplast Lipid Remodelling Protein 23 (CLRP23), früher als OEP23 (Outer Envelope Protein 23) bezeichnet, in den Mittelpunkt. CLRP23 wurde ursprünglich in den Chloroplastenhüllen von Erbsen entdeckt und aufgrund des Fehlens eines Transitpeptids der äußeren Hüllmembran zugeordnet. Subfraktionierungsanalysen und Protease-Assays deuten jedoch auf eine alternative Lokalisation in der inneren Hüllmembran hin. Die Charakterisierung von Mutanten, denen CLRP23 fehlt, zeigt deutliche Beeinträchtigungen der Photosynthese sowie veränderte Galaktolipidreaktionen unter Kälteeinfluss.

Diese Arbeit widmet sich daher vorrangig der Erforschung der alternativen Funktion von CLRP23 als Bestandteil der inneren Chloroplastenhülle und beleuchtet dessen Rolle bei Lipidumwandlungsprozessen während der Kälteakklimatisierung. Darüber hinaus wurden acht weitere Transporter-Kandidaten aus der Hüllmembran, deren molekulare Funktionen bislang unbekannt sind, mittels proteomischer Analysen identifiziert und einer ersten Charakterisierung unterzogen, um eine Grundlage für weiterführende Untersuchungen zu schaffen.

Figures

Tables

Abbreviations

A32gXYLT	Anthocyanin 3-O-glucoside xylosyltransferase
AGAP1	Acylated galactolipid associated phospholipase 1
AmiR	Artificial microRNA
ATP	Adenosine triphosphate
BN-PAGE	Blue native polyacrylamide gel electrophoresis
C17:0	Heptadecanoic acid
cDNA	Coding DNA
$CHCl_3$	Chloroform
Chl α	Chlorophyll a
CHI	Chalcone isomerase
CHS	Chalcone synthase
CHUP	Chloroplast unusual positioning
CLRP23	Chloroplast lipid remodelling protein 23
CO_2	Carbon dioxide
CRG	Cold-regulated genes
DAG	Diacylglycerol
DEG	Differentially regulated genes
DEP	Differentially regulated proteins
DFR	Dihydroflavonol 4-reductase
DGDG	Digalactosyldiacylglycerol
DNA	Deoxyribonucleic acid
DTT	Dithiothreitol
EDTA	Ethylenediaminetetraacetic acid
EGTA	Egtazic acid
ER	Endoplasmic reticulum
EtOH	Ethanol
F3H	Flavanone 3-hydroxylase (F3H)
FAD	Fatty acid desaturase
FAME	Fatty acid methyl ester
FAX1	Fatty acid export 1

FBPase	Fructose-1,6-bisphosphatase
FID	Flame ionisation detection
GC	Gas chromatography
gDNA	Genomic DNA
GFP	Green fluorescent protein
GO	Gene ontology
GTP	Guanosine triphosphate
HCl	Hydrochloric acid
HEPES	4-(2-hydroxyethyl)-1-piperazineethanesulfonic acid
HRG	High light regulated genes
IAA	Iodoacetamide
IE	Chloroplast inner envelope
IMS	Chloroplast envelope intermembrane space
JA	Jasmonic acid
KCl	Potassium chloride
LACS9	Long-chain acyl-CoA synthetase 9
LC	Liquid chromatography
LDOX	Leucoanthocyanidin dioxygenase
LDS	Lithium dodecyl sulphate
LFQ	Label-free quantification
MeOH	Methanol
MEX1	Maltose exporter 1
MGDG	Monogalactosyldiacylglycerol
mRNA	Messenger RNA
MS	Mass spectrometry
MTBE	Methanol:methyl tert-butyl ether
NaCl	Sodium chloride
OE	Chloroplast outer envelope
OEP	Chloroplast outer envelope protein
OPDA	Oxylipin-12-oxophytodieonic acid
RNA	Ribonucleic acid
PDV	Plastid division
PA	Phosphatidic acid

PC	Phosphatidylcholine
PCR	Polymerase chain reaction
PG	Phosphatidylglycerol
POE	Protein of the outer envelope
PRAT	Preprotein and amino acid transporter
PSI	Photosystem I
PSII	Photosystem II
psbO	Photosystem II extrinsic protein O
pSuT	Plastidic sugar transporter
PT	Protein transporter
RBL11	Rhomboid-like protease of the chloroplast IE 11
SDS-PAGE	Sodium dodecyl sulphate – polyacrylamide gel electrophoresis
SFR	Sensitive to freezing
SGC	Standard growth conditions
SQDG	Sulfoquinovosyldiacylglycerol
SRPBCC	START/RHO_alpha_C/PITP/Bet_v1/CoxG/CalC
TAG	Triacylglycerol
TAG C15:0	Tripentadecanoin
TGD	Trigalactosyldiacylglycerol complex
TeGDG	Tetragalactosyldiacylglycerol
TGDG	Trigalactosyldiacylglycerol
TIC	Translocon at the inner envelope of chloroplasts
TLC	Thin layer chromatography
TOC	Translocon at the outer envelope of chloroplasts
TurboID	Engineered biotin ligase
UDP-Gal	Uridine diphosphate galactose
VDAC	Voltage-dependent anion-selective channel
β-DM	β-Dodecyl maltoside
φ(NPQ)	Nonphotochemical quenching
φ(NO)	Nonregulated energy dissipation
φ(PSII)	PSII quantum yield

1. Introduction

1.1 The endosymbiotic origin of the chloroplast

Oxygenic photosynthesis is the process by which solar radiation is converted into chemical energy, accompanied by the splitting of water molecules and the release of oxygen into the atmosphere (Fischer et al., 2016). This ancient metabolic innovation not only enabled the fixation of carbon dioxide (CO_2) into biomass but also resulted in the increase of oxygen in the atmosphere, both of which were instrumental to the emergence and diversification of complex life on Earth (Sánchez-Baracaldo & Cardona, 2020). Oxygenic photosynthesis was also pivotal to the evolution of vascular plants, as approximately one billion years ago, a photosynthetic, cyanobacterium-like prokaryote was engulfed by a phagocytic eukaryotic host cell, ultimately giving rise to plastids, most notably chloroplasts, the hallmark organelles of modern plant cells (Fig. 1; Dyall et al., 2024; Gould et al., 2008).

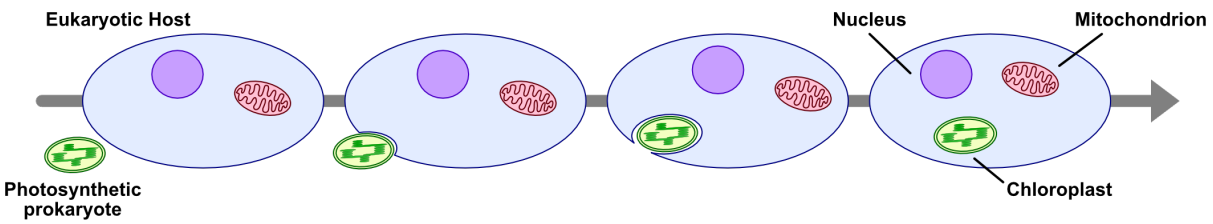

Figure 1 – The endosymbiotic origin of the chloroplast. Approximately one billion years ago, a photosynthetic, cyanobacterium-like prokaryote was engulfed by a phagocytic eukaryotic host cell.

As a result of this evolutionary history, the chloroplast is bound by a double membrane system consisting of the inner (IE) and outer (OE) envelope membranes. In total, the chloroplast is made up of three membrane systems: the IE, OE, and thylakoid membrane, which houses the protein complexes responsible for photosynthetic light reactions, including the photosystems I (PSI) and II (PSII). These membranes are organised to form three distinct aqueous compartments: the intermembrane space (IMS), which separates the IE and OE; the stroma, which is located between the IE and thylakoids; and the thylakoid lumen, which is enclosed within the thylakoid membrane system (Fig. 2). The light-independent metabolic reactions occur in the chloroplast stroma, while the thylakoid lumen is crucial for establishing the proton gradient driving ATP synthesis during light-dependent reactions (Kirchhoff, 2019).

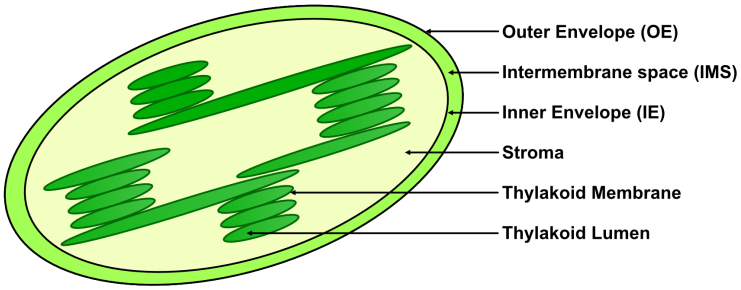

Figure 2 – Chloroplast membranes and sub-organellar compartments. The chloroplast is bound by a double membrane system consisting of the inner (IE) and outer (OE) envelope membranes, which are separated by the intermembrane space (IMS). The stroma is the aqueous compartment between the IE and thylakoid membranes, while the thylakoid lumen is enclosed within the thylakoid membrane system.

1.2 Functions of the chloroplast envelope

In addition to providing structural integrity and compartmentalisation, the chloroplast envelope membranes play an important role in coordinating chloroplast functions with the broader metabolic and regulatory networks of the plant cell (Block et al., 2007). Over the past decades, extensive research has revealed the chloroplast envelope to be involved in several essential processes, including, but not restricted to the import of nuclear-encoded proteins (Soll & Schleiff, 2004), the transport of ions and metabolites (Weber et al., 2005), and lipid metabolism (Hölzl & Dörmann, 2019).

1.2.1 Import of nuclear-encoded proteins across the chloroplast envelope

During endosymbiosis a substantial set of genes were transferred to the host nucleus, leading to a dependency on nuclear-encoded proteins and cytosolic translation machinery (Leister & Kleine, 2008; Martin et al., 1998). Of the approximately 2100 to 4500 proteins in the chloroplast proteome, less than 100 are encoded and synthesised in the chloroplast (Leister & Kleine, 2008). The rest are encoded by the nuclear genome and are imported post-translationally across the envelope in a process mediated by protein translocon complexes at the outer (TOC) and inner (TIC) envelope of chloroplasts (Strittmatter et al., 2010). Chloroplast proteins synthesised in the cytosol are targeted to the chloroplast with two different kinds of targeting signals. Most OE proteins (OEP) contain internal, non-cleavable signals, whereas proteins directed to the other intraplastidial compartments contain cleavable transit peptides at the N-terminus (Strittmatter et al., 2010). Targeting sequences can also consist of two parts, as

seen in thylakoid membrane/lumen proteins, which contain a cleavable N-terminal transit peptide targeting the protein precursor to the stroma, after which the non-cleavable C-terminal sequence targets the protein to its final intraplastidial destination (Richter & Lamppa, 2002).

Proteins targeted to the chloroplast first pass through the OE via the TOC complex. The core of the TOC complex, which has a molecular mass of approximately 500 kDa, includes four copies each of TOC34 and TOC75, as well as one copy of Toc159 (Schleiff et al., 2003). TOC75, the most abundant protein in the OE, forms the translocation channel, while TOC34 and TOC159 contain a GTP-binding domain and function as precursor protein receptors. TOC159 is also postulated to provide the driving force and conformational change required for precursor protein movement across the membrane (Tranel et al., 1995). In addition to the complex core, TOC64 and TOC12 are auxiliary components of TOC which, along with TIC22 and heat shock protein (HSP) 70 form a complex in the IMS to coordinate interactions between TOC and TIC (Becker et al., 2004; Tranel et al., 1995). After crossing the OE, protein precursors pass through the IE via the TIC complex, where TIC110 and TIC20 are postulated to form the translocation channels. Auxiliary subunits of the TIC complex include the putative redox-active regulatory components TIC32, TIC55, and TIC62, the chaperone coordinating factor TIC40, as well as TIC22, which resides in the IMS (Strittmatter et al., 2010).

1.2.2 Facilitating ionic/metabolic crosstalk between the plastid and cytosol

In vascular plants, the chloroplasts assimilate CO_2 into chemical energy in the form of sugars and carbohydrates through oxygenic photosynthesis. They also house the enzymatic machinery needed for the synthesis of amino acids, fatty acids, and isoprenoid compounds, positioning it as a central hub for plant metabolism (Buchanan et al., 2015; Weber & Fischer, 2009). As the interface separating the chloroplast from the cytosol, the envelope membranes are equipped with transporters and protein channels to facilitate ionic and metabolic flux between the two subcellular compartments. Decades of extensive research have elucidated the molecular mechanisms of many transport proteins responsible for the trafficking of solutes such as ions, sugars, sugar phosphates, organic acids and nucleotide/nucleotide derivatives across the IE (Facchinelli & Weber, 2011; Fischer, 2011; Weber & Fischer, 2009). A large number of these transport proteins are antiporters, which operate by exchanging one metabolite from one side of the membrane with a counter-exchange metabolite on the opposite side (Flügge, 1992, 1998). This exchange mechanism, which is also commonly found in other membrane systems, is particularly effective for linking metabolic pathways between organelles. By coupling the

movement of one substrate across the membrane with the simultaneous transport of another in the opposite direction, this ensures a coordinated and interdependent exchange of solutes/metabolites that integrates and regulates metabolic processes across subcellular compartments (Weber & Fischer, 2007).

Initially, efforts to study metabolite transport across the chloroplast envelopes have primarily focused on the IE, whereas the OE was widely regarded as a remnant of the endosymbiotic food vacuole that is freely permeable to small solutes (Day & Theg, 2018). Nevertheless, in recent years studies have revealed the presence of selective transport proteins localised to the OE, suggesting solute/metabolite traffic across the OE may be more selective than previously anticipated (Barth et al., 2022; Schwenkert, Leister, et al., 2023). To date, the OE is known to harbour more than 40 proteins involved in processes such as nuclear-encoded protein import (TOC), chloroplast positioning (CHUP), plastid division (PDV), and, most notably, metabolite transport. Of the (putative) OE transporters, OEP21, OEP24, OEP37, and OEP40, which are named according to their molecular weights, have a β-barrel structure resembling porins typically found in the outer membrane of Gram-negative bacteria (Bölter & Soll, 2001). OEP21 is a solute-selective porin that exports primary photosynthetic products such as triose phosphates (Bölter et al., 1999; Hemmler et al., 2006), while OEP40 forms a high-conductance channel transporting glucose and its phosphorylated derivatives (Harsman et al., 2016). OEP24 and OEP37 are thought to be less substrate specific. When expressed in the outer membranes of mitochondria, OEP24 and OEP37 are able to fully and partially complement the highly abundant voltage-dependent anion-selective channel (VDAC) in yeast (Goetze et al., 2006; Röhl et al., 1999; Ulrich et al., 2012). In contrast, OEP16 consists of four α-helices and is considered to be a eukaryotic addition to the OE proteome. OEP16 is a member of the preprotein and amino acid transporter (PRAT) family and exhibits *in vitro* permeability to amino acids (Pohlmeyer et al., 1997; Pudelski et al., 2012). Finally, JASSY is described to be neither β-barrel nor α-helical proteins but rather contain a mixture of both β-sheets and α-helices in their predicted structure. JASSY is a part of the START/RHO_alpha_C/PITP/Bet_v1/CoxG/CalC (SRPBCC) superfamily and has been shown to export oxylipin-12-oxophytodieonic acid (OPDA), the precursor of the plant hormone jasmonate (Guan et al., 2019). Figure 3 depicts the metabolite transporters of the chloroplast OE known to date.

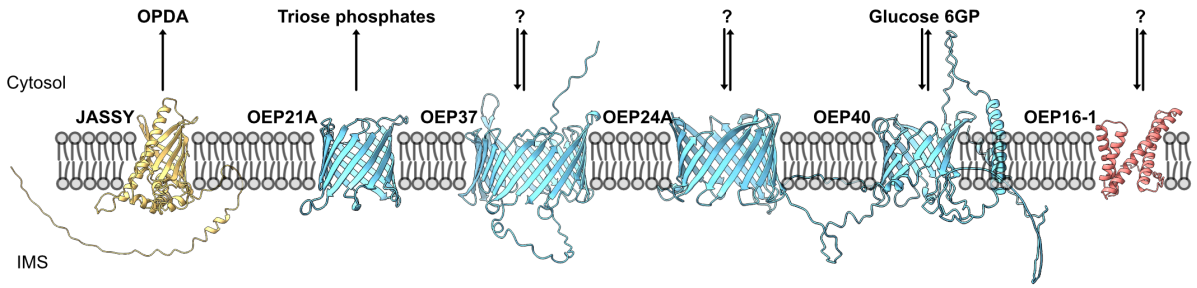

Figure 3 – Metabolite transporters of the chloroplast OE, adapted from Schwenkert, Leister et al. (2023). Proteins with a β-barrel structure (blue) are also found in mitochondria and bacteria and are thought to be of prokaryotic origin, whereas proteins that are α-helical (red) are thought to be eukaryotic additions. JASSY (yellow) represents an unusual structure where, unlike the classical β-barrel and α-helical OEPs, contains a mixture of both β-sheets and α-helices. Three-dimensional structural prediction was obtained from the AlphaFold Protein Structure Database.

1.2.3 Chloroplast lipid composition and the role of the envelope in lipid metabolism

Unlike the phospholipid-rich membranes of animal cells, most bacteria, and the extraplastidial membranes of plant cells, the membrane lipids of chloroplasts and cyanobacteria are composed primarily of glycolipids. In the chloroplast thylakoid membrane, glycolipids monogalactosyldiacylglycerol (MGDG) and digalactosyldiacylglycerol (DGDG) are most abundant, accounting for 52% and 26% of total thylakoid lipids, respectively (Block et al., 1983). In addition to MGDG and DGDG, the chloroplast thylakoid membrane also contains 6.5% of the sulfolipid sulfoquinovosyldiacylglycerol (SQDG) as well as 9.5% of the phospholipid phosphatidylglycerol (PG; Block et al., 1983). Although the lipid composition of the chloroplast IE highly resembles that of the thylakoid membrane, the OE is primarily enriched in DGDG and phosphatidylcholine (PC; Block et al., 1983). Notably, PC, a eukaryotic lipid that is only found in 15% of bacteria (Geiger et al., 2013), is only present in the outer leaflet of the OE and is postulated to have aided with the integration of the cyanobacteria-like prokaryote into the larger cellular network of its host during endosymbiosis (Barth et al., 2022).

In vascular plants, lipid biosynthesis is a complex process that spans multiple cellular compartments. While the chloroplast is the site of synthesis for 95% of fatty acids (Ohlrogge et al., 1979), depending on the plant species, lipid precursors phosphatidic acid (PA) and diacylglycerol (DAG) can be synthesised in both the chloroplast and the endoplasmic reticulum (Hölzl & Dörmann, 2019). In Arabidopsis, glycerolipid biosynthesis can occur via

the prokaryotic pathway, in which lipids are synthesised entirely within the chloroplast, or the eukaryotic pathway, which relies on lipid precursors imported from the endoplasmic reticulum (ER; Hölzl & Dörmann, 2019). Therefore, the trafficking of fatty acids and lipid precursors across the chloroplast envelope is an important aspect of plant lipid biosynthesis. Fatty acid export is mediated by fatty acid export (FAX) 1 and long-chain acyl-CoA synthetase (LACS) 9 in the IE and OE, respectively. It is postulated that FAX1 facilitates the diffusion of lipids across the envelope by bending the IE towards the OE (Könnel et al., 2019; Li et al., 2015), while LACS9 accelerates this process through the synthesis of acyl-CoA. This ATP-dependent coupling of free fatty acids to CoA results in a concentration gradient, thereby promoting fatty acid export (Kitajima-Koga et al., 2020; Könnel et al., 2019). Conversely, the re-import of lipid precursors is mediated by the trigalactosyldiacylglycerol (TGD) complex (Benning, 2008; Fan et al., 2015).

Other than the transport of fatty acids and lipid precursors, the chloroplast envelope is heavily involved with the synthesis of galactolipids, which make up the bulk of membrane lipids found in the chloroplast. The synthesis of MGDG involves the transfer of galactose from uridine diphosphate galactose (UDP-Gal) to DAG, which is catalysed by MGDG synthases (Dubots et al., 2010). Vascular plants possess two classes of MGDG synthases. MGD1, a type A MGDG synthase, is primarily expressed in green leaf tissue and localises to the IE, whereas type B MGDG synthases MGD2 and MGD3 localise to the OE and are only found in specific organs (Awai et al., 2001; Shimojima et al., 1997). While MGD1 expression is upregulated by light and cytokinin, MGD2 and MGD3 are upregulated by phosphate deprivation (Kobayashi et al., 2009; Yamaryo et al., 2003). Subsequently, MGDGs can be further synthesised into DGDGs through the transfer of another galactose from UDP-Gal to MGDG, which is catalysed by DGDG synthases at the OE: DGD1 and DGD2 (Kelly et al., 2003). Most DGDGs are synthesised by DGD1, which contains an extra N-terminal sequence directing the enzyme to the OE and facilitating the trafficking of lipids between the IE and OE (Dörmann et al., 1995; Kelly et al., 2016), whereas DGD2 is strongly upregulated by phosphate deprivation (Härtel et al., 2000). Beyond the synthesis of the major chloroplast galactolipids MGDG and DGDG, the envelope is also implicated in the synthesis of the less abundant chloroplast lipids SQDG and PG. SQD2, which catalyses the final step of SQDG synthesis by transferring the sulfoquinovose moiety to DAG from UDP-sulfoquinovose, has been reported in the chloroplast envelopes of Spinach (Seifert & Heinz, 1992). Meanwhile, enzymes involved in PG synthesis has also been found in proteomics studies of chloroplast envelopes (Ferro et al., 2003; Ferro et

al., 2002). An overview of lipid metabolism at the chloroplast envelope, adapted from Hölzl & Dörmann (2019) is depicted in figure 4.

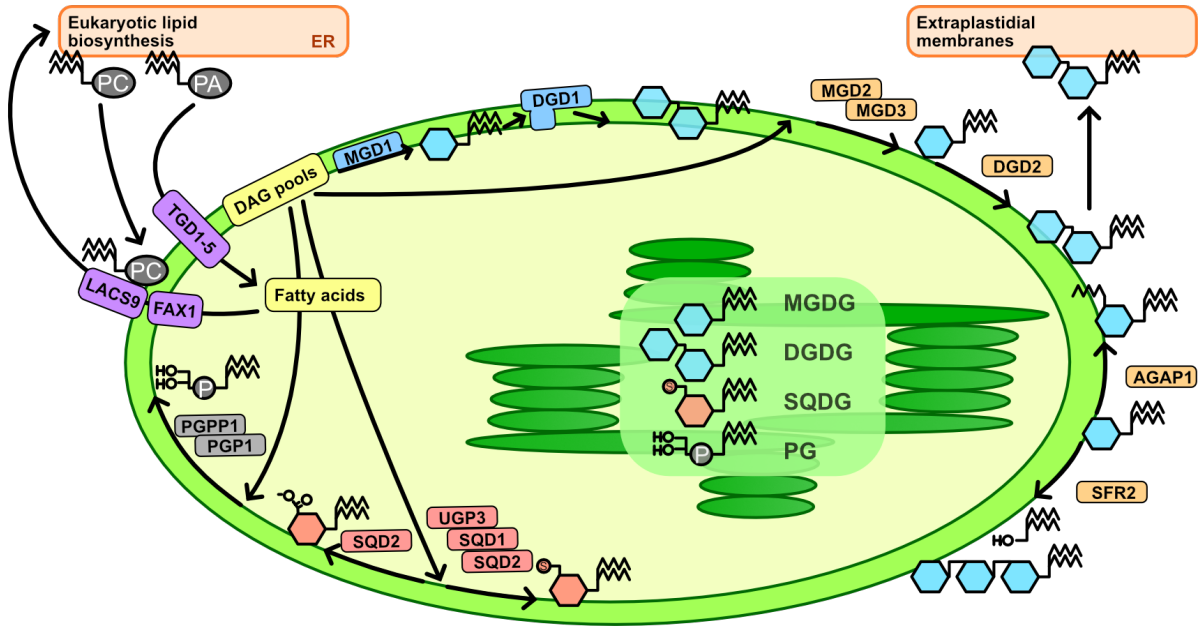

Figure 4 – Lipid metabolism at the chloroplast envelope membranes, adapted from Hölzl & Dörmann (2019). Fatty acids can be used directly for lipid biosynthesis via the prokaryotic pathway or exported to the ER by FAX1 and LACS9. Lipid precursors can also be reimported via the TGD (eukaryotic pathway). In addition to MGDG and DGDG, the chloroplast envelope is also involved in the synthesis of SQDG and PG. Under certain stress conditions, MGDGs can be converted into acyl-MGDG or oligogalactolipids by AGAP1 and SFR2, respectively.

1.2.4 Coordinating chloroplast function in changing environments

Far from being a passive barrier, the chloroplast envelope serves as a multifaceted and dynamic interface that integrates chloroplast function with the cellular environment. It is worth noting that the functions of the chloroplast envelope span beyond its role in nuclear-encoded protein import, metabolite trafficking and lipid metabolism described in previous sections, extending to processes such as chlorophyl synthesis (Block et al., 2007), chloroplast positioning (Oikawa et al., 2003) and plastid division (Yang et al., 2008). All such processes are essential not only for maintaining chloroplast homeostasis under favourable environmental conditions, but also for responses to both biotic and abiotic stress, underscoring the importance of chloroplast envelope proteins in plant acclimation processes.

1.3 The role of chloroplast envelope proteins in cold acclimation

Owing to their sessile lifestyle, to ensure survival vascular plants must possess the ability to respond to adverse environmental conditions *in situ*. While changes in factors such as nutrient or water availability can occur over extended periods, fluctuations in light and temperature can be much more abrupt. Consequently, molecular responses to such challenges must be both quick and reversible. The capacity of plants to rapidly adjust to adverse environmental conditions at the cellular or physiological level is referred to as plant acclimation, as opposed to plant adaption, which involves heritable changes occurring over the course of multiple generations. Due to the chloroplast's central metabolic position, plant acclimation is heavily reliant on changes in chloroplast metabolism (Weber & Fischer, 2009). Naturally, the import of nuclear-encoded chloroplast proteins, metabolite trafficking as well as lipid metabolism at the chloroplast envelopes play pivotal roles in these processes (Barrero-Sicilia et al., 2017; Eisa et al., 2020; Kleine et al., 2021; Li et al., 2020; Schwenkert et al., 2022). In recent years, proteins located at the chloroplast envelope are increasingly being recognised for their roles in plant acclimation processes, particularly with regards to cold acclimation (John, Keller, et al., 2024; Schwenkert, Lo, et al., 2023; Trentmann et al., 2020).

With just approximately 5% of the Earth's surface estimated to be frost free, freezing injury represents one of the major environmental challenges faced by vascular plants, and the extent to which different species can tolerate low temperature conditions is a key factor for determining their geographical distribution (Hurry, 2017). In cold tolerant species such as Arabidopsis, cold acclimation is triggered by the exposure to low but non-freezing temperatures and involves a series of physiological and metabolic changes that improve fitness during sub-optimal environmental conditions and increase freezing tolerance (Fürtauer et al., 2019; Hurry, 2017; Levitt, 1980).

1.3.1 Metabolic transport across the chloroplast envelope during cold acclimation

A key aspect of cold acclimation involves the reprogramming of carbohydrate metabolism to accumulate soluble sugars, which are known to play a wide variety of roles, including stabilizing membranes, maintaining osmotic balance, and protecting protein structure against dehydration-induced damage (Fürtauer et al., 2019; Pommerrenig et al., 2018). The availability of sucrose in the cytosol is particularly important, as it is cleaved by invertases to produce monosaccharides necessary for inducing cold-related gene expression (Klotke et al., 2004; Rekarte-Cowie et al., 2008). At the chloroplast IE, sucrose exporter pSUT is therefore essential

for sucrose compartmentation. Loss of pSUT has been shown to result in the accumulation of plastidic and reduction of cytosolic sucrose, leading to decreased freezing tolerance (Patzke et al., 2018). On the other hand, maltose exporter (MEX) 1, which also localises to the IE, has been identified to be heavily downregulated in chloroplast envelopes under cold acclimation (Trentmann et al., 2020). This downregulation is postulated to result in the accumulation of maltose in the chloroplast stroma, where it has been shown to contribute to frost tolerance (Cvetkovic et al., 2021).

Beyond carbohydrate metabolism, the jasmonic acid (JA) signalling pathway also plays a key role in plant response to both biotic and abiotic stress, including low temperatures (Ahmad et al., 2016; Hu et al., 2017). Loss of JASSY in the chloroplast OE, which exports the jasmonate precursor OPDA from the chloroplast, results in failure to accumulate JA and negatively affects cold tolerance (Guan et al., 2019).

1.3.2 Chloroplast envelope proteins in lipid remodelling during cold acclimation

Experimental evidence has established cellular membrane damage as a major contributor to freezing injury in vascular plants, affecting multiple membrane compartments (Hincha et al., 1987; Krause et al., 1988; Steponkus et al., 1984). At low temperatures, changes in lipid composition (i.e., lipid remodelling) are critical for maintaining optimal membrane fluidity, stability and functionality. In this context, chloroplast envelope proteins involved in lipid trafficking and metabolism play a key role in lipid remodelling during cold acclimation. The sugar residues of glycolipids are thought to have a cryoprotective effect on the membrane, and low temperatures have been shown to shift lipid biosynthesis to the prokaryotic pathway within the chloroplast (Janská et al., 2010; John, Keller, et al., 2024; Li et al., 2015; Wang et al., 2013). This shift is likely mediated by the downregulation of fatty acid exporter FAX1 (Trentmann et al., 2020), which is degraded by rhomboid-like protease of the inner chloroplast envelope RBL11 under cold conditions (John, Krämer, et al., 2024). Notably, both overexpression of FAX1 and loss of RBL11 redirect lipid biosynthesis to the eukaryotic pathway under cold, ultimately resulting in decreased chilling and freezing tolerance (John, Krämer, et al., 2024; Wang et al., 2013).

On a more mechanistic level, adjustments in membrane fluidity are essential for offsetting the rigidifying effects of low temperatures and are closely connected to fatty acid desaturation in membrane lipids (Fig. 5). The introduction of double bonds introduces conformational kinks in lipid carbon chains, thereby reducing intermolecular packing and enhancing membrane

fluidity (Hugly & Somerville, 1992; Murakami et al., 2000; Routaboul et al., 2000). In the chloroplast, lipid desaturation is catalysed by fatty acid desaturases (FAD), of which FAD6, FAD7 and FAD8 have been shown to reside in the chloroplast envelope (Bouchnak et al., 2019; Koo & Ohlrogge, 2002). Mutants deficient in FADs, namely *fad5*, *fad6*, as well as *fad7 fad8* double and *fade fad7 fad8* triple mutants have been reported to suffer from chlorosis and reduced growth under low temperature conditions (Hugly & Somerville, 1992; Murakami et al., 2000; Routaboul et al., 2000), further emphasising the importance of fatty acid desaturation on lipid remodelling during cold acclimation. Furthermore, MGDG is a non-bilayer forming lipid with the propensity to form inverted hexagonal H_{II} phases (Webb & Green, 1991). Under stress conditions, including low temperatures, vascular plants have been reported to reduce the ratio of non-bilayer forming MGDG to bilayer forming DGDG as an adaptive strategy to maintain membrane integrity and stability (Li et al., 2020; MacDonald et al., 2023; Moellering et al., 2010; Zheng et al., 2016). To reduce the MGDG/DGDG ratio, MGDGs can be converted into acyl-MGDG, or into oligogalactolipids by enzymes at the OE. Upon wounding or freezing stress, MGDGs can be converted into acyl-MGDG by acylated galactolipid associated phospholipase (AGAP) 1, which catalyses the addition of a third acyl group at the galactose C6 position of MGDG, concurrently producing lyso-MGDG as a byproduct (Nilsson et al., 2015). During freezing exposure, MGDGs can also be converted into oligogalactolipids and diacylglycerols through the processive transfer of galactoses from one molecule of MGDG to another, a process catalysed by sensitive to freezing (SFR) 2. Loss of SFR2 has been shown to result in chloroplast damage after exposure to freezing conditions (Moellering et al., 2010).

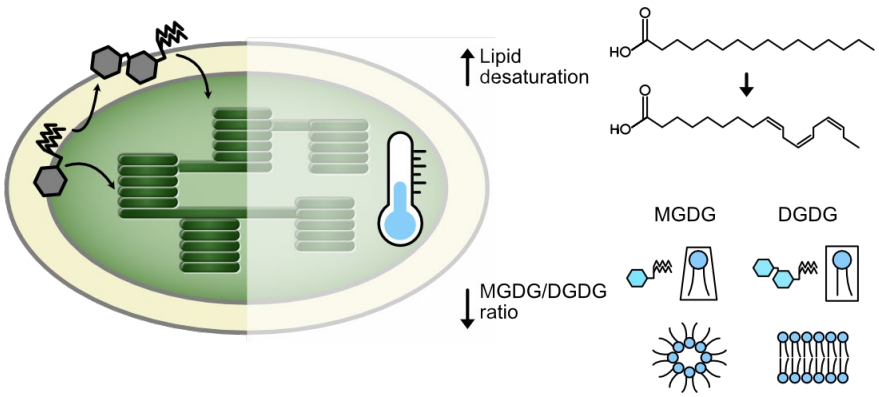

Figure 5 – Chloroplast lipid remodelling under cold acclimation. To offset the rigidifying effects of low temperature on membranes, desaturation of membrane lipids reduces intermolecular packing and maintains membrane fluidity. The ratio between non-bilayer forming MGDG and bilayer forming DGDG decreases to preserve membrane stability.

1.4 Aim of this work

The aim of this study is to explore the role of chloroplast envelope proteins in plant acclimation, with particular focus placed on lipid remodelling under low temperature stress. Although extensive efforts have provided invaluable insight to the multifaceted nature of the envelope and its potential involvement in cold acclimation, many of its constituent proteins have yet to be molecularly characterised. This work aims to explore the roles of chloroplast envelope proteins in plant acclimation processes, particularly during cold acclimation. AmiR based screens should be conducted to probe the chloroplast OE landscape. The chloroplast lipid remodelling protein (CLRP) 23 was also selected to be investigated in more detail. Formerly known in published literature as OEP23, CLRP23 (At2g17695) was originally identified in the chloroplast envelopes of Pea (Goetze et al., 2015) and assumed to localise to the OE due to the absence of a predicted transit peptide. However, the localisation of CLRP23 to the OE, has yet to be experimentally confirmed, and its exact molecular function remains elusive. Finally, chloroplast envelope transporter candidates of unknown molecular function should be selected and preliminarily characterised for future investigation.

2. Material and Methods

2.1 Material

2.1.1 Chemicals, molecular weight markers, enzymes and kits

Unless stated otherwise, all chemicals used in this study were purchased from Sigma Aldrich (Taufkirchen, Germany), Merck (Darmstadt, Germany), Thermo Fisher Scientific (Braunschweig, Germany) or Serva (Heidelberg, Germany). Liquid chromatography-grade solvents were purchased from Biossolve (Dieuze, France). Lipid standards were purchased from Avanti Polar Lipids, Inc (Alabaster, USA).

BlueStar Prestained Protein Marker (Nippon Genetics, Düren, Germany) was used as a molecular weight marker for SDS-PAGE. GeneRuler 1 kb Plus DNA-ladder (Thermo Fisher Scientific) was used as a molecular weight marker for agarose gel electrophoresis. Restriction endonucleases were purchased from Thermo Fisher Scientific, or New England Biolabs (Frankfurt am Main, Germany). RNAse free DNAse I was purchased from New England Biolabs. VeriFi Hot Start Polymerase (PCR biosystems, London, UK) was used for high fidelity/proofreading PCR.

The mi-Plasmid Miniprep Kit (Metabion) was used for the purification of plasmid DNA. The RNeasy Plant Mini Kit (Qiagen, Venlo, the Netherlands), was used for the extraction of RNA from plant tissue. The Fastgene Scriptase II cDNA kit (Nippon Genetics) was used for reverse transcription. The FastGene Gel/PCR Extraction kit (Nippon Genetics) was used for the extraction of DNA from agarose gel or PCR products.

2.1.2 Oligonucleotides

Oligonucleotides used in this work are listed in Table 1. All oligonucleotides were ordered from Metabion (Martinsried, Germany).

Table 1 – List of oligonucleotides used in this work.

Name	Sequence 5'-3'	Purpose
mir-for	CAAACACACGCTCGGAC	Genotyping (oemiR)
HSP-rev	CACAAATTCATAACACAACAAGC	Genotyping (oemiR)
CLRP23-for	TCACGAAGCATTGACATGTTTCA	Genotyping (CLRP23 mRNA/gDNA)
CLRP23-rev	ATGGTGTTCTTGAGTTGGGG	Genotyping (CLRP23 mRNA/gDNA)

gDNA-CLRP23-for	TCCTTCCCTTTCATCTTCATTTTTGG	Genotyping (CLRP23 gDNA only)
gDNA-CLRP23-rev	TGCAGGTTCTTCTTCTCTCTACAC	Genotyping (CLRP23 gDNA only)
GFP-rev	CTCGCCGGACACGCTGAACTTG	Plasmid sequencing (CLRP23-GFP)
TurboID-rev	GCTTATTAATGGCCGCTCGG	Plasmid sequencing (CLRP23-TurboID)
POE1-attb1-for	GGGGACAAGTTTGTACAAAAAAGCAGGCTTCATGGGGTCAAGGGACCAAAA	Gateway cloning
POE1-attb2-rev-nostop	GGGGACCACTTTGTACAAGAAAGCTGGGTCAGTAAGAAACAAATCCATCTGAGA	Gateway cloning
PT1-attb1-for	GGGGACAAGTTTGTACAAAAAAGCAGGCTTCATGGAGAGTCTCTCGATTCCC	Gateway cloning
PT1-attb2-rev-nostop	GGGGACCACTTTGTACAAGAAAGCTGGGTCGTAGTCATCTGGGAAGATGAACTGA	Gateway cloning
PT2-attb1-for	GGGGACAAGTTTGTACAAAAAAGCAGGCTTCATGACGCTTTTAGCTCTCTCTTCT	Gateway cloning
PT2-attb2-rev-nostop	GGGGACCACTTTGTACAAGAAAGCTGGGTCAACAATCATCCAAGTCAAGTGTCTG	Gateway cloning
PT3-attb1-for	GGGGACAAGTTTGTACAAAAAAGCAGGCTTCATGAGAATGTTAGTTCTTCGCACT	Gateway cloning
PT3-attb2-rev-nostop	GGGGACCACTTTGTACAAGAAAGCTGGGTCCCATCGTCTTATCAATGAAGTAAGCA	Gateway cloning
PT4-attb1-for	GGGGACAAGTTTGTACAAAAAAGCAGGCTTCATGGCTGCTAAACTTGTGTCC	Gateway cloning
PT4-attb2-rev-nostop	GGGGACCACTTTGTACAAGAAAGCTGGGTCAGACTGGTTTTGGGAAGGTGA	Gateway cloning
PT5-attb1-for	GGGGACAAGTTTGTACAAAAAAGCAGGCTTCATGGCTCTCTCCTCGTTGATC	Gateway cloning
PT5-attb2-rev-nostop	GGGGACCACTTTGTACAAGAAAGCTGGGTCTGTCTCTCCTTTGTGGAGA	Gateway cloning
PT6-attb1-for	GGGGACAAGTTTGTACAAAAAAGCAGGCTTCATGGCTCTTCTATTCACAGTGGT	Gateway cloning
PT6-attb2-rev-nostop	GGGGACCACTTTGTACAAGAAAGCTGGGTCTAATCGTTTGAGGACAAAAACTCCA	Gateway cloning
PT7-attb1-for	GGGGACAAGTTTGTACAAAAAAGCAGGCTTCATGTCACATATGGTGTTTCAGAGC	Gateway cloning
PT7-attb2-rev-nostop	GGGGACCACTTTGTACAAGAAAGCTGGGTCAGAGGCAGATGCAGCCAC	Gateway cloning

2.1.3 Plasmids

The oemiR plasmid collection was designed and generated by Philip Day and Beate Sculz prior to this work. The details of the plasmid collection can be found in the appendix (Supplementary Table 1) as well as the supplementary data of Schwenkert, Lo, et al. (2023). Other plasmids used in this work are listed in Table 2:

Table 2 – List of plasmids used in this work.

Gene	Description	Vector	Purpose	Source
AT2G17695	LII - Crispr-Cas9 - FastRed - CLRP23 - Guide 1+2	pICSL4723	CRISPR-Cas9	Lab Serena
AT2G17695	- stop	pDONR207	Gateway cloning	Lab Serena
AT2G17695	+ stop	pDONR207	Gateway cloning	Lab Serena
AT2G17695	- stop / GFP tag	pK7FWG2	GFP localisation	Lab Serena
AT2G17695	+ stop	pB7FWG2	Complementation	This work
AT2G17695	p35s-CLRP23-TurboID	pB7m34GW	Proximity labelling	This work
AT2G17695	- stop / His tag	pET21a+	Soluble protein expression	AG Hagn (TUM)
AT3G44380	-stop	pDONR207	Gateway cloning	This work
AT3G44380	-stop / GFP tag	pK7FWG2	GFP localisation	This work
AT5G22340	-stop	pDONR207	Gateway cloning	This work
AT5G22340	-stop / GFP tag	pK7FWG2	GFP localisation	This work
AT4G28210	-stop	pDONR207	Gateway cloning	This work
AT4G28210	-stop / GFP tag	pK7FWG2	GFP localisation	This work
AT1G44920	-stop	pDONR207	Gateway cloning	This work
AT1G44920	-stop / GFP tag	pK7FWG2	GFP localisation	This work
AT5G63040	-stop	pDONR207	Gateway cloning	This work
AT5G63040	-stop / GFP tag	pK7FWG2	GFP localisation	This work
AT5G13720	-stop	pDONR207	Gateway cloning	This work
AT5G13720	-stop / GFP tag	pK7FWG2	GFP localisation	This work
AT5G24000	-stop	pDONR207	Gateway cloning	This work
AT5G24000	-stop / GFP tag	pK7FWG2	GFP localisation	This work
AT5G24690	-stop	pDONR207	Gateway cloning	This work
AT5G24690	-stop / GFP tag	pK7FWG2	GFP localisation	This work

2.1.4 Plant species

Arabidopsis (*Arabidopsis thaliana*, Columbia-0 ecotype) was used for the majority of this study, with the exception of the sub-organellar localisation of CLRP23 to the chloroplast IE, which was performed in Pea (*Pisa sativum*, cv. 'Arvica', Prague, Czech Republic), and Tobacco (*Nicotiana benthamiana*), which was used for transient expression of proteins.

2.1.5 Bacterial strains

Competent TOP10 and DH5α cells were used for the propagation of plasmid DNA in *Escherichia coli*. For the propagation of plasmids containing CcdB selection, DB3.1 cells were used. LEMO21(DE3) competent *E. coli* (New England Biolabs) was used for the overexpression of His-tagged CLRP23 for *in vitro* experimentation. Agrobacteria (*Agrobacterium tumefaciens*, strain GV3101) was used for both stable expression in Arabidopsis and transient expression in Tobacco.

2.165 Antisera

Generation of antisera against CLRP23 was performed by Tim Lücke. The coding sequence of CLRP23 in Arabidopsis and Pea (psCLRP23) were separately cloned into pET51b(+) for protein overexpression and CLRP23 was purified from inclusion bodies for antisera generation. Antisera against PsbO, TIC110, FBPase in Arabidopsis and OEP37 and TIC40 in Pea were provided by the workgroup.

2.1.7 Accession numbers

The accession numbers of proteins investigated in this work are detailed in Table 3, with the exception of the proteins targeted by the oemiR plasmid library, which are detailed in the appendix (Supplementary Table 1).

Table 3 – Accession numbers of proteins investigated in this work

Gene	Gene name/Description
AT2G17695	Chloroplast Lipid Remodelling Protein (CLRP) 23
AT3G57990	Outer Envelope Protein (OEP) 40
AT2G43950	Outer Envelope Protein (OEP) 37
AT1G70480	JASSY-1 (OPDA exporter)
AT3G44380	Protein of the Outer Envelope (POE) 1
AT5G22340	Protein Transporter (PT) 1
AT4G28210	Protein Transporter (PT) 2
AT1G44920	Protein Transporter (PT) 3
AT5G63040	Protein Transporter (PT) 4
AT5G13720	Protein Transporter (PT) 5
AT5G24000	Protein Transporter (PT) 6
AT5G24690	Protein Transporter (PT) 7

2.2 Molecular Methods

2.2.1 Molecular cloning

Using the Gateway cloning system (Thermo Fisher Scientific), protein constructs with or without stop codons were first cloned into pDONR207 to generate entry clones, which were subsequently cloned into pB7FWG2 or pK7FWG2 (Karimi et al., 2002), according to manufacturer instructions. The Multi-site Gateway cloning system was used to tag the C-terminus of CLRP23 with TurboID, based on a method adapted from Arora et al. (2020). Expression vectors pEN-L4-2-R1 (Karimi et al., 2007), pDONR207-OEP23 (OEP23 cloned into pDONR207 vector via a BP reaction), and pEN_R2_LinkerTur (Arora et al., 2020) were cloned into the destination vector pB7m34GW (Karimi et al., 2007). Resulting plasmids were transformed into competent *E. coli* and subsequently purified with the mi-Plasmid Miniprep Kit (Metabion) according to manufacturer instructions. All plasmids were confirmed with Sanger Sequencing before proceeding with downstream experimentation.

2.2.2 Polymerase chain reaction (PCR)

PCR was performed using either genomic DNA (gDNA), coding DNA (cDNA) or plasmid DNA as templates. Homemade Taq polymerase was used for genotyping PCR. VeriFi Hot Start Polymerase (PCR biosystems, London, UK) was used for high fidelity/proofreading PCR if fragments were to be used for molecular cloning. Cycling settings were adjusted based on manufacturer guidelines, the melting temperatures (T_m) of the oligonucleotides, and the lengths of the amplified fragments. For oligonucleotides containing long non-template 5' overhangs, the initial 10 cycles were performed using the Tm calculated for the annealing region (excluding overhangs). Subsequent cycles used the Tm calculated for the full-length oligonucleotides (including overhangs). PCR fragments used for subsequent cloning were purified using the FastGene Gel/PCR Extraction kit (Nippon Genetics) according to manufacturer instructions.

2.2.3 Isolation of RNA and cDNA synthesis

Total RNA was extracted using the RNeasy Plant Mini Kit (Qiagen). After degradation of DNA with RNase free DNAse I (New England Biolabs), cDNA was synthesised with the Fastgene Scriptase II cDNA kit (Nippon Genetics). All steps were performed according to manufacturer instructions.

2.2.4 Isolation of gDNA for genotyping PCR

Genomic DNA was isolated in a method adapted from Kotchoni and Gachomo (2009). In short, samples were homogenised in 500 µl high purity extraction buffer (0.1 M Tris-HCl pH 7.5, 0.05 M NaCl, 0.05M EDTA pH 8.0, 1% (w/v) PVP 40), after which 66 µl of 10% (w/v) SDS and 166 µl 5M potassium acetate was added. After centrifugation at max speed for 15 min, the resulting supernatant (600-700 µl) was mixed with 500 µl isopropanol and incubated on ice for 15 min. This was followed by another centrifugation step before the pellet was washed with 500 µl 70% v/v EtOH, after which the samples were centrifuged again and the resulting DNA pellet was left to dry before resuspending in 50 µl H_2O.

2.2.5 Sequencing

Sequencing of plasmids and PCR products was performed by the sequencing service at the Faculty of Biology (Ludwig-Maximilians-Universität München, Germany).

2.3 Biochemical and Cell Biological Methods

2.3.1 Total protein extraction for SDS-PAGE

Fresh leaf tissue was homogenized with 100 µl extraction buffer (50 mM Tris pH 7.5, 300 mM NaCl, 5 mM EDTA, 20% (v/v) Glycerol, and 1% (v/v) Nonidet P40, 0.4M DTT), after which 10% w/v LDS was added to reach a final concentration of 2%. Samples were then incubated on rotation at 4ºC before centrifuging at full speed, 4ºC for 10 min. The resulting supernatant was then used for subsequent analysis with SDS-PAGE.

2.3.2 Sodium dodecyl sulphate-polyacrylamide gel electrophoresis (SDS-PAGE)

Proteins were separated by SDS-PAGE according to Laemmli (1970) with a 6% stacking gel and 12-15% separating gel. Samples were normalised according to total protein concentration via Bradford assay (Bradford, 1976) using ROTI®Quant (Carl Roth, Karlsruhe, Germany) and prepared for SDS-PAGE by adding 5x laemmli buffer (62.5 mM Tris/HCl pH 6.8, 2% (w/v) SDS, 10% (v/v) glycerol, 5% (v/v) β-mercaptoethanol, 0.004% (w/v) bromophenol blue) to a final concentration of 1x Laemmli. The system was filled with SDS running buffer (25 mM Tris, 192 mM glycine, 0.1% (w/v) SDS). After separation, gels were either stained directly with Coomassie brilliant blue (45% (v/v) MeOH, 9% (v/v) acetic acid, 0.2% (w/v) Coomassie

brilliant blue R-250) and destained (25% (v/v) MeOH, 10% (v/v) acetic acid), or used for immunoblotting analysis.

2.3.3 Blue Native PAGE (BN-PAGE)

Isolated chloroplasts normalised to 20 µg chlorophyll content were centrifuged at 6000 rpm, 4ºC for three min before being resuspended in 20 µl ACA buffer (750 mM Aminocaproic acid, 50 mM Bis-Tris pH 7, 0.5 mM EDTA-Na_2) and 2.25 µl 10% (w/v) β-Dodecylmaltosid (β-DM). After incubation for 10 min on ice, the solubilised chloroplasts were centrifuged at 14000 rpm, 4ºC for 10 min, after which the supernatant was combined with 1.25 µl loading dye (750 mM Aminocaproic acid, 5% (w/v) Coomassie Serva G-250). Samples were then loaded onto NativePAGE™ Bis-Tris Mini Protein Gels (3 to 12%, 1.0 mm; Thermo Fisher Scientific) and run at 200 V, 4ºC for 1-2h until samples reached a half to two thirds of the gel with blue cathode buffer (50 mM Tricine, 15 mM Bis-Tris pH 7, 0.02 % (w/v) Coomassie Serva G-250). The blue cathode buffer was then replaced by clear cathode buffer (50 mM Tricine, 15 mM Bis-Tris pH 7) for the rest of the run. 50 mM Bis-Tris pH 7 was used as the anode buffer. Individual lanes from the BN-PAGE were then excised for SDS-PAGE in the second dimension.

2.3.4 Immunoblotting analysis

After SDS-PAGE, proteins were transferred onto a PVDF membrane with a semi-dry blotting method using the TransBlot Turbo Transfer System (BioRad, Feldkirchen, Germany). The blot sandwich was assembled as follows onto the anode: two Whatman papers soaked in anode buffer I (0.3M Tris/HCl pH 10.4, 20% (v/v) MeOH), two Whatman papers soaked in anode buffer II (0.025M Tris/HCl pH 10.4, 20% (v/v) MeOH), PVDF membrane activated in MeOH and rinsed with water, SDS gel, and two Whatman papers soaked in cathode buffer (0.025 M Tris/HCl pH 9.4, 0.04M 6-aminohexanoic acid, 20% (v/v) MeOH). Western blotting was performed at 0.2 mA for 20 min. Unless stated otherwise, for immuno-hybridisation the PVDF membrane was blocked with (5% milk in TBS-T) before incubating with primary antisera (1:500-1000, 5% milk in TBS-T). The membrane was subsequently washed with TBS-T for 2x15 min before incubating with secondary α-rabbit-HRP (1:10,000-50,000, 5% milk in TBS-T). After washing for 4x10 min, the transferred proteins were developed with SuperSignal™ West Pico PLUS Chemiluminescent Substrate (Thermo Fisher Scientific) for immunodetection. Finally, the PVDF membrane was stained with Coomassie solution (25% (v/v) MeOH, 10% (v/v) acetic acid, 0.02% (w/v) Coomassie brilliant blue G-250) as a loading control.

2.3.5 Quantification of Anthocyanins

Anthocyanins were extracted and measured as described in Kitashova et al. (2023). In summary, plant material was ground in liquid nitrogen and suspended in 1M HCl before incubating at 25ºC for 30 min with shaking at 800 rpm. After centrifugation at 21,000 x g for 10 min, the supernatant was transferred to a fresh tube before the extraction process was repeated again at 80ºC for 30 min. Supernatants from both extraction steps were pooled and photometrically measured at 540 nm, with the resulting absorbance values normalised to fresh weight before proceeding with data analysis.

2.3.6 RNA Sequencing and data analysis

Total RNA was isolated from leaf tissue with TRIzol (Invitrogen, Carlsbad, USA) and purified with Direct-zol™ RNA MiniPrep Plus columns (Zymo Research, Irvine, USA) according to manufacturer instructions. The integrity and quality of the extracted RNA was evaluated with an Agilent 2100 Bioanalyzer (Agilent, Santa Clara, USA). Ribosomal RNA was then depleted to generate long non-coding RNA sequencing (lncRNA-seq) libraries encompassing both nuclear and organellar transcripts. After the preparation of directional lncRNA-seq libraries, 150 bp paired-end sequencing was conducted at a depth of approximately 6G on an Illumina NovaSeq 6000 system (Illumina, San Diego, USA) using standard Illumina protocols. The RNA-seq reads were then processed via the Galaxy platform (Jalili et al., 2020) according to Tang et al. (2024), with one exception: differential gene expression was determined using DESeq2 (Love et al., 2014) with fit type set to “parametric” multi-mapping allowed, and an adjusted P-value of <0.05. No fold-change cutoff was applied. Three biological replicates were analysed per genotype and condition, with one replicate of *clrp23* under standard growth conditions excluded as an outlier.

Paired-end sequencing was performed at Biomarker Technologies (BMK) GmbH (Münster, Germany). Extraction of total RNA and the processing of RNA-seq reads was performed by PD Dr. Tatjana Kleine.

2.3.7 Co-immunoprecipitation of GFP-tagged proteins with GFP-trap

CLRP23 with C-terminal tagged green fluorescent protein (GFP) was transiently expressed in Tobacco. Transiently transformed or wildtype Tobacco leaves were ground in liquid nitrogen. Approximately 1 g fresh weight of plant material was resuspended in 2 ml lysis buffer (50 mM

Tris/HCl pH 7.5, 5% glycerol, 10 mM DTT, 0.1% Nonidet P40, 1x Roche complete™ Protease Inhibitor Cocktail). After vortexing and solubilisation by rotating at 4ºC for 30 min, cell debris were removed by centrifugation at 20,000 x g, 4ºC for 15 min. For affinity chromatography, the resulting supernatant/lysate was added to 25 µl equilibrated GFP-Trap® Magnetic Agarose (ChromoTek, Planegg-Martinsried, Germany) and rotated end-over-end at 4ºC for 1h. For all subsequent wash and resuspension steps, the GFP-trap magnetic beads were pelleted with a magnetic tube rack. The beads were washed three times with lysis buffer and twice with washing buffer (50 mM Tris/HCl pH 7.5, 5% glycerol, 10 mM DTT) before proceeding with on-bead trypsin digestion.

For on-bead trypsin digestion, beads were resuspended with 25µl Elution Buffer I (50 mM Tris-HCl/pH 7.5, 2 M urea, 5 µg/ml Sequencing Grade Trypsin, 1 mM DTT) and incubated at 30ºC, 400 rpm for 30 min. The beads were then pelleted and the supernatant was collected and transferred to a fresh tube. The beads were then sequentially resuspended twice with 50 µl Elution buffer II (50 mM Tris-HCl pH 7.5, 2M urea, 5 mM iodoacetamide (IAA)), pelleted, and supernatants collected. All three supernatants (125 µl total) were pooled and digested overnight at 32ºC, 400 rpm. The digestion reaction was terminated the next day with 1µl formic acid, before purifying with homemade C18 stage tips for mass spectrometry analysis, according to Rappsilber et al. (2003). Mass spectrometry (MS) analysis was performed at the MSBioLMU core facility (Ludwig-Maximilians-Universität München).

2.3.8 Proximity labelling with Turbo-ID

CLRP23 with C-terminal tagged engineered biotin ligase (TurboID) was transiently expressed in Tobacco. Tobacco leaves were infiltrated with 2 mM biotin in PBS 24 hours after transient expression to allow for the biotinylation of proteins in close proximity to the CLRP23-TurboID fusion protein. Wildtype tobacco leaves were also infiltrated with biotin as a negative control. To verify successful biotinylation of proteins, total protein extracts from the infiltrated tobacco leaves were analysed by SDS-PAGE followed by western blotting with the Vectastain ABC Kit (BIOZOL Diagnostica Vertrieb, Eching, Germany) according to manufacturer instructions.

Pull-down of biotinylated proteins with affinity chromatography was performed based on a method adapted from Mair et al. (2019). Leaves were ground in liquid nitrogen, of which approximately 3 ml of material was suspended in 2 ml extraction buffer (50 mM Tris pH 7.5, 150 mM NaCl, 0.1% SDS, 1% Triton-x-100, 0.5% Na-deoxycholate, 1 mM EGTA, 1 mM DTT, 1x Roche complete™ Protease Inhibitor Cocktail) and incubated on a rotor wheel at 4ºC for

25 min. Samples were then sonicated 4x30 seconds, with 90 second breaks in between. To remove cellular debris, samples were centrifuged for 15 min at 15,000 x g, 4ºC for 15 min, after which the supernatant was collected and desalted with PD-10 desalting columns (Cytiva, Freiburg, Germany) using the spin protocol.

The protein concentration of the desalted samples were then measured with Bradford assay, after which sample containing 800 µg total protein was incubated with 100 µl equilibrated streptavidin Sepharose beads on a rotor wheel at 4ºC for 1h-overnight. For all wash and resuspension steps, beads were collected by centrifuging at 1000 x g, 4ºC for 30 seconds. After pull-down, beads were washed three times with 1 ml extraction buffer (without protease inhibitor), twice with 1 ml wash buffer I (50 mM Tris pH 7.5), and twice with 1 ml wash buffer II (50 mM Tris pH 7.5, 2 M Urea). The washed beads were then resuspended in 160 µl trypsin buffer (50 mM Tris pH 7.5, 1M Urea, 1 mM DTT, 0.8 µg Trypsin) and incubated at 25ºC with shaking for 3h. The supernatant was then transferred to a fresh tube, after which the beads were washed twice with 120 µl wash buffer III (50 mM Tris pH 7.5, 1 M Urea) the supernatants of which were pooled to a 400 µl total sample volume. The pooled supernatants were then reduced by adding DTT to a final concentration of 4 mM. After another incubation step at 25ºC with shaking for 30 min, IAA was added to a final concentration of 10 mM and incubated at 25ºC with shaking for 45 min. Finally, 1 µg trypsin was added to each sample before they were left to digest overnight at 25ºC with shaking. Samples were then purified the next day with homemade C18 stage tips for mass spectrometry analysis, according to Rappsilber et al. (2003). MS analysis was performed at the MSBioLMU core facility (Ludwig-Maximilians-Universität München).

2.3.9 Proteomic analysis with LC-MS/MS

Proteomic analysis with liquid chromatography (LC)-MS/MS was performed at the MSBioLMU core facility (Ludwig-Maximilians-Universität München).

For Arabidopsis shotgun proteomics, 3-week-old rosette leaves were ground in liquid nitrogen, after which 100 mg of frozen ground plant material was suspended in 0.3 ml extraction buffer (100 mM 4-(2-hydroxyethyl)-1-piperazineethanesulfonic acid (HEPES) pH 7.5, 150 mM NaCl, 10 mM DTT, 6 M Guanidine Chloride, and 1x Roche complete™ Protease Inhibitor Cocktail). After sonification with a Branson Sonifier B-12 (Branson Ultrasonics, Danbury, USA) for three

20-second cycles, the suspension was incubated at 60ºC for 10 min. Cellular debris was removed by centrifugation at 10,000 x g for 15 min. MeOH:chloroform:water (4:2:3, v/v) was added to the clarified supernatant. After centrifugation at 10,000 x g for 10 min, the protein interphase was collected and washed five times with MeOH. The resulting protein pellet was then dried before it was dissolved in 3 M Urea/2 M Thiourea in 50 mM HEPES (pH 7.8). The Pierce 660 nm Protein Assay Kit (Thermo Fisher Scientific) was used to determine protein concentration, and 100 µg of protein was reduced with 10 mM DTT for 30 min at 37ºC, alkylated with 50 mM IAA at room temperature for 20 min in darkness before digesting with 1 µg Trypsin (Thermo Fisher Scientific) at 37ºC overnight.

For envelope proteomics, chloroplast IE and OE membranes fractions, which were fractionated from pea chloroplasts according to Waegemann et al. (1992), were provided by PD Dr. Bettina Bölter. 30 µg protein of each membrane sample was resuspended in 250 µl extraction buffer. Samples were then sonicated, incubated at 60ºC, and centrifuged as described for plant powder, before processing with the Filter Aided Sample Preparation (FASP) method according to Wiśniewski et al. (2009).

All digested peptides were then purified using homemade C18 stage tips according to Rappsilber et al. (2003). For LC-MS/MS analysis, 1 µg of peptides was separated using a nano-LC system (Ultimate 3000 RSLC, Thermo Fisher Scientific) with linear gradients of 5% to 80% ACN (v/v) at a flow rate of 250 nl/min. Gradient lengths varied by sample complexity: 90 min for total proteins and 60 min for envelope samples. Chromatography was performed with Acclaim Pepmap nano-trap (C18, 100 Å, 100 µm × 2 cm) and analytical (C18, 100 Å, 75 µm × 50 cm) columns, with the column temperature maintained at 50°C. MS/MS was conducted on an Impact II high-resolution Q-TOF mass spectrometer (Bruker Daltonics, Bremen, Germany) using CaptiveSpray nano-electrospray ionization. MS1 spectra (m/z 200–2000) were acquired at 3 Hz, and the 18 most intense peaks were subjected to MS/MS at 4–16 Hz based on intensity. A dynamic exclusion duration of 0.5 min was applied.

Raw data were processed using MaxQuant (version 2.4.4.0) with peak lists matched against the Arabidopsis reference proteome (UniProt) using default parameters. Protein quantification was performed using the LFQ algorithm. Data were further analysed using Perseus (version 2.0.6.0), excluding contaminants, reverse hits, and proteins identified only by site modification. Proteins quantified in at least three out of four replicates were retained. LFQ intensities were $\log_2$-transformed, and missing values were imputed using a normal distribution in Perseus. The

Database for Annotation, Visualization, and Integrated Discovery (DAVID) was used to identify enriched gene ontology (GO) terms based on biological process (Huang et al., 2009; Sherman et al., 2022).

2.3.10 Lipidomic analysis with LC-MS

Lipidomic analysis with LC-MS was performed at the MSBioLMU core facility (Ludwig-Maximilians-Universität München).

Lipids and free fatty acids were extracted as described in Hummel et al. (2011). In short, 50 mg of each sample was suspended 1 ml of pre-chilled MeOH:methyl tert-butyl ether (MTBE) solution (1:1, v/v) at −20°C. Internal standards, namely 2 µg ml-1 corticosterone, 0.25 µg ml-1 ampicillin, and 1 µg ml-1 chloramphenicol, were also added to the extraction mixture. Samples were shaken at 4°C for 10 min before they were ultrasonicated for an additional 10 min on ice. 500 µl of H_2O:MeOH (3:1, v/v) was then added, after which the mixture was vortexed for 10 sec and centrifuged at maximum speed at 4°C for 5 min. After phase separation, the upper organic phase (500 µl) was collected, dried under vacuum under argon gas, and stored at −80°C until further analysis.

For LC-MS analysis, a Dionex Ultimate 3000 UHPLC system (Thermo Fisher Scientific) coupled with a timsTOF mass spectrometer (Bruker Daltonik) was used. The dried extracts were reconstituted in 100 µl of acetonitrile:isopropanol (7:3, v/v), of which 5 µl was injected onto a C8 reversed-phase column (Ultra C8, 100 × 2.1 mm; Restek) with a flow rate of 300 µl min^{-1} at 60°C. (A) water and (B) acetonitrile:isopropanol (7:3, v/v) were used as mobile phases, both of which contain 1% (v/v) ammonium acetate and 0.1% (v/v) acetic acid. A 26 min gradient was used, from 55% B to 99% B over 15 min. This was followed by a 5 min washing step at 99% B before returning to 55% B with a 5 min equilibration phase.

For mass spectrometry, an electrospray ionization (ESI) source in positive mode was employed. Nitrogen was used as the dry gas at a flow rate of 8 l min^{-1}, a pressure of 8 bar, and a temperature of 200°C. Mass spectra were recorded in MS mode with a range of 50–1300 m/z, resolution of 40,000, scan speed of 1 Hz, and mass accuracy of 0.3 ppm. Compounds were annotated with a targeted approach based on specific m/z values at defined retention times and their isotopic patterns. Data acquisition was performed using otofControl 6.2, with further analysis conducted using DataAnalysis 5.3 and MetaboScape 2021 software. Quantification was normalized to fresh weight and internal standards, excluding features detected in blanks or

wash samples with a threshold of >10%. Three independent biological replicates were measured per genotype/condition for cold treatment, four for freezing recovery. For freezing recovery, one replicate of the *clrp23* mutant grown at room temperature was excluded due to technical reasons and was replaced by taking the average value of the remaining replicates.

2.3.11 Analysis of fatty acid composition with GC-FID

Lipids were extracted for Thin-Layer Chromatography (TLC) and fatty acid methyl ester (FAME) analysis using a method adapted from Yu et al. (2020). 500 mg of frozen and ground plant material was ground in liquid nitrogen and suspended in 6 ml $CHCl_3$:MeOH (1:2 v/v), with 50 µl of 5 mg ml-1 tripentadecanoin (TAG C15:0) added to each sample as an internal standard. Cellular debris were removed by centrifugation at 2100 g, 4ºC for 5 min. 2 ml of $CHCl_3$ and 1.2 ml of KCl (0.45 % v/v) was added to the resulting supernatant for phrase separation, and the lower green organic phase was collected. The solvent was evaporated by nitrogen stream and the lipids were resuspended in 250 µl $CHCl_3$:MeOH (9:1 v/v).

For TLC, lipid samples were applied to a silica gel coated glass plate (20 x 20 cm) using an automatic TLC sampler (CAMAG® ATS 4). For each sample, a total of 8 µl of lipids were separated with acetone:toluene:H_2O (91:30:8, v/v/v) and visualised with 0.05% primuline in acetone:H_2O (8:2 v/v) under UV light (Hölzl & Dörmann, 2021). 4 µl each of MGDG and DGDG (2.5 mg/ml, Avanti Polar Lipids, Inc.) were also applied to the plate as external standards. Water was applied to MGDG and DGDG bands to prevent particle formation, and the silica was scraped with a spatula into a fresh glass tube. The silica containing MGDG or DGDG was then suspended in 0.5 ml anhydrous MeOH and sonicated for 5 min, before evaporating the MeOH by nitrogen stream.

Fatty acid methyl esters (FAMEs) were generated as described in Pålsson et al. (2024), slightly modified from Leonova et al. (2008). In short, 2 ml of MeOH:H_2SO_4 (98:2 v/v) was added to either 8 µl lipid extract (for total lipid analysis) or dried silica from the previous TLC step (for MGDG and DGDG analysis). 10 µl of 0.25 mg ml-1 heptadecanoic acid (C17:0) was also added as an internal standard for the methylation reaction. Samples were methylated in a heat block at 80ºC for 45 min, after which 2 ml of water and 2 ml heptane was added for phase separation. The upper heptane phase was collected and evaporated under nitrogen gas and the FAMEs were resuspended in 50 µl cyclohexane.

The resulting FAMEs from the methylation step were then analysed on a Trace 1300 gas-chromatography (GC) machine equipped with an ISQ single quadrupole mass spectrometer (MS), a flame ionisation detector (FID) and an auto-sampler (Thermo Scientific). FAMEs were separated on a Zebron ZB-FAME column (20m x 0.18mm i.d. x 0.15 µm film thickness). The GC oven was set to a starting temperature of 90ºC, which was held for 1.5 min before ramping at 5.5ºC/min to 240ºC. The oven was held at 240ºC for 4 min until the end of the program, with a total run time of 33 min. The MS was set with an MS line temperature and ion source temperature of 250ºC, and a full scan was performed with mass range of 50-500 amu and dwell time of 0.2 seconds. FAMEs were identified based on the retention time compared with the external reference standard GLC 426 (Nu-Check-Prep) and further confirmed with MS spectra using GC-MS, after which FID was then employed for the quantification of each FAME. The FID was set to a detection temperature of 260ºC.

GLC 426 standard mix was used as the external standard to both identify the retention time and calculate the response factor for each FAME. The response factor, which accounts for the difference in detector response of each fatty acid (FA) compared to the internal standard C17:0 (IS), was calculated as follows:

$$DFA = RFA/RIS = (AFA/WFA)/(AIS/WIS)$$

D = response factor; R = response; A = peak area (pA*min); W = weight. The response factor of C17:0 was set to 1.

After subtracting the peak areas detected in the reaction blanks, the peak areas of each FAME were normalized according to the response factor of each FAME. For FAMEs C16:2 and C16:3, which were not included in the external standard, the response factor for the C16:1 FA was used for normalization. The final quantification of each FAME is reported as mol%. Total lipid content was calculated based on the sum of the normalized peak areas of all FAMEs, relative to the normalized peak area of the TAG IS C15:0, which was added as tripentadecanoin (Larodan, Sweden) to each sample prior to lipid extraction. Four independent biological replicates were used per genotype/condition for all measurements.

2.3.12 Protein overexpression in E. coli

CLRP23 with a C-terminal His-tag cloned into the pET21a(+) inducible expression vector was provided by Prof. Dr. Franz Hagn, and transformed into LEMO21(DE3) competent *E. coli* (New England Biolabs). Transformed cells were then inoculated into 5 ml LB medium with

supplemented with chloramphenicol and ampicillin, and incubated for 37ºC in a shaker overnight before transferring into 400 ml LB medium the next morning. The main culture was supplemented with chloramphenicol, ampicillin and 0-250 µM L-Rhamnose. After incubation at 37ºC in a shaker until an OD_{600} of 0.4-0.6 was reached, overexpression was induced with the addition of IPTG to reach a final concentration of 400 µM. Protein overexpression took place overnight at 16-18 ºC to maximise the yield of soluble proteins. The cells were then centrifuged at 4000 rpm, 4ºC for 15 min and stored at -20ºC until purification.

2.3.13 Purification of soluble his-tagged proteins with affinity chromatography and size exclusion chromatography (SEC)

Cell pellet from protein overexpression (0.4 L culture volume) was resuspended in 20-30 ml protein buffer (50 mM Tris pH 8.0, 200 mM NaCl, 10 mM Imidazol). The cells were passed through a microfluidic device twice for cell lysis. The lysate was then centrifuged at 20,000 x g, 4ºC for 30 min, after which the supernatant was added to 50-100 µl equilibrated Ni Sepharose™ High Performance histidine-tagged protein purification resin (Cytiva, Freiburg, Germany) and incubated at RT on rotation for 30 min to 2h. The lysate/resin mixture was then passed through a gravity flow column, after which the resin was washed twice with protein buffer. His-tagged proteins were eluted with 4 x 200 µl elution buffer (50 mM Tris pH 8.0, 200 mM NaCl, 500 mM Imidazol). For MST, 10% (v/v) glycerol was added to the elution buffer to prevent protein precipitation. SEC was performed on a Superdex™ 200 10/300 GL column (GE Healthcare, Düsseldorf, Germany) with protein buffer used as running buffer.

2.3.14 Microscale thermophoresis (MST)

Soluble His-tagged CLRP23 eluted from Ni-sepharose was desalted using PD10 columns before being fluorescently labelled with the His-Tag Labeling Kit RED-tris-NTA 2nd Generation (Nanotemper, Munich, Germany) according to manufacturer instructions. The concentration of fluorescently labelled CLRP23 was kept constant at 600 nM, while the concentration of MGDG or DGDG varied between 30 nM and 1 mM. The final reaction conditions of the MST assay contained 1x PBS-T, 2.5% (v/v) glycerol, and 10% (v/v) DMSO. Samples were incubated for 30 min before they were loaded onto Monolith Capillaries (Nanotemper) and MST was performed on the Monolith NT.115 Red/Green decide (Nanotemper) with 40% LED power and 80% MST power. The Nanotemper Analysis Software was used for data analysis to determine the overall affinity (K_D).

2.4 Plant Biological Methods

2.4.1 Plant material and growth conditions

Arabidopsis plants were grown on soil in a growth chamber under long-day conditions [16 h/8 h day-night cycle, 120 µmol photons $m^{-2}s^{-1}$, temperatures 21°C/ 18°C (light/dark)] for three weeks. For cold and light treatment, plants were grown at the indicated conditions. Pea plants were grown on vermiculite for 10 days in a climate chamber s [14 h/10 h day-night cycle, 120 µmol photons $m^{-2}s^{-1}$, temperatures 20°C/ 14°C (light/dark)].

Freezing treatment of Arabidopsis was performed by Katharina Ebel according to Trentmann et al. (2020) with small changes. Briefly, four-week-old plants were cold acclimated for 4 days under short day conditions (light 10 h/4°C; dark 14 h/4°C). The diurnal cycle was turned off the following day and the temperature was gradually lowered from 4°C to -10°C, with a stepwise temperature decrease of 2 to 4°C per h. The temperature was kept at -10ºC for 15 h, after which the temperature was raised again to 22°C with a stepwise temperature increase of 2 to 4°C/h. The diurnal cycle was turned on again after 1 day, when the temperature was recovered back to 22°C (light 10 h/22°C; dark 14 h/18°C). Two rounds of freezing experiments were performed on a combined total of 110 Col-0 and *clrp23* mutant plants each. After freezing, samples were collected for lipidomic analysis after temperatures were recovered for 1 hour at 22ºC.

2.4.2 Stable transformation of Arabidopsis

The floral dip method (Clough & Bent, 1998) was used to stably transform Arabidopsis plants. 2 µg plasmid containing the appropriate construct was transformed into competent Agrobacteria. The transformed cultures were sequentially grown in 3 ml, 25 ml, and 400 ml of LB or YEP medium, with each step incubated overnight in a 28 °C shaker. The final culture was centrifuged at 3500 rpm for 20 min, before resuspended in Silwet-medium (5% sucrose, 0.05% silwet L-77) and adjusted to an OD_{600} of 0.8. Five-week-old, flowering plants were dipped in the resulting bacterial suspension and covered overnight. The dipping procedure was repeated after seven days. Transformed plants in the T_1 generation were selected by either kanamycin (50 µg/ml) or BASTA.

2.4.3 Transient transformation of Tobacco

Transformed agrobacteria was inoculated in 5 ml LB/YEP medium supplemented with appropriate antibiotics and grown in a 28ºC until an OD_{600} of 0.6-1. For GFP localisation, helper phage p19 was also grown in a separate inoculation. After centrifugation at 4000 x g for 15 min, the agrobacteria/helper phage was resuspended with infiltration media (10 mM MES, pH 6, 10 mM $MgCl_2$, 150 µM Acetosyringone) to an OD_{600} of 1, before rotating in darkness for 2h. Tobacco leaves were infiltrated with a 1 ml syringe.

2.4.4 Isolation of chloroplasts from Arabidopsis

Arabidopsis plants were grown for three weeks under long day conditions and placed in darkness the evening before chloroplast isolation. Plants were harvested with a sharp razor blade before being homogenized in isolation buffer (0.3 M Sorbit, 5 mM $MgCl_2$ x 6 H_2O, 5 mM EDTA, 20 mM HEPES-KOH, 10 $NaHCO_3$, 50 mM ascorbic acid, adjusted to pH 8 with KOH) with a Polytron mixer. After filtering through 1 layer of gauze/miracloth, the homogenate was centrifuged at 3000 rpm, 4ºC for 4 min. The chloroplast pellet was washed with wash buffer (50 mM HEPES, 0.3 Sorbit, 0.5 mM $MgCl_2$, adjusted to pH 8 with KOH), centrifuged, and resuspended in a small volume of wash buffer. Chlorophyl concentration was determined by adding 1 µl isolated chloroplasts to 1 ml 80% acetone, before spectrophotometrically measured at 645, 663 and 750 nm and calculated as follows:

$$\mu g\ chlorophyll/\mu l\ =\ 8.02 * (Abs\ 663 - Abs\ 750)\ +\ 20.2 * (Abs\ 645 - Abs\ 750)$$

2.4.6 Isolation of protoplasts from Tobacco for GFP localisation

One tobacco leaf was cut with a razor blade in 10 ml freshly prepared enzyme solution (1% cellulase R10, 0.3% Mazerozyme R10, 10 mM KNO_3, 3 mM $CaCl_2$ x 2 H_2O, 1.5 mM $MgSO_4$ x 7 H_2O, 1.25 mM KH_2PO_4, 20 mM NH_4 Succinate, 2 mM MES, approx. 320 mM sucrose adjusted to 550 mOsm). After vacuum-infiltration, the leaves were shaken at 40 rpm in the dark for 90 min, before the protoplasts were released with 80 rpm shaking for 1 min. The protoplast suspension was then filtrated through 100 µm gauze into a 15 ml centrifugation tube before overlaying with 2 ml F-PCN (10 mM KNO_3, 3 mM $CaCl_2$ x 2 H_2O, 1.5 mM $MgSO_4$ x 7 H_2O, 1.25 mM KH_2PO_4, 20 mM NH_4 Succinate, 2 mM MES, approx. 444 mM glucose adjusted to 550 mOsm) and centrifuged at 70 x g, low brake and acceleration for 10 min. Intact protoplasts were carefully removed in the layer between the enzyme solution and F-PCN, and washed with

10 ml W5 buffer (150 mM NaCl, 125 mM $CaCl_2$, 5 mM KCl, 2 mM MES pH 5.7, adjusted to 550-580 mOsm), before centrifuged at 50 x g for 10 min and resuspended in 0.5-1 ml W5 buffer. GFP signal was visualised under the Stellaris 5 point scanning confocal microscope (Leica Microsystems, Wetzlar, Germany).

2.4.7 Chlorophyll fluorescence measurements

The photosynthetic activity of PSII was assessed by measuring chlorophyll *a* fluorescence using the HEXAGON-IMAGING-PAM system (Walz, Effeltrich, Germany). Photosynthetic parameters were calculated using IMAGING-PAM software based on the equations described by Klughammer and Schreiber (2008).

2.5 Computational Methods

2.5.1 Molecular docking analysis

Molecular docking was performed by Dr. Eslam Abdel-Salam. The 3D structure of OEP23 protein (At2g17695) was downloaded in PDB format (UPF0548) from the AlphaFold Protein Structure Database (Jumper et al., 2021; Varadi et al., 2022). With AutoDock 4.2 (Morris et al., 2009) the PDF file was prepared by removing, water molecules, repairing missing atoms, adding polar hydrogens, adding Kollman charges (Singh & Kollman, 1984), as well as checking the total charges on residues. Ligands used for the docking analysis include MGDG (CID: 5771744), DGDG (CID: 363608285), PC (CID: 52923341), and SQDG (CID: 363648189). The 3D conformation of the different ligands was obtained either as SDF files from the PubChem database (Kim et al., 2025) or generated based on the 2D conformations SDF files using OpenBabel v3.1.1 (O'Boyle et al., 2011). SDF files were then converted into PDBQT format in the AutoDock 4.2.

Docking simulations in this work were performed using AutoDock 4.2 and AutoDock Vina 1.2.0 (Eberhardt et al., 2021; Trott & Olson, 2010). Default docking parameters were chosen with a globally searching exhaustiveness of 8. The docking grid size was set to 44 × 64 × 58 Å where its centre corresponding to the centre of the receptor protein. The docking conformation with the lowest binding affinity (kcal mol-1) was used. Molecular graphing software ChimeraX-1.8 (Pettersen et al., 2004) and PyMOL (Schrodinger, 2010) were used for further visualisation and identification of contact sites.

2.5.2 Sequence alignment analysis

To investigate residue conservation, the BLAST search function in Phytozome 13 (Goodstein et al., 2011) was used to identify CLRP23 homologs across a list of nine species spanning dicots, monocots, lycophytes and bryophytes. Homologs of CLRP23 were identified in Soybean (Schmutz et al., 2010), Tomato (Hosmani et al., 2019), Black cottonwood (Tuskan et al., 2006), Common grape vine (Jaillon et al., 2007), Amborella trichopoda (Amborella Genome Project, 2013), Rice (Ouyang et al., 2006), Maize (EnsemblPlants), Selaginella moellendorffii (Banks et al., 2011) and Physcomitrella patens (Lang et al., 2018). CLC Main Workbench 20.0.4 (QIAGEN, Aarhus, Denmark) was used to conduct sequence alignment with CLRP23 in Arabidopsis.

2.5.3 Statistical analysis and data availability

In addition to the software mentioned above, Microsoft Excel, Graphpad Prism, R and R studio were also used for statistical analysis and data visualisation. Raw data files of transcriptomic, proteomic and lipidomic analysis can be accessed on DataPlant (Schwenkert et al., 2025, doi: 10.60534/qsh62-7p088, https://www.nfdi4plants.de/).

3. Results

3.1 OemiR plasmid library

3.1.1 Screening for potential OEPs implicated in cold acclimation

To obtain a broad overview of the OEP landscape, an initial screen to identify potential OEPs of interest was conducted using artificial microRNA (amiR) to generate knockdown mutants. In the past, efforts to elucidate the molecular roles of OEPs with loss of function mutants have been complicated by genetic redundancies, with presence of multiple genes coding for protein homologs serving similar molecular functions (Cutler & McCourt, 2005). This was addressed with amiR, an approach that can target and downregulate multiple protein homologs to account for potential genetic redundancies (Hauser et al., 2013; Jover-Gil et al., 2014). Thus, a library of 36 plasmids (oemiR) was designed to contain amiR constructs targeting all known OEPs to date (Appendix Table 1) and subsequently transformed into wildtype Arabidopsis plants (Col-0) for phenotypic analysis.

Chloroplast envelope proteins are increasingly being recognised for their roles in plant acclimation processes, particularly with regards to cold acclimation (John, Keller, et al., 2024; Trentmann et al., 2020). To investigate the role played by OEPs in cold acclimation, the resulting transformants were screened for cold sensitivity. Transformants in the T_1 generation were subjected to seven days of cold treatment (4ºC, 100 µmol photons $m^{-2}s^{-1}$, 16 h light), before and after which Fv/Fm levels were measured as a general parameter to assess photosynthetic performance and overall plant fitness (Fig. 6A). In total, 80 transformants were subjected to the cold screen. After seven days at 4ºC, Fv/Fm values of Col-0 and control plants declined to around 0.7. While most transformants showed similar decreases in Fv/Fm, ten *oemiR* lines were identified to have average Fv/Fm values below 0.55 ($p<0.05$, Student's *t*-test). Since transformants may contain any of the 36 *amiR* constructs from the oemiR library, PCR-based Sanger's sequencing revealed that seven of the ten mutants harbour amiR constructs targeting SFR2, CHUP1, OEP40, TOC159, OEP16-2, PDV2 and WBC7, respectively (Fig. 6B-C), indicating a potential involvement of these proteins in cold acclimation processes. Three of these identified proteins, namely SFR2, CHUP1 and OEP40, have been previously linked to low temperature sensitivity (Harsman et al., 2016; Kitashova et al., 2021; Moellering et al., 2010), providing proof of principle for this amiR-based screening method. Three mutants showed inconclusive sequencing results, presumably due to the presence of multiple insertions.

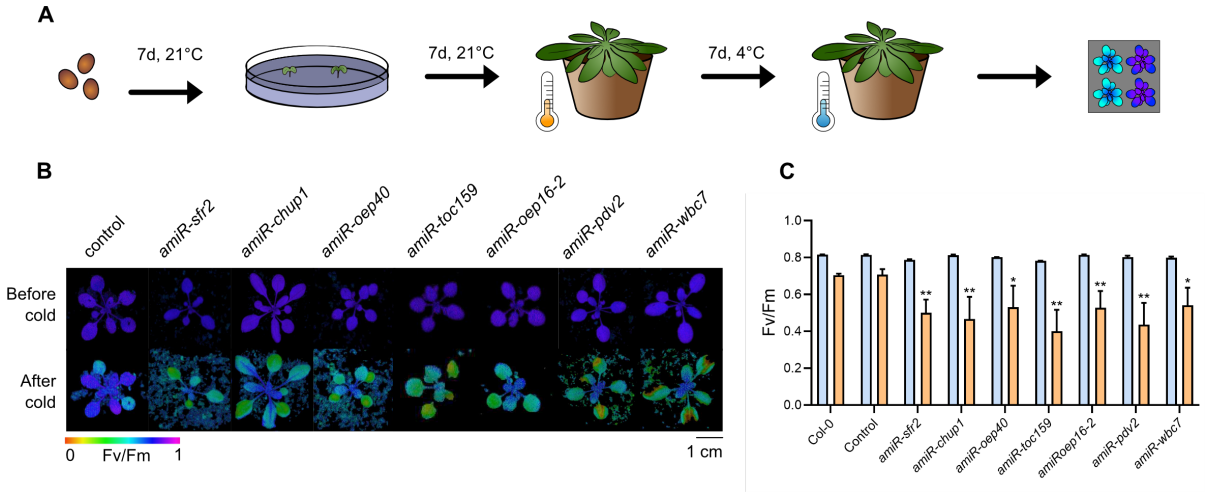

Figure 6 – OemiR library screen for potential OEPs implicated in cold acclimation. A) Schematic of the cold screen workflow. **B)** Plant images showing Fv/Fm of *oemiR* transformants exhibiting cold sensitivity. **C)** Average Fv/Fm values before and after cold treatment of cold-sensitive transformants. Four leaves were measured for each plant in the T_1 generation. Asterisks indicate statistically significant differences according to Student's t-test (*p<0.05; **p<0.01; ***p<0.001). Figure adapted from Schwenkert et al. (2023).

This specific experiment was part of a larger collaboration with the work group of Prof Dr. Hans Henning Kunz. The oemiR plasmid library was designed by Philip Day, with the plasmids cloned by Beata Szulc. The design of the OemiR plasmid library, as well as the results of the cold screen, were published in Schwenkert, Lo, et al. (2023).

3.1.2 Double mutant mini libraries: probing metabolite transport across the OE

In addition to genetic redundancies, functional redundancies may also be present, particularly among certain OEPs. In principle, the same cold screen could be applied to different knockout mutant backgrounds. However, identifying multiple independent lines for each double mutant would require extensive screening efforts, making this approach impractical. Therefore, smaller "mini" libraries were generated in a more focused approach to probe the role of metabolite transport across the OE in cold acclimation. A subset of the oemiR library targeting (potential) channels and transporters of the OE (Appendix table 1, ID 1-11) were transformed into OE knockout mutants available in our research group. This included mutants lacking OEP37 (Goetze et al., 2006), OEP40 (Harsman et al., 2016), JASSY1 (Guan et al., 2019), and CLRP23. *Clrp23* was generated by former lab members using CRISPR-Cas9 technology. A total of 53 double mutants were obtained, with 21, 11, 15, and 6 *oemiR* lines in the *oep37*, *clrp23*, *oep40* and *jassy1* knockout mutant backgrounds, respectively (Fig. 7).

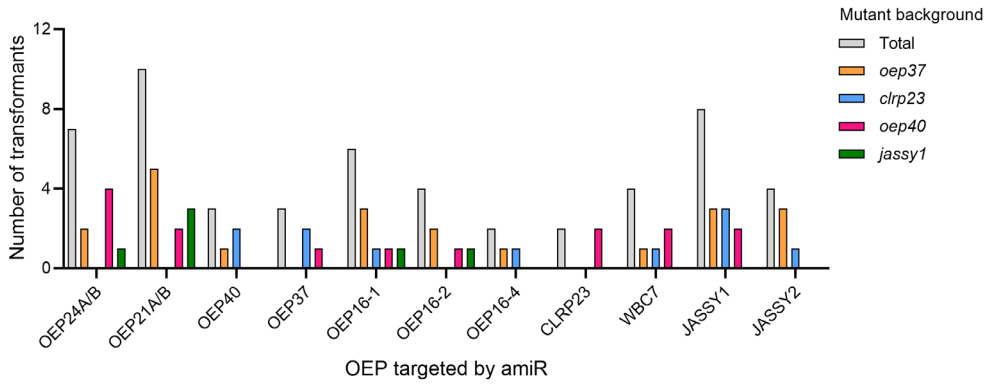

Figure 7 – Distribution of double mutants with OEP-targeting *amiRs* in knock-out mutant backgrounds. A total of 53 double mutants were obtained, with 21, 11, 15 and 6 *oemiR* lines in the *oep37*, *clrp23*, *oep40*, and *jassy1* knockout backgrounds, respectively.

The double mutants from the *oep37* mutant background were additionally screened for cold sensitivity. A representative line was selected for each available double mutant combination, from which nine biological replicates of the T_2 generation were exposed to cold conditions as described previously. Fv/Fm values were measured before and after cold treatment. *Oep37 x oemiR* mutants harbouring amiR constructs targeting OEP16-1, OEP21, OEP40, OEP16-4 and OEP24 were found to have significantly lower Fv/Fm values compared to Col-0 after cold treatment (Fig. 8), suggesting a potential for these proteins to function synergistically with OEP37 during cold acclimation.

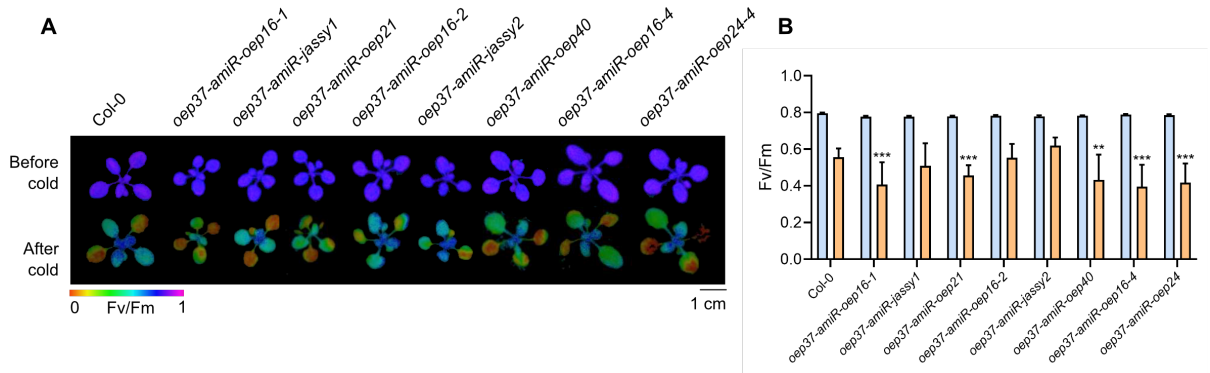

Figure 8 – *OemiR* double mutants in the *oep37* mutant background screened for cold sensitivity. A) Plant images depicting Fv/Fm values of each double mutant before and after cold treatment. **B)** Average Fv/Fm values across nine biological replicates of each double mutant before and after cold treatment. Asterisks indicate statistically significant differences according to Student's t-test (*p<0.05; **p<0.01; ***p<0.001).

Preliminary cold screens were also conducted for double mutants in the *clrp23* mutant background. Surprisingly, all *clrp23 x oemiR* mutants in the T_1 generation exhibited severe impairments in photosynthetic performance after cold treatment (Fig. 9). The consistency of this cold-sensitive phenotype across all *clrp23 x oemiR* mutants suggests that the loss of CLRP23 is responsible, prompting us to focus our efforts on elucidating the molecular function of CLRP23 and its role in cold acclimation.

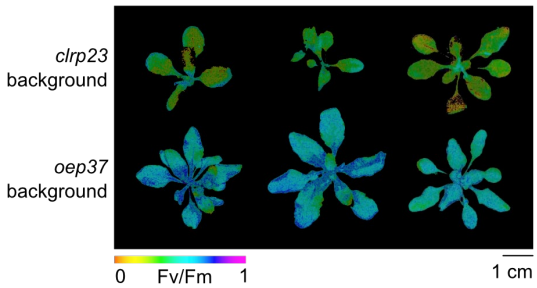

Figure 9 – Fv/Fm of *clrp23 x oemiR* and *oep37 x oemiR* double mutants after cold treatment. All *clrp23 x oemiR* mutants in the T_1 generation exhibited severe impairments in Fv/Fm.

3.2 CLRP23

3.2 1 CLRP23 is structurally similar to members of the SRPBCC fold protein superfamily

Since the original identification of CLRP23 by Goetze et al. (2015), advances in computational biology have significantly enhanced the accuracy of *in silico* protein structure prediction (Meng et al., 2025), allowing us to revisit the three-dimensional structure of CLRP23. The predicted structure of CLRP23 in the AlphaFold Protein Structure Database (AlphaFold DB; Jumper et al., 2021; Varadi et al., 2022) shows a presence of both α-helix and β-sheets . The β-sheets form an incomplete β-barrel, a structure that differs from the typical β-barrel or α-helical structures found in chloroplast envelope protein transporters (Fig. 10A). This was supplemented by a second search using Phyre2.2, a template-based modelling software. 139 residues with 68% coverage were modelled with 86.4% confidence, revealing a structure highly similar to that in the AlphaFold DB (Fig. 10B). Intriguingly, all three top ranking protein templates from this analysis contain a STAR-related lipid transfer (START) domain (Fig. 10C), suggesting a high degree of similarity between CLRP23 and members of the START/RHO_alpha_C/PITP /Bet_v1/CoxG/CalC (SRPBCC) superfamily (Radauer et al., 2008; Soccio & Breslow, 2003).

A

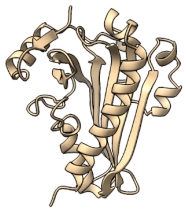

B

C

Rank	Template ID	Coverage (%)	Confidence	Sequence identity (%)
1	c2d4rA	73	86.4	12
2	c2d4rD	73	86.4	12
3	c2pcsA	72	82.1	8

Figure 10 – *In silico* structural predictions of CLRP23 A) from the Alphafold Protein Structure Database, and **B)** using the template-based modelling software Phyre2.2. **C)** The top three ranking templates from Phyre2.2 analysis.

3.2.2 CLRP23 is strongly attached to the membrane

To characterise the attachment of CLRP23 to the chloroplast envelope membrane, Arabidopsis leaf tissues were treated with either acidic or chaotropic agents, after which the insoluble (membrane) and soluble fractions were collected via centrifugation and separated by SDS-PAGE. Subsequent immunoblots with antisera against CLRP23 of membrane and soluble fractions revealed a strong attachment of CLRP23 to the membrane, where CLRP23 remained in the membrane fraction in the presence of HCl, NaCl or Urea (Fig. 11). Antisera against the photosystem II extrinsic protein O (PsbO) and TIC110 were used as markers, respectively, for peripheral and integral membrane association. As expected, lithium dodecyl sulfate (LDS) treatment released all proteins from the membrane fraction and served as a positive control.

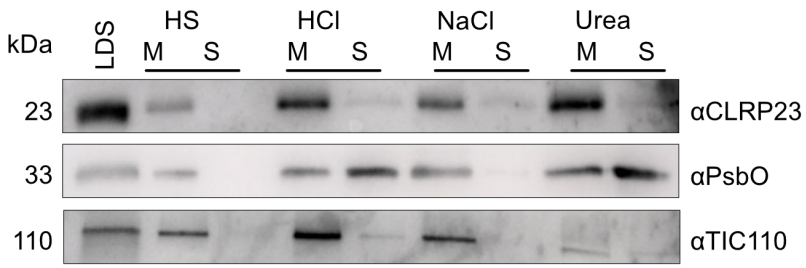

Figure 11 – Membrane association of CLRP23. Arabidopsis leaves (approx. 500 mg FW) were ground with liquid nitrogen and treated with LDS, buffer (HS), HCl, NaCl or Urea and subsequently separated into membrane (M) and soluble (S) fractions. Samples were separated on SDS gels, transferred onto PVDF and immunolabeled with α-CLRP23, α-PsbO, and α-Tic110.

3.2.3 CLRP23 interaction partners

While previous electrophysiological measurements of CLRP23 have suggested the presence of cation-selective activities *in vitro* (Goetze et al., 2015), it remains unclear how CLRP23 is able to form a channel with its incomplete β-barrel structure. To determine whether CLRP23 complexes with itself or other proteins, a BN-PAGE was performed, followed by SDS-PAGE for separation in the second dimension. Subsequent immunoblotting with antisera against CLRP23 in Arabidopsis revealed the presence of CLRP23 in Col-0 chloroplasts at three different sizes at 70, 150 and 250 kDa, respectively, suggesting a potential for complex formation (Fig. 12A). Chloroplasts from *clrp23* knockout mutants were used as a negative control, where no CLRP23 was observed (Fig. 12B).

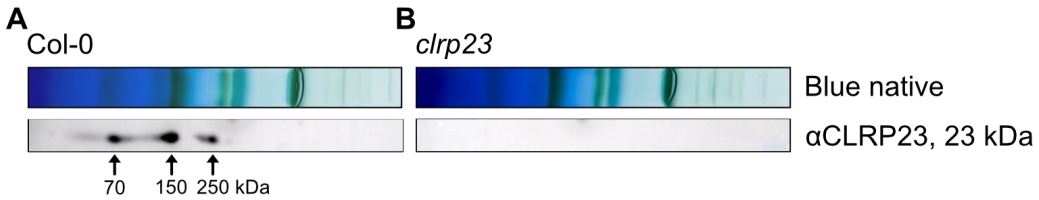

Figure 12 – Potential interaction partners of CLRP23 A-B) Blue native PAGE and second dimension SDS-PAGE of **(A)** Col-0 and **(B)** *clrp23* chloroplasts. Second dimension SDS-PAGE was transferred to PVDF and immunoblotted with antisera against CLRP23.

Next, green fluorescent protein (GFP)-trap was used to search for potential interaction partners of CLRP23 (Fig. 13A). The C-terminus of CLRP23 was tagged with GFP (CLRP23-GFP) and transiently expressed in Tobacco leaves under the 35S promoter. GFP-tagged protein complexes in plants expressing CLRP23-GFP were subsequently isolated with affinity chromatography and analysed with mass spectrometry, with plants expressing GFP-tagged OEP37 (OEP37-GFP) and wildtype Tobacco serving as negative controls. The identified proteins were then blasted against the Arabidopsis proteome for better annotation. To show statistically enriched proteins in CLRP23-GFP, a Student's *t*-test was performed comparing CLRP23-GFP with the wildtype control, and proteins were plotted according to the $\log_2$ fold change and negative $\log_{10}$ p-value (Fig. 13B). 17 unique Arabidopsis homologs were identified to be exclusively and significantly enriched in the CLRP23-GFP pull-down, each with a $\log_2$ fold change greater than two (Fig. 14C). Among these there were several heat shock proteins, which may indicate that overexpression of CLRP23-GFP leads to protein unfolding or

aggregation. Of the eight enriched proteins predicted to localise to the plastid, several are thylakoid associated, making direct interaction with CLRP23 unlikely *in vivo*.

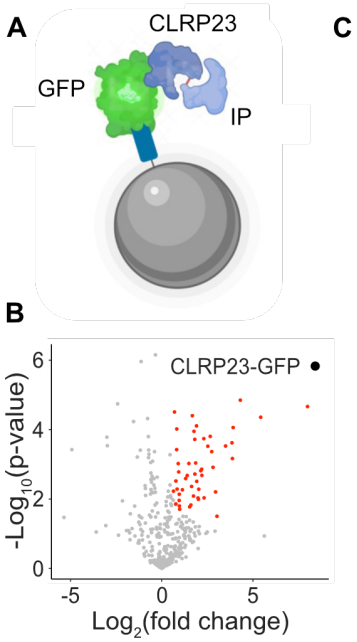

C

Gene	Gene name/function	Localisation	TMD
AT4G05050	Ubiquitin 11	Nucleus	-
AT5G36230	ARM repeat superfamily protein	Mitochondrion	-
AT4G35090	catalase 2	Plastid	-
AT4G03280	photosynthetic electron transfer C	Plastid	1
AT1G55670	photosystem I subunit G	Plastid	2
AT3G12580	heat shock protein 70	Unknown	-
ATCG00800	structural constituent of ribosome	Plastid	-
AT3G62290	ADP-ribosylation factor A1E	Mitochondrion	-
ATCG00670	plastid-encoded CLP P	Plastid	2
AT3G05560	Ribosomal L22e protein family	Cytosol	-
AT5G55220	trigger factor type chaperone family protein	Plastid	-
AT5G02500	heat shock cognate protein 70-1	Unknown	-
AT1G78300	general regulatory factor 2	Unknown	-
AT2G45290	Transketolase	Plastid	2
AT1G02560	nuclear encoded CLP protease 5	Plastid	2
AT5G56030	heat shock protein 81-2	Nucleus	2
AT1G75780	tubulin beta-1 chain	Unknown	2

Figure 13 – Identification of interaction partners with GFP-trap. A) Schematic showing the pulldown of GFP-tagged protein complexes with affinity chromatography before being analysed with mass spectrometry. **B)** Volcano plot showing the $\log_2$ fold change and $-\log_{10}$ p value from a Student's *t*-test comparing proteins quantified in the CLRP23-GFP pull-down vs wildtype control. Proteins significantly enriched in CLRP23-GFP are highlighted in red. **C)** Accession numbers, description, localisation and predicted transmembrane domains (TMD) of seventeen unique Arabidopsis protein homologs that were found to be significantly enriched in CLRP23-GFP, with a $\log_2$ fold change of greater than two.

To validate the results obtained from GFP-trap co-immunoprecipitation, proximity labelling with TurboID was used. The C-terminus of CLRP23 was tagged instead with TurboID (CLRP23-TurboID), an engineered biotin ligase that enables the *in vivo* biotinylation of proteins coming into close proximity with CLRP23 (Fig. 14A-B). 24 hours after transiently expressing the construct in Tobacco leaves under the 35S promoter, the tobacco leaves were infiltrated with 2 mM biotin for biotinylation. Biotinylated proteins were purified with affinity chromatography and analysed with mass spectrometry. Unfortunately, no biotinylated proteins were significantly enriched in plants expressing CLRP23-TurboID (Fig. 14C). It was therefore assumed that proteins enriched in CLRP23-GFP were false positives, perhaps due to complex formation during the cell lysis and protein solubilisation process. C-Terminal tagging of

CLRP23 with GFP could also disturb the localisation of CLRP23, resulting in complex formation that would otherwise not occur in wildtype.

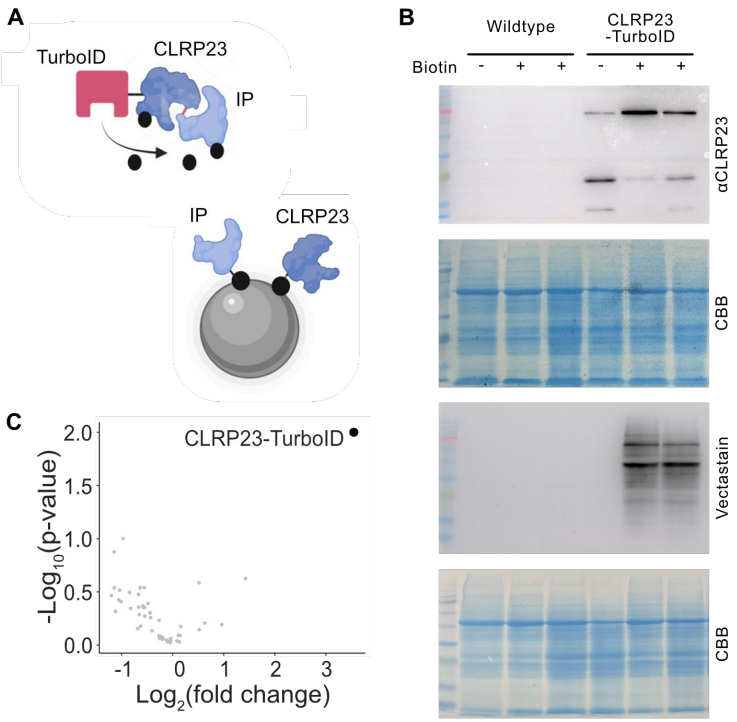

Figure 14 – Proximity labelling with TurboID. A) Schematic showing the biotinylation of proteins in close proximity with CLRP23-TurboID. Biotinylated proteins were subsequently isolated via affinity chromatography. **B)** Immunoblots showing the biotinylation of proteins with CLRP23-TurboID. Total protein of tobacco leaves transformed with CLRP23-TurboID before and after biotin infiltration were extracted and separated according to size with SDS-PAGE. Subsequent immunoblot analysis using antisera against CLRP23 shows the presence of CLRP23 at ~70 kDa, which is the expected size for the CLRP23-TurboID construct. Simultaneous analysis with vectastain, which binds to biotinylated proteins, shows the biotinylation of proteins in CLRP23-GFP after infiltration with tobacco. Total protein from wildtype tobacco under the same conditions were used as a negative control, while coomassie brilliant blue (CBB) was used as a loading control. **C)** Volcano plot showing the $\log_2$ fold change and $-\log_{10}$ p value from a Student's *t*-test comparing proteins quantified in the CLRP23-TurboID pull-down vs wildtype control. No proteins were found to be significantly enriched in CLRP23-TurboID.

Unfortunately, efforts to generate overexpression mutant lines in Arabidopsis for CLRP23-GFP (*35s:clrp23-gfp*) and CLRP23-TurboID (*35s:clrp23-turboID*) were unsuccessful. Total protein extracts from 26 plants in the T_2 generation for each construct were separated by SDS-PAGE and analysed by immunoblotting with antisera against CLRP23. For *35s:clrp23-turboID*, only one line exhibited a signal at 72 kDa, corresponding to the expected molecular weight of the

CLRP23-TurboID fusion protein (Fig. 15A). Expression levels, however, were insufficient for downstream experimentation. For *35s:clrp23-gfp*, despite several lines displaying strong signals at 23 kDa, consistent with the size of CLRP23, no bands were visualised at 50 kDa, the expected molecular weight of the CLRP23-GFP fusion protein (Fig. 15B). It is plausible that tagging the C-terminus of CLRP23 with GFP or TurboID disrupts its structural integrity and functionality, leading to degradation of the fusion protein. Therefore, although CLRP23 can be detected in larger complexes in BN-PAGE, whether CLRP23 complexes with itself or with other proteins and the identity of such interacting partners remain inconclusive.

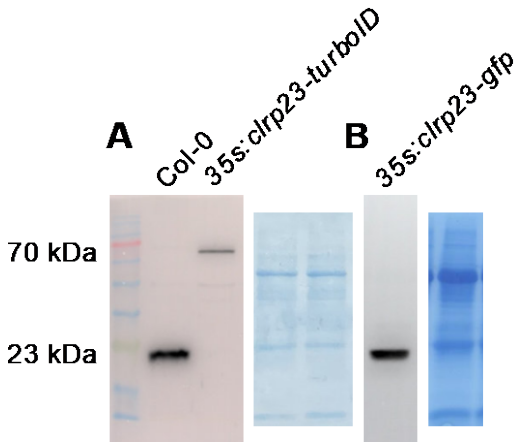

Figure 15 – Transformation of CLRP23-GFP and CLRP23-TurboID in Arabidopsis. Total protein from a representative lines of **A)** *35s:clrp23-turboID* and **B)** *35s:clrp23-gfp* were separated by SDS-PAGE and subsequently analysed with immunoblotting using antisera against CLRP23. CBB was used as a loading control.

3.2.4 CLRP23 localisation and topology

Since the original designation of CLRP23 to the chloroplast OE remains to be experimentally confirmed, a subfractionation analysis was performed. Chloroplasts from Arabidopsis and Pea were isolated and fractionated into envelopes (Env), thylakoids (Thy) and Stroma (Str). High-purity envelope separations can only be obtained in Pea, whereas only mixed envelopes can be isolated in Arabidopsis (Bölter et al., 2020). To confirm OE/IE localisation, immunoblots were also performed on pea chloroplast IE and OE fractions provided by PD Dr. Bettina Bölter. The resulting fractions for Env, Thy and Str in Arabidopsis (performed by Denise Winkler), as well as the IE and OE in Pea, were subsequently separated by SDS-PAGE and analysed with immunoblotting using antisera against CLRP23 in Arabidopsis and Pea, respectively (Fig. 16).

Antisera against FBPase, PsbO, and TIC110 were used as markers for Str, Thy and Env in Arabidopsis, while TIC40 and OEP37 were used as markers for IE and OE in Pea. AtCLRP23 was detected in the Env, confirming its localisation to the chloroplast envelope (Fig. 16A). However, psCLRP23 was only detected in the IE fraction (Fig. 16B), a finding that contrasts with the prior assumption of CLRP23 as an OE protein (Goetze et al., 2015).

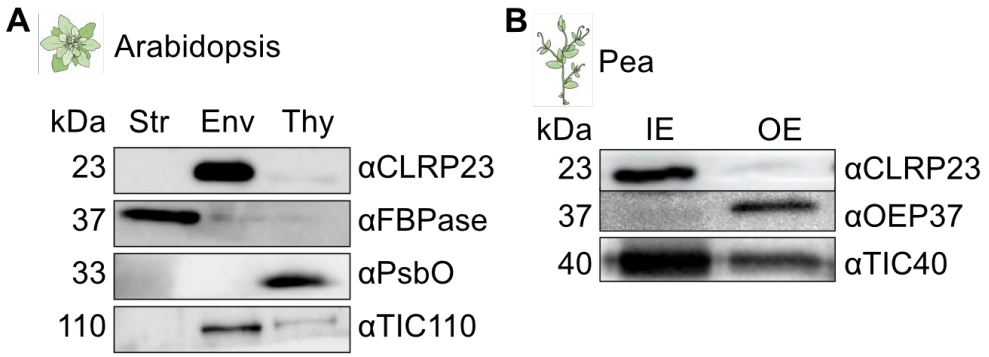

Figure 16 – Localisation of CLRP23 to the chloroplast IE. Subfractionation of A) Arabidopsis chloroplasts into stroma (Str), envelope (Env) and thylakoid (Thy), and **B)** Pea chloroplast envelopes into inner (IE) and outer (OE) envelope factions. Fractions were separated by SDS-PAGE, transferred to PVDF and analysed by immunoblotting with antisera against CLRP23 in Arabidopsis and Pea. Antisera against fructose-1,6-bisphotphatase (FBPase), PsbO, TIC110, OEP37 and TIC40 were used as markers for Str, Env, Thy, IE and OE, respectively. CLRP23 was detected in the Arabidopsis Env and Pea IE fractions, thereby localising it to the chloroplast IE. Subfractionation analysis in Arabidopsis was performed by Denise Winkler. Pea chloroplast IE and OE fractions were provided by PD Dr. Bettina Bölter.

In addition to immunoblot analysis, proteomics was also performed on the pea envelope fractions. Proteins from five biological replicates of IE and six of OE were analysed with mass spectrometry and quantified with label-free quantification (LFQ). To enable a more comprehensive annotation of their known functions and localisations, identified proteins were blasted against the Arabidopsis proteome. A total of 858 proteins, with 767 unique Arabidopsis homologs were identified. After manual annotation of each protein with known descriptors, the purity of the IE and OE fractions was assessed. Mean LFQ intensities of proteins in the IE fractions were plotted against their mean LFQ intensities in the OE (Fig. 17A). Proteins known to reside in the IE exhibited systematically higher LFQ intensities in the IE fraction and vice versa, suggesting a clear separation between the envelope fractions. Subsequently, a Student's *t*-test was performed to determine differentially enriched proteins in either fraction, after which

each protein was plotted according log_2 fold change and the $-log_{10}$ p-value (Fig. 17B). Excluding proteins with previously known localisations to other subcellular compartments, proteomic analysis of the chloroplast IE and OE membrane fractions revealed a list of 473 nonredundant envelope proteins, with 427 showing significant enrichment in either membrane fraction. IE proteins generally showed a positive log_2 fold change when comparing IE vs. OE, while OE proteins showed a negative log_2 fold change. With a log_2 fold change of 2.04, CLRP23 was found to be significantly enriched in the IE fraction, further confirming its localisation to the chloroplast IE.

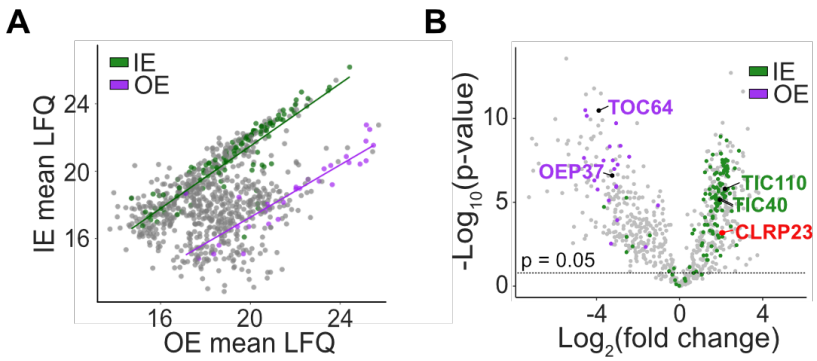

Figure 17 – Proteomic analysis of pea chloroplast envelopes. A) Scatter plot according to mean label-free quantification (LFQ) intensities of proteins quantified in IE vs. OE fractions. IE proteins exhibited systematically higher LFQ intensities in the IE fraction while OE exhibited higher LFQ intensities in the OE fraction, suggesting a clear separation between the fractions. **B)** Volcano plot showing the log_2 fold change and $-log_{10}$ p value from a Student's *t*-test comparing proteins quantified in the IE vs. OE. CLRP23 is found to be enriched in the IE fraction.

With the help of PD Dr. Bettina Bölter, we were able to investigate the localisation and topology of CLRP23 in more detail. In a "dual protease" approach, whole Arabidopsis chloroplasts were digested with increasing concentrations of either Trypsin or Thermolysin (Fig. 18A). Under the appropriate reaction conditions, Thermolysin digests OE proteins facing the cytosol. While Thermolysin leaves the OE intact, Trypsin partially disrupts the OE and also digests proteins residing in the IMS (Froehlich, 2011). The degradation of CLRP23 by Trypsin but not Thermolysin suggests that CLRP23 is anchored to the chloroplast IE with a significant portion of the protein residing in the IMS (Fig. 18B).

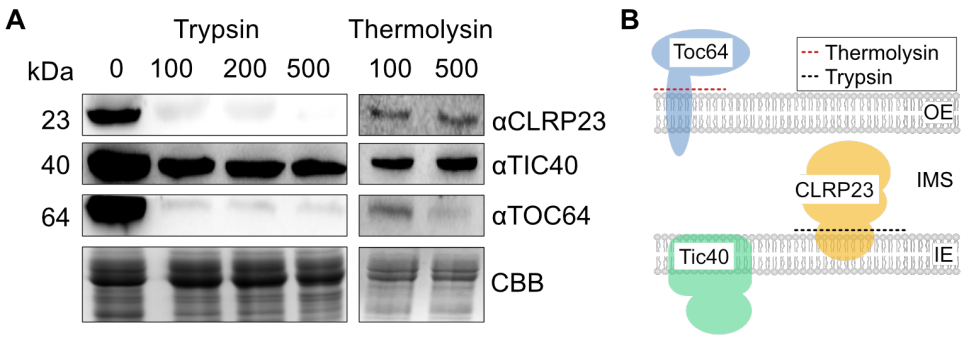

Figure 18 – Treatment of intact Arabidopsis chloroplasts with Trypsin or Thermolysin, performed by PD Dr. Bettina Bölter. A) Intact chloroplasts treated with increasing concentrations of either Trypsin or Thermolysin are separated by SDS-PAGE, transferred to PVDF and analysed by immunoblotting with antisera against CLRP23. Antisera against TIC40 and TOC64 were used as markers for IE and OE proteins, while Coomassie brilliant blue (CBB) was used as a loading control. CLRP23 is digested by Trypsin, but not Thermolysin. **B)** Schematic showing the digestion of IE and OE proteins by Trypsin and Thermolysin. CLRP23 is concluded to reside in the IE facing the IMS.

3.2.5 clrp23 knockout mutants are cold sensitive

As mentioned previously, all *oemiR* double mutants in the *clrp23* knockout background suffered from impaired photosynthetic performance when plants were exposed to cold conditions, leading to the hypothesis that the loss of CLRP23 is responsible. To investigate this further, the CRISPR-Cas9-generated *clrp23* knockout mutants used in the double mutant library were analysed. Complementation lines were generated by expressing *CLRP23* cDNA in the knockout mutants under the 35S promoter to confirm that phenotypic differences resulted solely from the *CLRP23* knockout. Knockout lines were verified through Sanger sequencing (Fig. 19A-C). For downstream analysis, a representative line from both the knockout and complementation mutants was selected and further confirmed with immunoblotting (Fig. 19D). These lines were designated *clrp23* and *clrp23 com*, respectively.

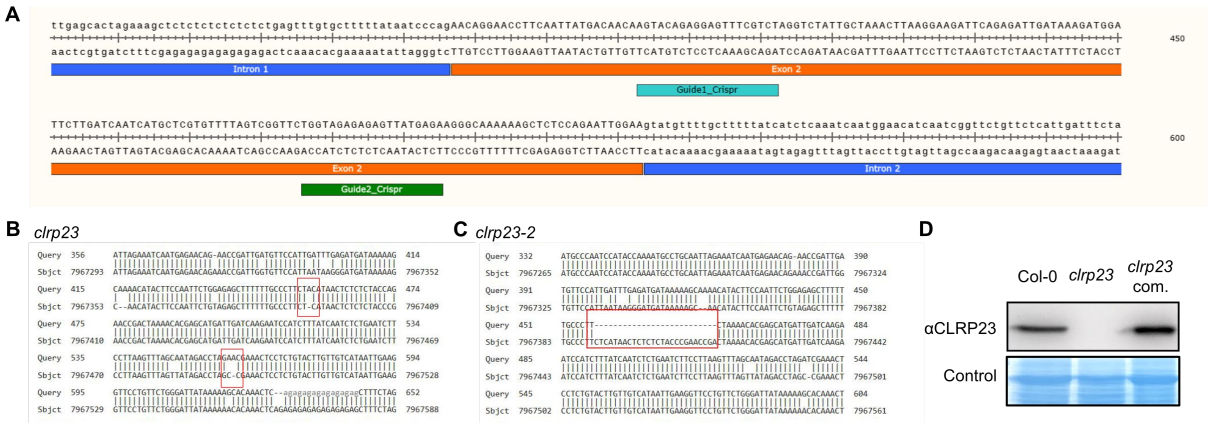

Figure 19 – *clrp23* knock-out mutants generated with CRISPR/Cas9 technology A) gDNA sequence of *CLRP23*. The two specific guide RNAs designed for mutant knock-out are marked in blue and green. **B-C)** Verification of knockout lines **(B)** *clrp23* and **(C)** *clrp23-2* with Sanger sequencing. **D)** Immunoblot showing successful knockout and complementation of CLRP23 in *clrp23* and *clrp23 com*. Immunoblots were performed using antisera against CLRP23, and CBB was used as a loading control.

Col-0, *clrp23* and *clrp23 com* plants were subsequently grown on soil under standard growth conditions (SGC) for 20 days before being transferred to low temperature conditions (4ºC, 250 µmol photons $m^{-2}s^{-1}$, 16h light). Chl α fluorescence parameters were measured before and during cold treatment as well as after the plants were returned to SGC for 7 days to monitor their photosynthetic performance. After several days of cold treatment, Col-0 and *clrp23 com* started to accumulate anthocyanins, which was particularly visible in the centre of the plant rosette. This effect was not observed in *clrp23* (Fig. 20A). A closer look at the Chl α fluorescence parameters also revealed that while Col-0 plants showed a slight decrease in Fv/Fm values after one day of cold treatment, the difference observed in *clrp23* was significantly more severe. Significant decreases in PSII quantum yield (φ(PSII)), nonphotochemical quenching (φ(NPQ)), as well as a significant increase in nonregulated energy dissipation (φ(NO)) were also observed in *clrp23* after just one day of cold treatment, effects that are indicative of photosynthetic dysregulation and oxidative stress (Fig. 20C). After five days of cold treatment, Fv/Fm values plateau at around 0.6 in Col-0, but continue to decrease to around 0.4 in *clrp23* (Fig. 20B). The cold sensitive phenotype in *clrp23* was not observed in *clrp23 com*, where no statistical differences were found in the Chl α fluorescence parameters compared to the wildtype-control. The same experiment was repeated with the second CLRP23 knockout line (*clrp23-2*) and its respective complementation (*clrp23-2 com*), which exhibited the same phenotype (Fig. 20D).

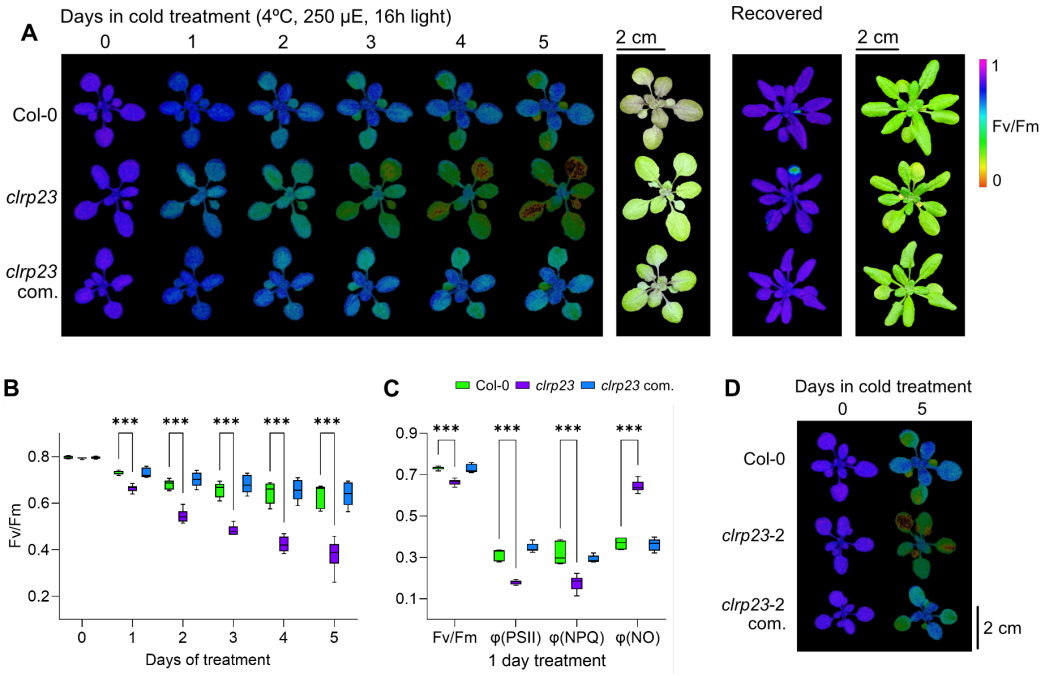

Figure 20 – Cold sensitive phenotype of *clrp23*. 20-day old plants grown under standard growth conditions (SGC) were shifted to low temperature conditions (4ºC, 250 µmol photons $m^{-2}s^{-1}$, 16 h light) for six days before recovered to SGC for seven days. A) Chlorophyll α fluorescence imaging showing Fv/Fm of Col-0, *clrp23* and *clrp23 com* during the first five days of cold treatment and one week after recovery. **B)** Fv/Fm values of Col-0, *clrp23* and *clrp23 com* during the first five days of cold treatment. **C)** Fv/Fm, PSII quantum yield (φ(PSII)), nonphotochemical quenching (φ(NPQ)), and nonregulated energy dissipation (φ(NO)) of Col-0, *clrp23* and *clrp23 com* after one day of cold treatment. Asterisks indicate statistically significant differences according to a Student's *t*-test (*p<0.05; **p<0.01; ***p<0.001). **D)** Chlorophyll α fluorescence imaging showing Fv/Fm of Col-0, *clrp23-2* and *clrp23-2 com* before and after five days of cold treatment.

Intriguingly, despite the cold sensitive phenotype in *clrp23*, no noticeable differences in freezing tolerance were observed. A total of 110 plants each for Col-0 and *clrp23* were subjected to freezing treatment in two separate experiments to ensure reproducibility. Freezing treatment result in survival rates of 69% in Col-0 and 74% in *clrp23*. A stacked bar graph of (A) the percentage of plants that survived and died, as well as (B) a representative diversity of plants after recovery from freezing treatment is visualised in Figure 21. Freezing tolerance experiments were performed by Katharina Ebel from AG Neuhaus, at the University of Kaiserslautern-Landau (RPTU).

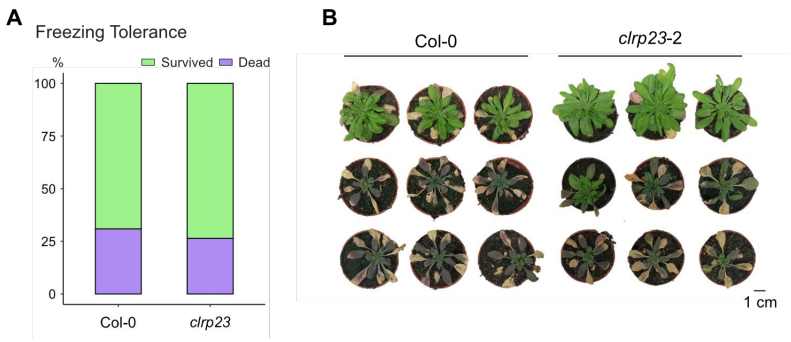

Figure 21 – Freezing tolerance of Col-0 and *clrp23*, performed by Katharina Ebel, AG Neuhaus. A) Survival rates of Col-0 and *clrp23* after freezing treatment. **B)** Representative diversity of Col-0 and *clrp23* plants after recovery from freezing treatment.

During low temperature stress, enzyme activity slows while the light-harvesting system is not impacted, a discrepancy that may lead to the accumulation of reactive oxygen (ROS) and increase the likelihood of light-induced damage (Miura & Furumoto, 2013). To separate the effects of low temperature and light stress on *clrp23* during cold treatment, plants were also subjected to cold/low light (4ºC, 80 µmol photons $m^{-2}s^{-1}$, 16 h light) and room temperature/ high light (22ºC day/18ºC night, 500 µmol photons $m^{-2}s^{-1}$, 16 h light) conditions. *Clrp23* exhibited significantly lower Fv/Fm values compared to Col-0 in both treatment conditions (Fig. 22A-B). However, Fv/Fm levels in *clrp23* returned to wild-type levels after three days of room temperature/high light treatment, whereas Fv/Fm levels continued to decline to around 0.6 after five days under cold/low light. After three days, *clrp23* mutants exhibited significantly lower Fv/Fm and φ(PSII) under cold/low light, and under both treatments exhibited significantly lower φ(NPQ) and higher φ(NO) compared to Col-0 (Fig. 22C-D). It is therefore likely that the cold-sensitive phenotype observed in *clrp23* is largely attributed to low temperature but can be further aggravated by high light stress.

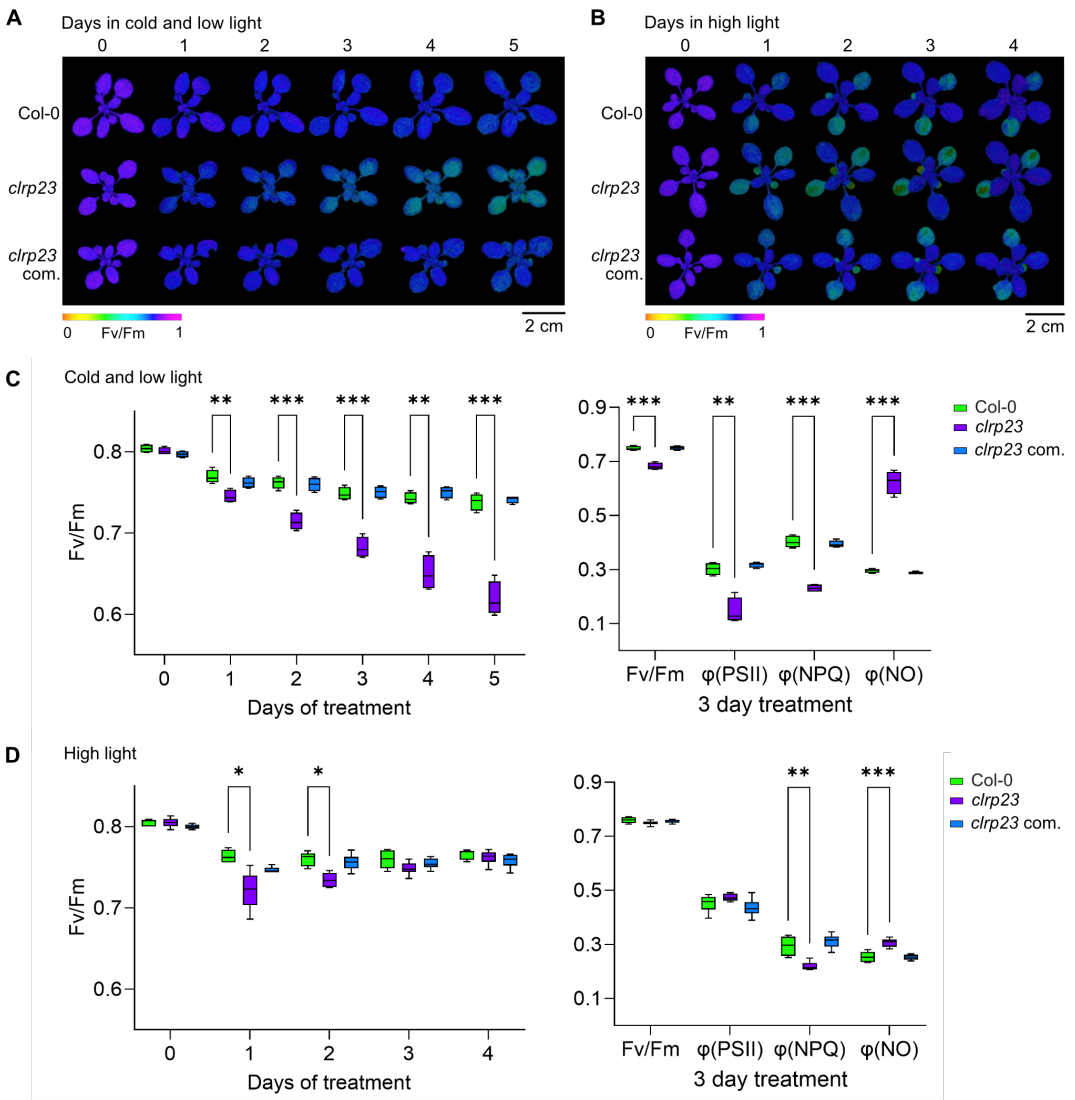

Figure 22 – Col-0, *clrp23* and *clrp23 com* under cold/low light and room temperature/high light conditions. 20-day old plants were shifted to **(A, C)** cold/low light (4ºC, 80 µmol photons $m^{-2}s^{-1}$, 16 h light) and room **(B, D)** temperature/high light (22ºC day/18ºC night, 500 µmol photons $m^{-2}s^{-1}$, 16h light) conditions. **(A-B)** Chlorophyll α fluorescence imaging during **(A)** cold low light and **(B)** room temperature high light treatment. **(C-D)** Fv/Fm values at 0-5 days, as well as Fv/Fm, PSII quantum yield (φ(PSII)), non-photochemical quenching (φ(NPQ)) and nonregulated energy dissipation (φ(NO)) after three days of **(C)** cold low light **(D)** and room temperature high light treatment. Asterisks indicate statistically significant differences according to Student's t-test (*p<0.05; **p<0.01; ***p<0.001).

3.2.6 clrp23 transcriptomic and proteomic analysis under cold stress

To elucidate the cellular pathways responsible for the cold-sensitive phenotype observed in *clrp23* mutants, transcriptomic and proteomic analyses were performed to compare cold-treated plants (4ºC, 250 µmol photons $m^{-2}s^{-1}$, 16h light, 4 days) with plants grown under SGC. A Student's *t*-test was performed for both Col-0 and *clrp23* to identify differentially regulated

genes (DEGs) and proteins (DEPs) after cold treatment vs SGC, the results of which are depicted in volcano plots (Fig. 23).

Next, a list of genes found to be differentially expressed after at least 48 hours of cold exposure (CRGs) was obtained from a comprehensive meta-analysis of multiple studies (Hannah et al., 2005). To evaluate the effect of cold treatment on the transcriptome and proteome of Col-0 and *clrp23*, we compared the CRGs with the DEGs and DEPs identified in our analyses. Overlapping CRGs and DEGs/DEPs are highlighted in volcano plots, where CRGs that are upregulated or downregulated by cold are marked in green or brown, respectively (Fig. 23A, C, E, G). Similarities and differences between CRGs and DEGs/DEPs in response to cold treatment are depicted in Venn diagrams. A similar analysis was also performed with a list of high light regulated genes (HRGs) obtained from a meta-analysis of high light exposure (48-120 hours; Bobrovskikh et al., 2022). Overlapping HRGs that are up- or downregulated by highlight are marked in yellow or blue, respectively (Fig. 23B, D, F, H).

Among the overlapping CRGs, 84% in the transcriptome and 91% in the proteome displayed a similar response in Col-0 when comparing cold-treated plants with SGC (Fig. 23A, C). Accordingly, 77% and 84% of overlapping CRGs the transcriptome and proteome of *clrp23* displayed a similar response to cold treatment (Fig. 23E, G). In contrast, a much weaker alignment was observed among the overlapping HRGs. Only 38% and 34% of the overlapping HRGs displayed a similar response in the transcriptome and proteome of Col-0 in response to cold treatment (Fig. 23B, D). In *clrp23*, the percentages are 38% and 14%, respectively (Fig. 23F, H). This suggests that transcriptomic and proteomic responses in *clrp23* to cold treatment are not only primarily driven by low temperature stress, but they are also predominantly in line with previously published transcriptomic research on long-term cold exposure in Arabidopsis. It can therefore be assumed that the cold-sensitive phenotype observed in *clrp23* is unlikely to be a result of disruptions in cold stress signalling.

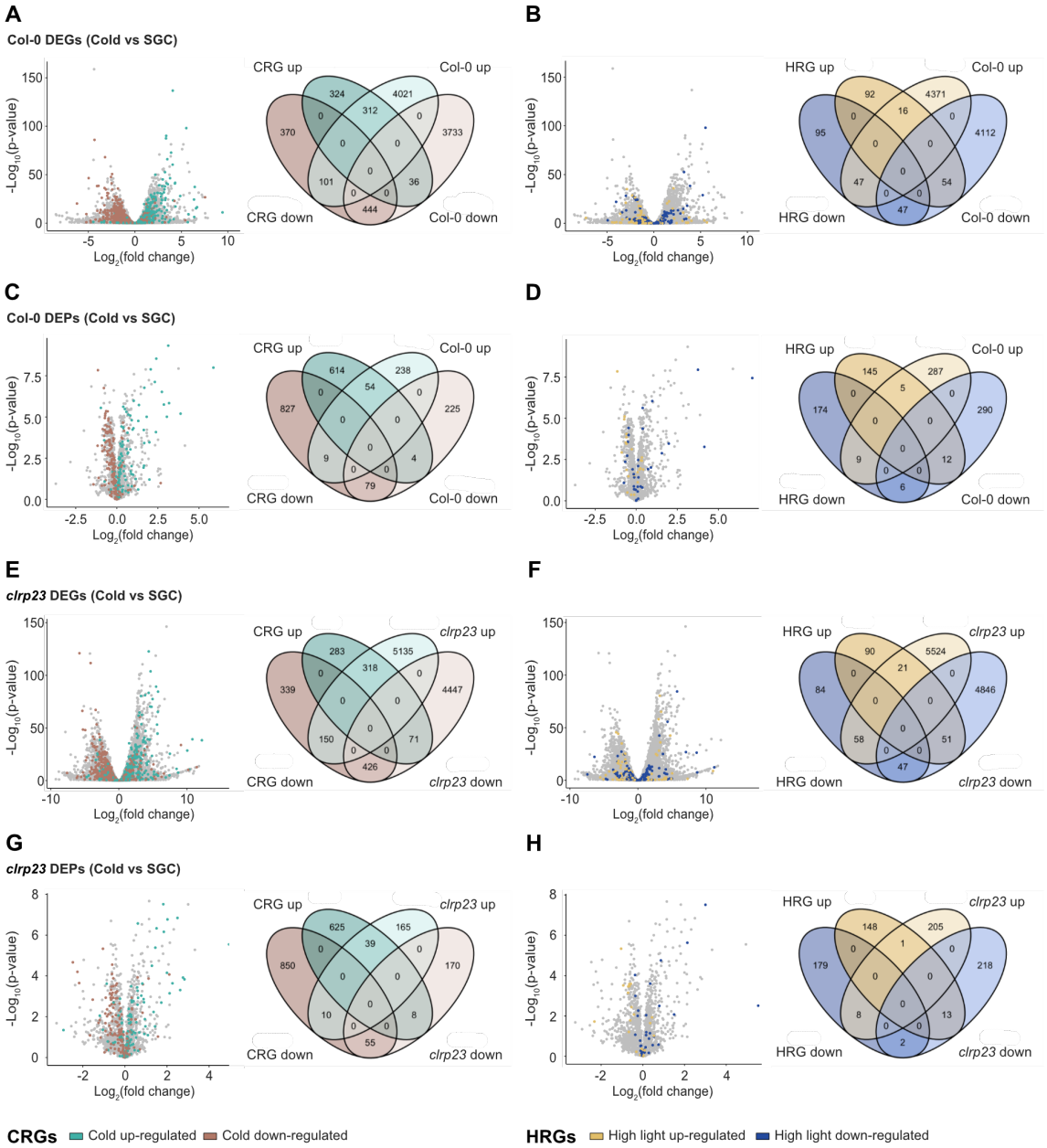

Figure 23 – Transcriptomic (A, B, E, F) and proteomic (C, D, G, H) analysis of Col-0 and *clrp23* after cold treatment vs. standard growth conditions (SGC). Differentially expressed genes (DEGs) and proteins (DEPs) under cold treatment vs. SGC were identified with DESeq2 (Love et al., 2014) and Student's *t*-test, respectively. Results were plotted in volcano plots according to the $\log_2$ fold change and negative $\log_{10}$ p value for both **(A-D)** Col-0 and **(E-H)** *clrp23*. Genes and proteins found in published literature to be up- or downregulated by >48 hours cold treatment (CRGs; Hannah et al., 2005) are respectively marked in green and brown **(A, C, E, G)**. Genes and proteins found in published literature to be up- or downregulated by 48-120 hours high light treatment (HRGs; Bobrovskikh et al., 2022) are respectively marked in yellow and blue **(B, D, F, H)**. Overlap between CRGs and the DEGs and DEPs identified in our analyses is depicted in Venn diagrams.

To investigate further, the proteome of *clrp23* was also compared with Col-0 under SGC and after cold treatment. While the proteome of *clrp23* did not show significant alterations compared to Col-0 under SGC (Fig. 24A), a number of DEPs were identified after four days of cold treatment (Fig. 24B). In particular, gene ontology (GO) term enrichment analysis of biological process revealed that proteins involved in flavonoid biosynthesis are significantly downregulated. These proteins include chalcone synthase (CHS), chalcone isomerase (CHI3), and flavanone 3-hydroxylase (F3H), in addition to proteins acting in the later stages of anthocyanin biosynthesis, namely dihydroflavonol 4-reductase (DFR), leucoanthocyanidin dioxygenase (LDOX) and anthocyanin 3-O-glucoside xylosyltransferase (A32gXYLT). Accordingly, anthocyanins were also extracted and photometrically measured, revealing a lack of anthocyanin accumulation in *clrp23* after cold treatment (Fig. 24C).

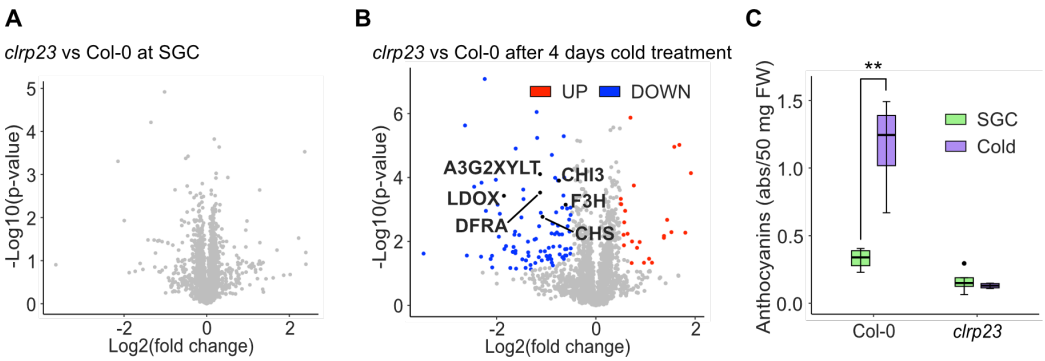

Figure 24 – Proteomic analysis of *clrp23* vs. Col-0 plants under A) SGC and **B)** after four days of cold treatment. Gene ontology (GO) term enrichment analysis of biological process revealed a significant downregulation of proteins involved in flavonoid biosynthesis. **C)** Extraction and photometric measurements of anthocyanins in *clrp23* show a lack of anthocyanin accumulation after cold treatment compared to Col-0. For proteomic analysis, statistical significance was determined with a p-value of <0.05, adjusted to a false discovery rate (FDR) of 0.05 and a $\log_2$ fold-change cut-off of ± 0.5. Proteins found to be significantly up- and downregulated are highlighted in red and blue, respectively. For anthocyanin quantification, asterisks indicate statistically significant differences according to Student's t-test (*p<0.05; **p<0.01; ***p<0.001).

3.2.7 clrp23 lipid remodelling under cold stress

Proteins belonging to the SRPBCC protein superfamily are known for their ability to interact with hydrophobic ligands (Radauer et al., 2008). Structural similarities between CLRP23 and proteins from the SRPBCC superfamily, combined with the importance of lipid remodelling in

cold acclimation (Barrero-Sicilia et al., 2017; Degenkolbe et al., 2012), prompted the investigation of lipid composition in *clrp23*. An LC-MS based method was used to quantify the lipidomes of *clrp23* and Col-0 under SGC as well as after four days of cold treatment. Z-score based k-means clustering analysis was used to organise each lipid into one of five clusters based on their response in each genotype/condition (Fig. 25).

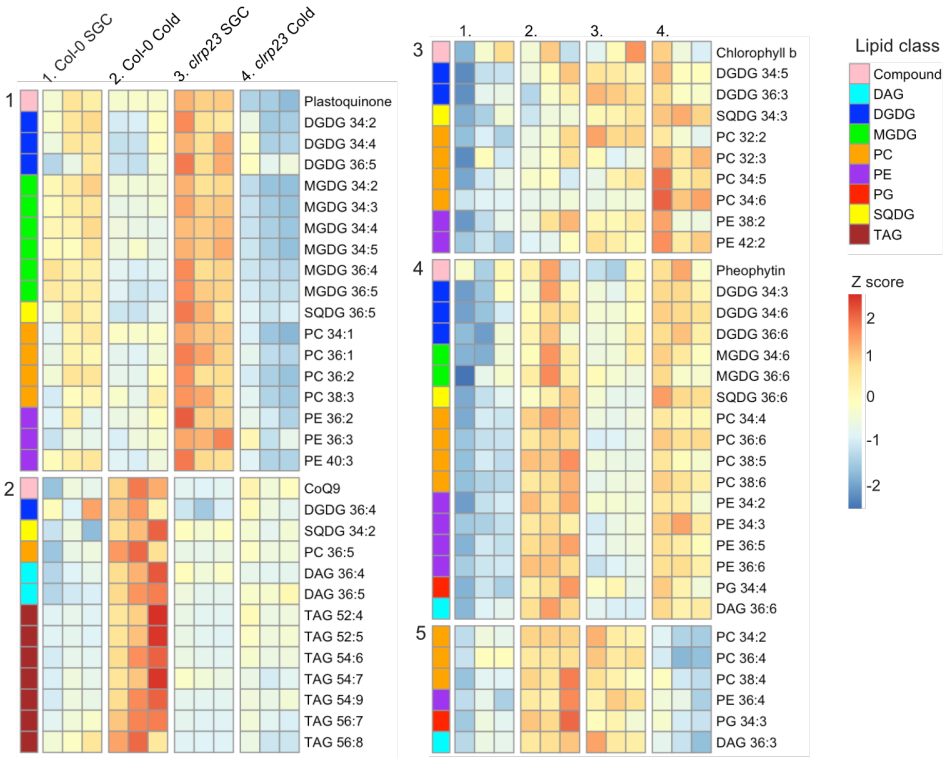

Figure 25 – LC-MS based lipid quantification of *clrp23* and Col-0 under SGC and after four days of cold treatment. Z-score based k-means clustering was used to group each quantified lipid into five clusters. Heatmap shows the z-scores of lipids quantified from every biological replicate in each genotype/condition.

Next, GC-FID was used to analyse the fatty acid profile of total lipids, as well as the major chloroplast galactolipids MGDG and DGDG. Fatty acids detected in the total lipid samples (Fig. 26A) of *clrp23* and Col-0 were summed and quantified against the internal standard C:15 to determine the total lipid content of each genotype under SGC and after cold treatment, where no significant differences were observed (Fig. 26B). To assess the coverage of MGDG and DGDG lipid species quantified by LC-MS, they were compared with their corresponding fatty acid profile measured by GC-FID. The most abundant fatty acids in the MGDG lipid class were C16:3 and C18:3 (Fig. 26C), which is consistent with the most abundant MGDG lipids

quantified by LC-MS, namely 34:6 and 36:6 (Fig. 26D). Correspondingly, the most abundant fatty acids in the DGDG lipid class were C16:0 and C18:3 (Fig. 26E), which is also reflected in the high abundance of DGDG 34:3 quantified by LC-MS (Fig. 26F). Overall, significant differences were observed in a number of lipid species and fatty acid composition in *clrp23* when compared Col-0 (Fig. 26). In the Z-score based clustering analysis of LC-MS quantified lipids, neutral (DAG and TAG) and MGDG lipid classes also exhibited clear grouping patterns (Fig. 25). This prompted further analysis into the respective lipid classes.

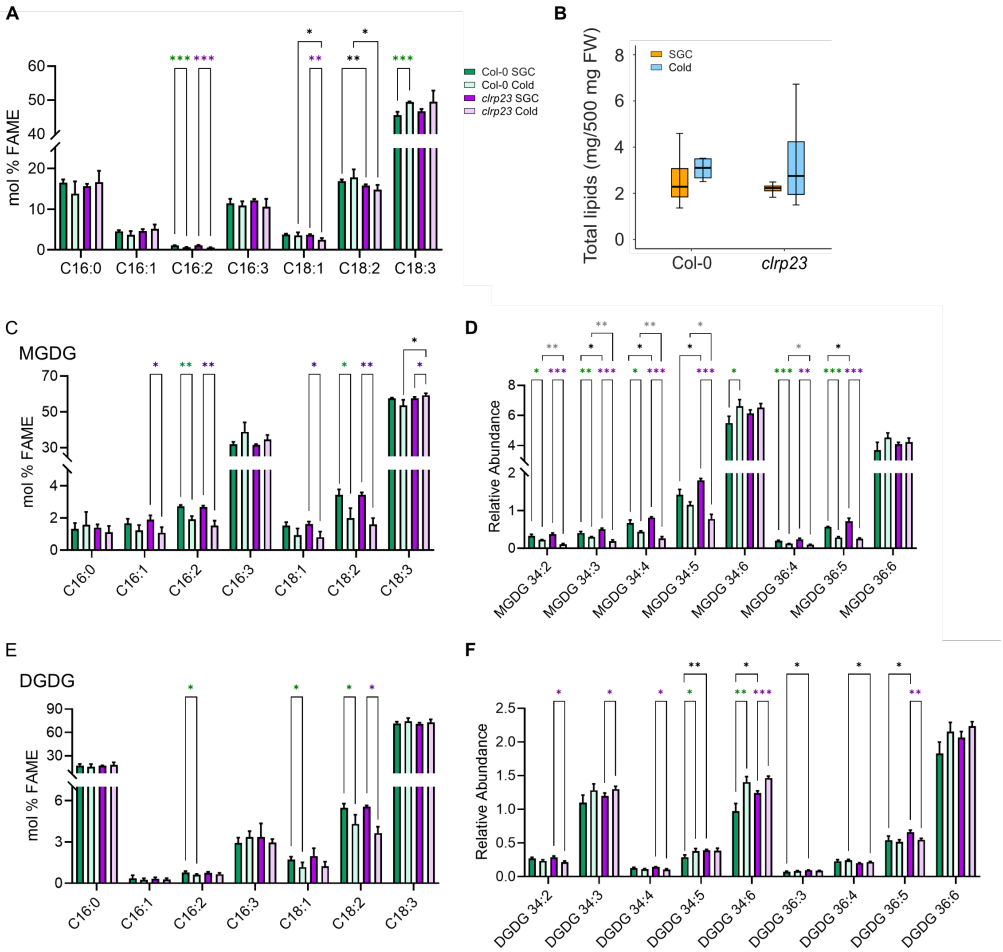

Figure 26 – LC-MS and GC-FID based lipid analysis of *clrp23* and Col-0 under SGC and after cold treatment. A) Fatty acid profile of total lipids, quantified by GC-FID. **B)** Fatty acids measured in total lipid samples were summed and quantified with internal standard C15:0 to determine total lipid content. **C-F)** Side-by-side comparison of **(C,E)** fatty acids measured with GC-FID and **(D, F)** lipid species measured with LC-MS for **(C, D)** MGDG and **(E, F)** DGDG lipid classes, respectively. LC-MS quantified lipids reported as relative abundance (peak area relative to internal standard corticosterone). GC-FID quantified fatty acids reported as molar percentage (mol%). Asterisks indicate statistically significant differences according to Student's t-test (*p<0.05; **p<0.01; ***p<0.001).

Ten neutral lipid species, in particular two out of three diacylglycerol (DAG) and all triacylglycerols (TAG), grouped in cluster two, where their levels increased in Col-0 after cold treatment, but not in *clrp23* (Fig. 25, Fig. 27A). Total neutral lipid levels were determined by summing up all DAG and TAG species measured, and normalisation against Col-0 levels under SGC revealed an approximate 3.6-fold increase after cold treatment in Col-0, while this increase was not observed in *clrp23* (Fig. 27B). Prior research has shown that neutral lipid accumulation occurs in Arabidopsis during cold acclimation, potentially as a means of storing excess fixed carbon when plant growth is slowed at low temperature conditions (Degenkolbe et al., 2012). Beyond carbon storage, however, neutral lipids can also accumulate as a result of adaptive changes in membrane fluidity and stability as part of the cold acclimation response. Under freezing conditions, for example, DAGs, which are eventually converted to TAGs, can be derived from MGDG through the activity of SFR2 (Moellering et al., 2010). To rule out the involvement of the SFR2 pathway, the lipidomes of Col-0 *clrp23* before and after freezing treatment were also analysed with LC-MS. After one hour of freezing recovery, *clrp23* showed neutral lipid levels comparable to those in Col-0 (Fig. 27C). This suggests that the reduced accumulation of neutral lipids observed in *clrp23* can likely be attributed to limited fixed carbon availability, stemming from impaired photosynthetic activity.

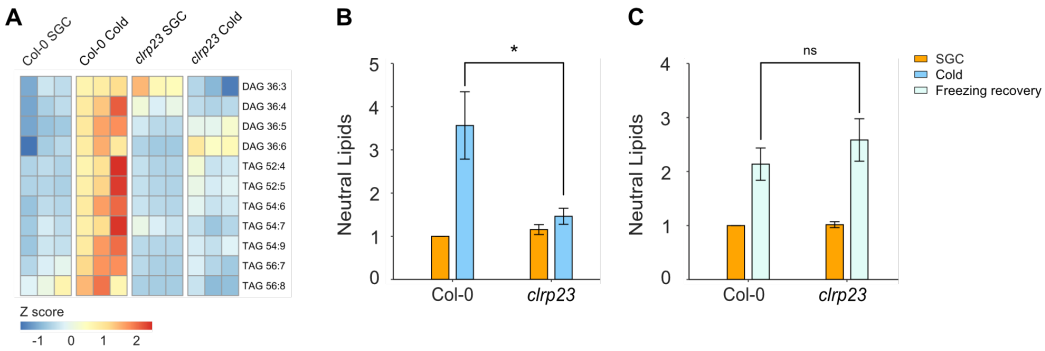

Figure 27 – Neutral lipids (DAGs and TAGs) in *clrp23* and Col-0 under SGC, after cold treatment, and after freezing recovery, quantified with LC-MS. A) Heatmap showing the z-scores of neutral lipids quantified from every biological replicate in each genotype under SGC and after four days of cold treatment. Relative abundance values of neutral lipids were summed and normalised against Col-0 under SGC for both **B)** cold and **C)** freezing treatment. Asterisks indicate statistically significant differences according to Student's t-test (*p<0.05; **p<0.01; ***p<0.001).

Meanwhile, a large number of MGDG species were found in cluster one (Fig. 25). These MGDG species were characterised by a decrease in abundance in Col-0 after cold treatment, an effect that appeared to be exaggerated in *clrp23*. The differing responses of these MGDG species, as opposed to the two most unsaturated and abundant species 34:6 and 36:6, suggested broader implications on MGDG saturation (Fig. 28A). Hence, the double bond index (DBI; Σ (% lipid or fatty acid × number of double bonds)) was determined for all MGDG lipid species and fatty acids measured with LC-MS and GC-FID, respectively. Cold treatment led to an increase in the DBI of MGDG lipids in Col-0, with an even more pronounced elevation observed in *clrp23* (Fig. 28B). In line with this, a significant increase in the DBI of MGDG fatty acids was observed in *clrp23* but not in Col-0 (Fig. 28C).

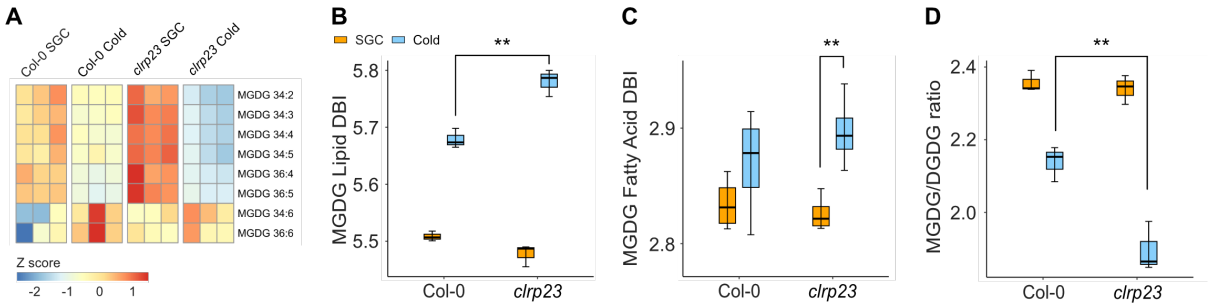

Figure 28 – MGDGs in *clrp23* and Col-0 under SGC and after cold treatment. A) Heatmap showing the z-scores of MGDG lipids quantified from every biological replicate in each genotype under SGC and after Cold. **(B, C)** Double bond index (DBI; Σ (% lipid or fatty acid × number of double bonds)) of MGDG **(B)** lipid species measured with LC-MS and **(C)** fatty acids measured with GC-FID in *clrp23* and Col-0 under SGC and after cold treatment. **D)** MGDG/DGDG ratio of *clrp23* and Col-0 under SGC and after cold treatment. Asterisks indicate statistically significant differences according to Student's t-test (*p<0.05; **p<0.01; ***p<0.001).

Since MGDG is a non-bilayer forming lipid with a propensity to adopt inverted hexagonal (H_{II}) phases (Webb & Green, 1991), the ratio between MGDG and bilayer-forming DGDG was also examined. The relative abundance values of all MGDG and DGDG species measured with LC-MS were respectively summed to determine MGDG/DGDG ratio. In Col-0, the MGDG/DGDG ratio was observed to decrease after cold treatment. Strikingly, this effect was also significantly more pronounced in *clrp23* (Fig. 28D), suggesting a dysregulation in galactolipid remodelling response in *clrp23* during cold acclimation.

3.2.8 clrp23 lipid interactions

To investigate potential interactions between CLRP23 and chloroplast lipids *in silico*, Autodock 4.2 (Morris et al., 2009) was used. The structural prediction of CLRP23 was downloaded from AlphaFold DB and docked against a number of major chloroplast lipids, namely MGDG, DGDG, SQDG, and PC (Fig. 29). Molecular docking of CLRP23 revealed the strongest binding affinity for MGDG with a docking score of -6.7 kcal/mol, followed by PC (-6.4 kcal/mol), DGDG (-4.6 kcal/mol) and SQDG (-4.3 kcal/mol). All lipids investigated in the simulations docked to the same hydrophobic binding pocket of CLRP23. However, while the hydrophilic heads of MGDG and PC face inwards towards the inside of the binding pocket, the heads of DGDG and SQDG face outwards.

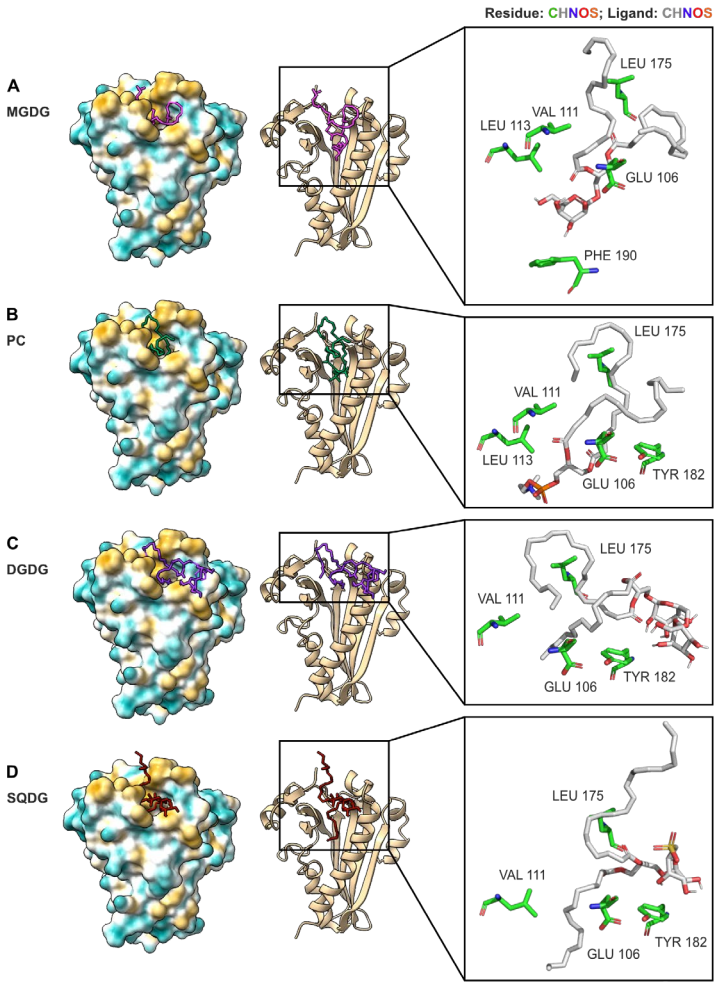

Figure 29 – Molecular docking of CLRP23 against chloroplast lipids A) MGDG, B) PC, C) DGDG and D) SQDG. A distance-based approach (<3.5 Å) was used to identify lipid-interacting amino acid residues. Residues identified to come into contact with three or more of the lipids investigated, along with residue F190, is shown. Molecular docking was performed by Dr. Eslam Abdel-Salam.

To gain insight into CLRP23 lipid interactions, a distance-based approach (<3.5 Å) was adopted to identify potential contact sites (Fig. 29, Fig. 30). A total of 17 amino acid residues were identified to interact with at least one lipid investigated in the docking simulations (Fig. 30). To investigate how the residues are conserved, sequence alignment of CLRP23 homologs across a list of nine species spanning dicots, monocots, lycophytes and bryophytes was conducted against CLRP23 in Arabidopsis. Out of the lipid interacting residues identified, four (H143, E148, L175 and F190) were found to be fully conserved among the nine homologs analysed, while other less conserved residues were often replaced by amino acids of comparable physiochemical properties. The amino acid residue F190 was of particular relevance, as it had the shortest ligand distance of 2.5 Å to MGDG. Although F190 was only identified as an interacting residue in the docking simulation with MGDG, it was found in the sequence alignment to be fully conserved among the homologs analysed.

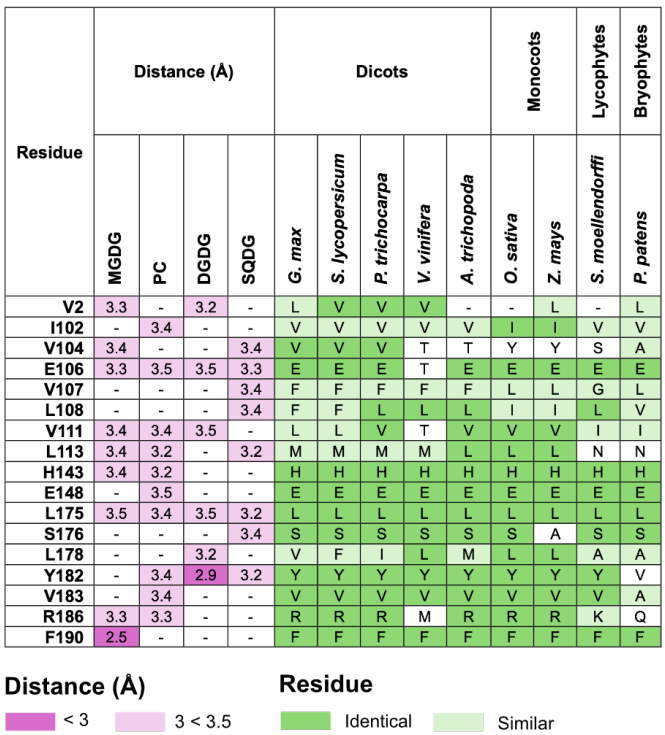

Residue	Distance (Å)				Dicots					Monocots		Lycophytes	Bryophytes
	MGDG	PC	DGDG	SQDG	*G. max*	*S. lycopersicum*	*P. trichocarpa*	*V. vinifera*	*A. trichopoda*	*O. sativa*	*Z. mays*	*S. moellendorffii*	*P. patens*
V2	3.3	-	3.2	-	L	V	V	V	-	-	L	-	L
I102	-	3.4	-	-	V	V	V	V	V	I	I	V	V
V104	3.4	-	-	3.4	V	V	V	T	T	Y	Y	S	A
E106	3.3	3.5	3.5	3.3	E	E	E	T	E	E	E	E	E
V107	-	-	-	3.4	F	F	F	F	F	L	L	G	L
L108	-	-	-	3.4	F	F	L	L	L	I	I	L	V
V111	3.4	3.4	3.5	-	L	L	V	T	V	V	V	I	I
L113	3.4	3.2	-	3.2	M	M	M	M	L	L	L	N	N
H143	3.4	3.2	-	-	H	H	H	H	H	H	H	H	H
E148	-	3.5	-	-	E	E	E	E	E	E	E	E	E
L175	3.5	3.4	3.5	3.2	L	L	L	L	L	L	L	L	L
S176	-	-	-	3.4	S	S	S	S	S	S	A	S	S
L178	-	-	3.2	-	V	F	I	L	M	L	L	A	A
Y182	-	3.4	2.9	3.2	Y	Y	Y	Y	Y	Y	Y	Y	V
V183	-	3.4	-	-	V	V	V	V	V	V	V	V	A
R186	3.3	3.3	-	-	R	R	R	M	R	R	R	K	Q
F190	2.5	-	-	-	F	F	F	F	F	F	F	F	F

Figure 30 – Sequence alignment of CLRP23 in Arabidopsis with homologs. CLRP23 homologs were identified across nine species spanning dicots, monocots, lycophytes and bryophytes. Lipid-interacting residues were identified in a distance-based approach (<3.5 Å), and residues with a ligand distance of <3 Å highlighted in a deeper purple. Conserved amino residues are highlighted in dark green, while residues substituted with amino acids of similar physiochemical properties (hydrophobic, hydrophilic, acidic, or basic) highlighted in a lighter green.

Despite extensive efforts, whether CLRP23 interacts with chloroplast lipids *in vitro* remains inconclusive. CLRP23 with a C-terminal His tag (CLRP23-His) was successfully expressed in *E. coli* under the lac operon (Fig. 31A). However, attempts to purify correctly folded CLRP23-His at sufficient purity and yield for downstream experiments were significantly hampered by its strong propensity to precipitation and degradation. After expression in *E. coli*, CLRP23-His was isolated by nickel affinity chromatography and eluted with Imidazole. Analysis of the resulting eluate with SDS-PAGE and subsequent CBB staining revealed the presence of contaminants along with CLRP23-His, with particularly strong bands visualised approximately at 60 kDa and 20 kDa, in addition to CLRP23-His at 23 kDa (Fig. 31B). While attempts to further purify the CLRP23-His eluate with size exclusion chromatography (SEC) seemed promising (Fig. 31C, D), analysis of the purified eluate with MS revealed a heavy contamination of cAMP-activated global transcriptional regulator CRP, which also had a molecular size of 23 kDa. The MS intensity of CRP in the eluate was 12,000-fold of that of CLRP23. It was therefore assumed that overnight storage and removal of buffer components with SEC resulted in the precipitation and degradation of CLRP23-His.

Dot blots of fresh eluates of CLRP23-His from nickel affinity chromatography using antisera against both His Tag and CLRP23 suggested a successful pulldown of CLRP23-His (Fig. 31E), albeit at inadequate purity for more sophisticated *in vitro* binding assays such as Circular dichroism spectroscopy and isothermal titration calorimetry. Nevertheless, fresh eluates of CLRP23-His were used for protein lipid overlay assay and microscale electrophoresis (MST) in attempts to demonstrate CLRP23-lipid interactions *in vitro*.

For protein lipid overlay assay, chloroplast lipids MGDG, PC, DGDG and SQDG were spotted onto a nitrocellulose membrane and analysed by immunoblotting with anti-His Tag antisera. While faint spots could be visualised where the membrane was spotted with chloroplast lipids (Fig. 31F), reproduction of these findings with appropriate negative controls were unsuccessful. On a similar note, MST with fluorescently labelled CLRP23-His with MGDG and DGDG initially yielded promising findings with binding affinities (K_D) of 133 µM and 154 µM respectively (Fig. 31G). However, binding was also observed between MGDG and the negative control peptide. Presumably, ligand concentrations that are too high disrupt the thermophoresis of fluorescently labelled molecules regardless of ligand binding. Higher purity CLRP23-His is therefore needed such that reaction conditions with lower ligand concentrations can be used for MST.

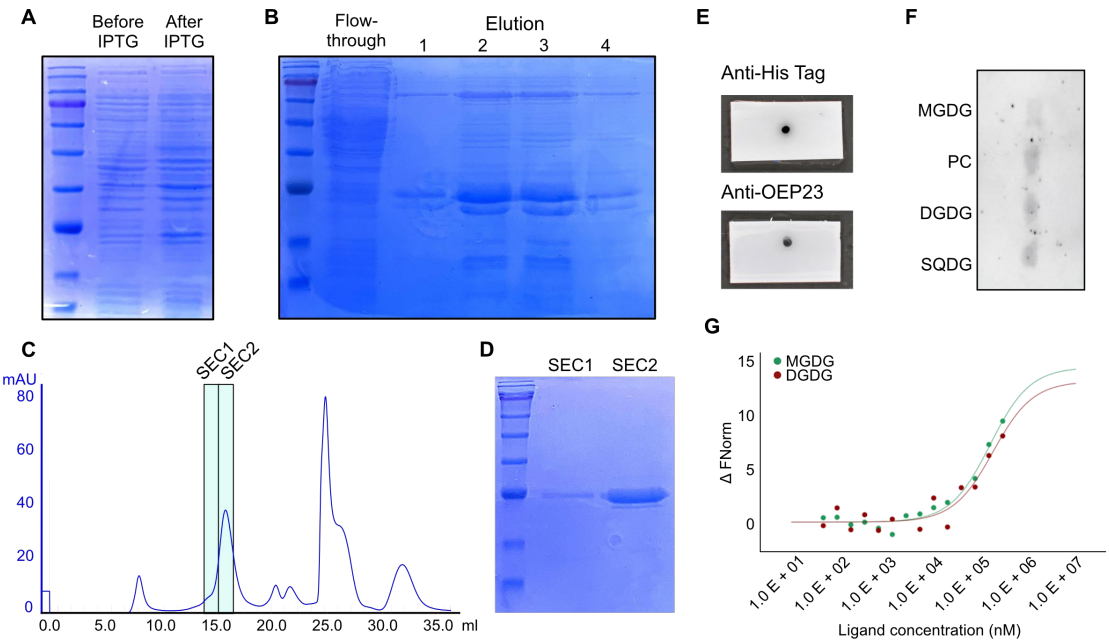

Figure 31 – Expression of C-terminal his tagged CLRP23 (CLRP23-His) for *in vitro* CLRP23-lipid binding assays. A-B) CLRP23-His was expressed in *E. coli* under the lac operon and isolated with nickel affinity chromatography. Samples were taken from Culture samples taken before and after IPTG induction (A), as well as the protein flow through and first four elutions of His purification (B) were analysed with SDS-PAGE and stained with CBB. **C-D)** Further purification of CLRP23-His eluate with size exclusion chromatography (SEC). Elution fractions at around 15 ml (SEC1 and SEC2) were analysed with SDS-PAGE and stained with CBB. **E)** Dot blots of fresh eluates of CLRP23-His from nickel affinity chromatography using antisera against both His tag and CLRP23. **F)** Protein lipid overlay assay. MGDG, PC, DGDG and SQDG lipid standards were spotted onto a nitrocellulose membrane before being incubated with a protein solution containing freshly eluted CLRP23-His and analysed by immunoblotting with anti-His Tag antisera. **G)** Microscale thermophoresis (MST) of fluorescently labelled CLRP23-His with MGDG (green) and DGDG (brown). Unfortunately, reproduction of protein lipid overlay assay with appropriate controls was unsuccessful, and binding was also observed in MST of MGDG with the negative control peptide. Whether CLRP23 interacts with chloroplast lipids *in vitro* therefore remain inconclusive.

3.3 On the hunt for new transporters of the chloroplast envelope

3.3.1 Identification of potential candidates from pea envelope proteomics study

In addition to revealing the localisation of CLRP23 to the chloroplast IE, the proteomic study of the chloroplast IE and OE fractions in Pea also revealed a number of potential chloroplast envelope transporter proteins with currently unknown molecular functions. Out of the 767 unique Arabidopsis homologs identified in the proteomic analysis, 583 localised to the plastid,

eight of which were chosen as potential candidates for further investigation (Fig. 32). Protein candidates significantly enriched in the OE or IE fractions were termed Putative Outer Envelope Protein (POE) or Putative Transporter (PT), respectively. All eight candidates were also identified in at least one other MS study to localise to the chloroplast and, with the exception of POE1, harboured at least two predicted transmembrane domains. POE1 was also chosen as a candidate due to its predicted three-dimensional structure, which appears to resemble that of a classic β-barrel protein.

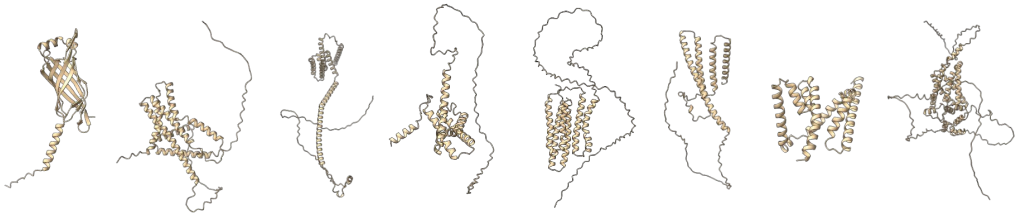

	POE1	PT1	PT2	PT3	PT4	PT5	PT6	PT7
TMD	-	4	7	4	5	3	10	4
SUBA5 MS	4	7	6	10	5	13	1	15
kDa	28	36	37	27	42	30	47	57

Figure 32 – Potential transporters of the chloroplast with currently unknown molecular functions. All nine candidates were identified in the proteomics experiment on pea OE and IE fractions localising CLRP23 to the chloroplast IE. Protein candidates significantly enriched in the OE or IE are termed putative outer envelope protein (POE) or putative transporter (PT), respectively. The accession number of each candidate was searched in the plant membrane protein database (Aramemmnon) and the subcellular localisation database for Arabidopsis proteins (SUBA5) to identify predicted transmembrane domains (TMD) and prior localisation to the plastid with MS (SUBA5 MS). The predicted three-dimensional structure of each candidate from the AlphaFold DB and their respective molecular weights (kDa) are also shown.

3.3.2 Verification of localisation to the chloroplast envelope with fluorescence microscopy

To verify their localisation to the chloroplast envelope, each protein candidate was cloned with a C-terminal GFP tag under the control of the 35S promoter. Among the envelope protein candidates, the POE1, PT2, PT3 and PT4 -GFP constructs were transiently expressed in Tobacco, after which protoplasts were isolated for fluorescent microscopy. While the eGFP signal of protoplasts expressing POE1, PT2 and PT4 -GFP form rings around the Chl a autofluorescence, confirming its localisation to the chloroplast envelope, PT3-GFP show needle like structures over and in between the Chl a autofluorescence signals (Fig. 33).

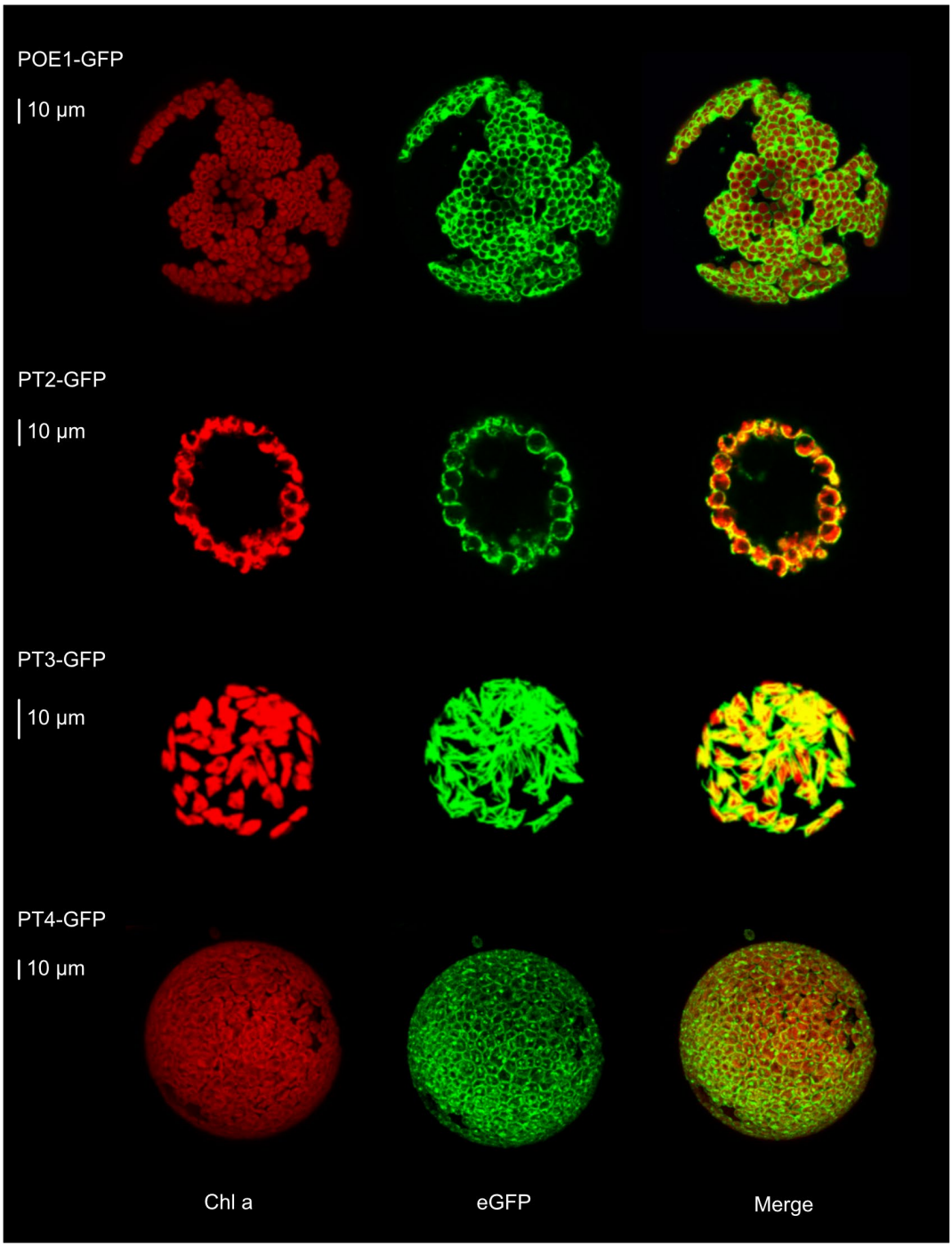

Figure 33 – GFP fluorescence microscopy of protoplasts expressing POE1, PT2, PT3 and PT4-GFP in Tobacco. In POE1, PT2, and PT4 -GFP, the eGFP signal form rings around chlorophyll a (Chl a) autofluorescence, thereby confirming their localisation to the chloroplast envelope.

4. Discussion

4.1 Screening for OEPs implicated in cold acclimation with the OemiR *plasmid library*

The capacity of plants to acclimate to adverse environmental conditions is heavily reliant on chloroplast metabolism. Located at the interface between the chloroplast and the cytosol, many proteins of the chloroplast envelope are naturally implicated in such acclimation processes (Kleine et al., 2021; Schwenkert et al., 2022). In the past, research has primarily focused on proteins of the chloroplast IE, whereas the OE was often regarded as either a nonspecific molecular sieve or simply an endosymbiotic remnant of the food vacuole (Day & Theg, 2018). However, studies in recent years have illuminated the significance of OE proteins in specific metabolite transporter and biological processes, particularly those related to cold acclimation (Neuhaus & Wagner, 2000; Trentmann et al., 2020). By targeting all known OE proteins with amiR technology, the *oemiR* plasmid library served as a powerful tool to probe the OE protein landscape in a way that also accounts for functional redundancies on the genetic level.

Of the *oemiR* mutants identified in the pilot cold screen, three have already been previously linked to low temperature sensitivity. SFR2 is a galactolipid:galactolipid galactosyltransferase (GGGT) responsible for the freeze-dependent transglycosylation of MGDG into DGDG, tri- (TGDG), and tetragalactosyldiacylglycerol (TeDG). This ultimately leads to the reduction of MGDG, thereby reducing the ratio of non-bilayer to bilayer forming lipids and stabilising the membrane during freezing conditions (Moellering et al., 2010; Thorlby et al., 2004). Mutants deficient in SFR2 are therefore sensitive to freezing and suffer from chloroplast damage after freeze treatment (Fourrier et al., 2008). Next, OEP40 is a glucose-permeable β-barrel protein channel, the loss of which results in early flowering under cold conditions due to carbohydrate imbalance, especially in the floral meristem (Harsman et al., 2016). Finally, CHUP1 contains an actin binding domain essential for chloroplast positioning and movement (Oikawa et al., 2003; Oikawa et al., 2008). Under a combination of cold and ambient light conditions, *chup1* mutants exhibited lower Fv/Fm values compared to wildtype plants (Kitashova et al., 2021), a cold-sensitive phenotype that was recapitulated in *amiR-chup1*. The identification of *ami-sfr2*, *ami-oep40* and *ami-chup1* mutants in the pilot cold screen therefore confirms the capabilities of the screening procedure to identify OEPs that play a role in cold acclimation processes.

In addition to SFR2, OEP40 and CHUP1, the cold screen of *oemiR* transformants also revealed OE proteins TOC159, OEP16-2, PDV2 and WBC7 to potentially be involved in the low temperature stress response. TOC159, also known as PLASTID PROTEIN IMPORT 2 (PPI2),

is a membrane GTPase forming an integral part of the chloroplast's TOC complex. Responsible for the quantitative import of photosynthetic proteins, *ppi2* knockout mutants are seedling lethal with an albino phenotype when supplemented with sucrose (Bauer et al., 2000). Although this phenotype was not observed in the *amiR-toc159 knockdown* line, the identification of its cold-sensitive response in the pilot screen underscores the value of milder mutant variants in uncovering nuanced aspects of more complex physiological responses to stress. Notably, *ppi* knockout mutants have also been found to exhibit alterations in chloroplast lipid composition (Afitlhile et al., 2015; Afitlhile et al., 2013; Afitlhile et al., 2021). This raises the question of whether the cold-sensitive phenotype observed in *amiR-toc159* could be due to imbalances in lipid remodelling under low temperature conditions, a possibility that can be addressed in future studies by analysing the lipid composition of *amiR-toc159* before and after cold treatment.

OEP16, a member of the preprotein and amino acid transporter (PRAT) family, is an α-helical eukaryotic addition to the chloroplast OE with *in vitro* permeability to amino acids but is impermeable to phosphoglyceric acid and uncharged sugars (Pohlmeyer et al., 1997; Pudelski et al., 2012). Four isoforms of OEP16 are found in higher plants, with OEP16-1, OEP16-2 and OEP16-4 localising to the chloroplast while OEP16-3 is targeted to the mitochondria (Schwenkert, Leister, et al., 2023). The identification of *amiR-oep16-2* and not *amiR-oep16-1* in the pilot screen was unexpected, as OEP16-1 is the most abundant isoform in leaf tissue, whereas OEP16-2 is primarily expressed during germination and late seed development (Pudelski et al., 2012). While this finding may indicate unexpected off-targeting towards *OEP16-1* in the *amiR-oep16-2* mutant, it remains plausible that OEP16-2 has a previously unknown role in cold acclimation. The same holds true for PDV2 which, along with its homolog PDV1, is responsible for plastid division (Chang et al., 2017; Miyagishima et al., 2006). Lastly, WBC7 is a putative member of the ABC protein superfamily (Sánchez-Fernández et al., 2001), although its exact molecular function has yet to be determined. Still, WBC7 has been found in a proteomic study to be downregulated in chloroplast envelopes under cold conditions (Trentmann et al., 2020), confirming the cold-sensitive phenotype of *amiR-WBC7* identified in the pilot screen.

In the mini cold screen of *oemiR* mutants in the *oep37* knockout background, the cold sensitivity observed in *oep37-amiR-oep40* was unsurprising due to the same phenotype exhibited by *amiR-oep40* single mutants in the pilot cold screen. Notably, *oep37-amiR-oep16-1* and *oep37-amiR-oep16-4* also exhibited lower Fv/Fm values after cold treatment while no

significant differences were observed between *oep37-amiR-oep16-2* and the wildtype control. This is suggestive of unpredicted off-targeting towards OEP16-1 of OEP16-4 in the *amiR-oep16-2* line captured in the pilot cold screen. Intriguingly, *oep37-amiR-oep21* and *oep37-amiR-oep24* also exhibited cold sensitivity. Along with OEP37 and OEP40, OEP21 and OEP24 share significant structural similarities to β-barrel porins typically found in the outer membrane of gram-negative bacteria (Reddy & Saier Jr, 2016). OEP21 is a solute-selective porin known to function as a major exporter for primary products of photosynthesis, while OEP24 is less specific and postulated to function as a homolog for the voltage-dependent anion-selective channel (VDAC). Intriguingly, OEP24 is able to fully, and OEP37 partially complement VDAC in yeast (Goetze et al., 2006; Röhl et al., 1999; Ulrich et al., 2012), suggesting an at least partially overlapping function between the proteins (Schwenkert, Leister, et al., 2023). The identification of *oep37-amiR-oep21* and *oep37-amiR-oep24* in the mini cold screen further highlights the potential functional overlap between these porins and prompts speculation about their possible synergistic roles during cold acclimation.

In future, additional verification steps will be needed in order to further dissect the molecular mechanisms causing the cold-sensitive phenotypes that were observed. This can be done with the employment of homozygous T-DNA or CrispR knockout mutants, or, in the case of the pilot cold screen, in subsequent generations of the *oemiR* mutant lines to enable the characterisation of more biological replicates. Nevertheless, the single and double mutant cold screens of the *oemiR* plasmid library transformants revealed a number of OE protein candidates potentially implicated in cold acclimation, reinforcing the significance of the chloroplast OE in such processes.

4.2 Role of CLRP23 in lipid remodelling during cold acclimation

CLRP23 was originally identified in chloroplast envelopes in pea and assumed to localise to the OE due to its lack of a predicted transit peptide (Kim et al., 2019). Due to electrophysiological measurements suggesting cation-selective activities *in vitro* (Goetze et al., 2015), it was often described as a chloroplast OE protein channel. Nevertheless, prior to this study, the localisation of CLRP23 to the chloroplast OE has yet to be experimentally confirmed and its exact molecular function remains elusive.

Structural predictions with AlphaFold2 and Phyre2 revealed a mixture of both α-helixes and β-sheets in the predicted structure of CLRP23, with the β-sheets forming an incomplete β-barrel. While analysis with BN-PAGE suggest the presence of CLRP23 in larger protein complexes, attempts to identify interaction partners with GFP-trap and TurboID were ultimately inconclusive. Additional experiments, either with alternative methods or modified protocols are therefore needed to follow up on the identification of CLRP23 interaction partners.

The predicted structure of CLRP23 also shared a high degree of similarity to proteins from the SRPBCC superfamily, which is characterised by a low sequence identity but shared 3-dimensional structure. Proteins in this superfamily also contain a large binding domain for hydrophobic ligands such as membrane lipids, secondary metabolites, polycyclic aromatic hydrocarbons, and plant hormones (Radauer et al., 2008). Subfractionation analysis of CLRP23, combined with protease treatments, also revealed the localisation of CLRP23 to the chloroplast IE, as well as its orientation to the IMS. Although it remains unclear how CLRP23 targets to the chloroplast IE/IMS without a predicted transit peptide, structural predictions of CLRP23, combined with experimental evidence of its localisation, suggest an alternative function for CLRP23 which differs from its previously assumed role as an OE channel.

Preliminary findings from screening *oemiR* mutants in the *clrp23* knockout background revealed all *clrp23 x oemiR* double mutants to exhibit severe impairments in photosynthetic performance after cold treatment. CLRP23 has also been identified in a proteomic study of the chloroplast envelope to be differentially expressed under cold (Trentmann et al., 2020), prompting further investigation into the role of CLRP23 itself in cold acclimation. Indeed, *clrp23* single knockout mutants exhibit impaired photosynthesis compared to Col-0 under cold conditions, adding to the growing body of evidence connecting proteins of the chloroplast envelope with plant acclimation processes (John, Keller, et al., 2024; Schwenkert, Lo, et al., 2023; Trentmann et al., 2020).

In addition to suffering from impaired photosynthesis, *clrp23* mutants also accumulated less anthocyanins and exhibited a significant downregulation in proteins involved in flavonoid biosynthesis after cold treatment. Anthocyanins comprise one of the major groups of flavonoids, secondary metabolites with a polyphenolic three-ring chemical structure that are involved in numerous abiotic stress responses in plants (Di Ferdinando et al., 2012; Kitashova et al., 2023; Kitashova et al., 2024; Petrussa et al., 2013; Shomali et al., 2022). Synthesised from photosynthetically derived carbon along the Phenylpropanoid pathway, flavonoid

accumulation occurs after several days of exposure and has been previously shown to help balance the C/N metabolism and maintain protein homeostasis (Kitashova et al., 2024). Despite this, in contrast to the cold-sensitive phenotype observed in *clrp23*, photosynthetic performance in mutants deficient in flavonoid biosynthesis are comparable to Col-0 during cold acclimation (Kitashova et al., 2023). Hence, while the downregulation of flavonoid metabolism in *clrp23* may have detrimental effects on low temperature tolerance, it is unlikely to be the primary driver of its cold-sensitive phenotype.

On the contrary, Arabidopsis mutants suffering from impaired photosynthesis have previously been shown to synthesise and accumulate less flavonoids (Scherer et al., 2024; Vicente et al., 2023). Therefore, the downregulation of flavonoid biosynthesis and reduction of anthocyanin accumulation observed in *clrp23* exposed to cold temperatures are more likely attributable to a shortage of fixed carbon caused by compromised photosynthetic activity. Supporting this, triacylglycerol accumulation is also negatively affected in *clrp23* under cold, suggesting a more widespread disturbance in carbon distribution.

Aside from flavonoid metabolism, lipid remodelling comprises another major aspect of cold acclimation, a process that maintains the fluidity and structural integrity of membranes during low temperature stress (Barrero-Sicilia et al., 2017; Degenkolbe et al., 2012; Li et al., 2020). For chloroplast membranes, which host the plants photosynthetic machinery and accounts for 80% of all glycerolipids in leaves, lipid remodelling is of particular importance (Hölzl & Dörmann, 2019). Upon cold exposure, the primary chloroplast membrane lipids MGDG and DGDG undergo both structural and compositional modifications. To reduce intermolecular packing and enhance membrane fluidity to counteract the rigidifying effects of low temperatures, membrane lipids become more unsaturated, introducing double bonds and thereby creating conformational kinks in the lipid carbon chains (Hugly & Somerville, 1992; Murakami et al., 2000; Routaboul et al., 2000). Since MGDG is a non-bilayer forming lipid with the propensity to form inverted hexagonal H_{II} phases (Webb & Green, 1991), plants also reduce the proportion of MGDG to bilayer-forming DGDG to maintain membrane integrity and stability. This reduction in MGDG/DGDG ratio is typically used by plants as an adaptive strategy to a variety of environmental stresses, including low temperature (Li et al., 2020; MacDonald et al., 2023; Moellering et al., 2010; Zheng et al., 2016). To our intrigue, both MGDG fatty acid desaturation and MGDG/DGDG ratio reduction was exaggerated in *clrp23* after cold treatment compared to Col-0, findings that are indicative of imbalances in lipid remodelling on multiple levels during cold acclimation.

Although the biophysical properties of lipid desaturation make it critical for cold acclimation, lipid remodelling is highly complex and requires a delicate balance between fluidity and stability to maintain optimal membrane functionality. Studies have also demonstrated that, in addition to lipid desaturation, other factors such as lipid shape also play a major role in lipid remodelling under cold conditions (Barkan et al., 2006; Degenkolbe et al., 2012). The cold-sensitive phenotype of the Arabidopsis *fatty acid biosynthesis 1* (*fab1*) mutant, in which fatty acid 16:0 over-accumulates, can be rescued by a further increase in MGDG saturation levels via a mutation in the *FATTY ACID DESATURATION 5* (*FAD5*) gene (Barkan et al., 2006). Barkan et al. (2006)proposed that, since saturated species of MGDG are predicted to be narrower in shape compared to their more unsaturated, conical counterparts (Gounaris et al., 1983; Gruner et al., 1985), this compensates for structural changes in other lipid classes resulting from 16:0 overaccumulation. Increases in MGDG saturation have also been postulated to help stabilise the membrane by preventing the formation of H_{II} phases, and the more saturated MGDG species 34:2 and 34:2 were also positively correlated with acclimated freezing tolerance in a separate lipidomic analysis of 15 Arabidopsis accessions (Degenkolbe et al., 2012).

Furthermore, despite their propensity to form H_{II} phases, MGDG lipids account for 50% of all thylakoid lipids and, along with other lipids in the thylakoid membrane, are integral to photosynthetic complex assembly and function (Hölzl & Dörmann, 2019; Yoshihara & Kobayashi, 2022). In a study using single-molecule force spectroscopy, MGDG has been found to significantly increase the mechanical stability of trimeric light-harvesting complex II (LHCII), an effect that is likely caused by the steric complementarity between the conical shape of MGDG and the hourglass shape of LHCII (Seiwert et al., 2017). Arabidopsis, despite being more tolerant to low temperature, also maintains a higher MGDG/DGDG ratio than Rice, suggesting that the ability to effectively modulate this ratio, rather than its absolute value, is more important during cold acclimation (Zheng et al., 2016). Therefore, exaggerations in galactolipid remodelling observed in *clrp23* after cold treatment may result in imbalances in chloroplast lipid composition, ultimately destabilising the membrane and disrupting lipid-protein interactions that are essential for the function of photosynthesis.

In addition to structural similarities to the SRPBCC protein superfamily and changes in galactolipid composition observed in the *clrp23* lipidome, the involvement of CLRP23 in lipid remodelling during cold acclimation is further supported by *in silico* docking simulations. CLRP23 exhibited an affinity for chloroplast membrane lipids MGDG, DGDG, SQDG and PC

in silico, with the strongest binding affinity observed between CLRP23 and MGDG. The amino acid residue F190, with the shortest ligand distance docking exclusively to MGDG, was also found to be fully conserved in all homologs of CLRP23 investigated in the sequence alignment analysis, further emphasising the potential preference for CLRP23 to bind or interact with MGDG *in vivo*. Unfortunately, whether or not CLRP23 interacts with MGDG *in vitro* remains inconclusive, as efforts to produce soluble, properly folded CLRP23 in *E. coli* at adequate yield, stability and purity for downstream interactions were unsuccessful. It is likely that fusion tags at either the N- or C-terminus compromise the protein's structural integrity and fusion, which is also reflected in the difficulty of obtaining stable Arabidopsis overexpression lines expressing C-terminal tagged CLRP23. Consequently, more advanced expression strategies will be required for future investigations into *in vitro* CLRP23 protein-lipid interactions.

Strikingly, CLRP23 represents one of the rare examples of chloroplast envelope proteins that orient toward the IMS. Among the few IMS-facing proteins identified so far is MGD1, the principle enzyme responsible for MGDG synthesis in leaves (Vojta et al., 2007), prompting the speculation of whether CLRP23 functions in close association with MGD1 during galactolipid remodelling responses upon cold acclimation. Combined, the findings from this study indicate the involvement of CLRP23 in modulating the dynamics of MGDG, a process integral to the maintenance of chloroplast membrane fluidity, stability and function. We speculate that CLRP23 potentially serves as an MGDG-binding scaffold protein and negative regulator of the galactolipid response during cold acclimation (Fig. 34). Such a role may contribute to the fine-tuning required for effective lipid remodelling under cold acclimation.

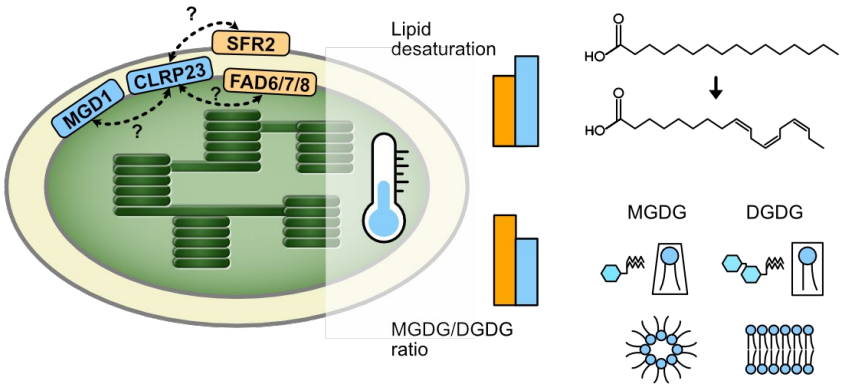

Figure 34 – Role of CLRP23 in lipid remodelling during cold acclimation. We speculate that CLRP23 works in close association with MGD1 in the IMS, where it potentially acts as an MGDG-binding scaffolding protein and regulator of galactolipid responses under low temperature stress.

4.3 Putative chloroplast envelope transporters with unresolved molecular functions

Previous proteomic approaches have provided extensive insights into the core proteome of the chloroplast envelope (Bouchnak et al., 2019; Cheng et al., 2020; Ferro et al., 2003; Ferro et al., 2002; Froehlich et al., 2003). However, the distinct characterisation of the IE and OE membranes has been limited, largely due to the challenges associated with isolating highly pure membrane fractions. To date, the most comprehensive analysis of the IE and OE proteomes in Pea was conducted by Gutierrez-Carbonell et al. (2014), identifying a nonredundant set of 409 chloroplast envelope proteins, 229 of which were significantly enriched in either the IE or OE. In our current proteomic analysis of IE and OE fractions in pea, a total of 473 nonredundant envelope proteins were identified, with 427 showing significant enrichment in the IE or OE. These findings underscore the potential of recent advances in mass spectrometry (MS)-based proteomics to achieve deeper coverage and enhanced resolution of the IE and OE proteomes. The expanded proteomic dataset enabled not only the localisation of CLRP23 to the IE, but also the identification of eight potential envelope transporter proteins with currently unknown molecular functions, seven of which were not identified in the 2014 study.

A literature search of the eight envelope proteins selected as transporter candidates revealed several connections with abiotic stress, including drought, salt and light/low temperature. Annotation of POE1 in the UniProt database showed the presence of a water stress and hypersensitive response (WHy) domain. The WHy protein family is typically expressed in late embryogenesis as well as under desiccation conditions (Ciccarelli & Bork, 2004). Consistent with this, POE1 has been found to be upregulated upon dessication stress in the streptophyte green algae *Klebsormidium* (Holzinger et al., 2014), further supporting its potential role in water stress response. Intriguingly, cold acclimation has also been found to induce the differential localisation of POE1 away from the chloroplast envelope (Trentmann et al., 2020), raising the question of whether or not it functions as a metabolite channel despite its β-barrel structure. It is plausible that the differential localisation of POE1 observed during cold acclimation is related to cellular dehydration at subzero temperatures (Nagao et al., 2008). On the other hand, PT3 has been identified in the interactomes of proteins associated with salt stress (Castro-Bustos et al., 2022; Michaeli et al., 2014), while PT1 has been found in a transcriptomic study to be significantly downregulated in Arabidopsis under excess light and low temperature (Alboresi et al., 2011).

In addition to these stress-related associations, two candidate envelope transporters have also been linked to embryonic defects. PT2, also known as embryo defective (EMB) 1923 was originally identified in a forward genetic screen in Arabidopsis to be implicated in normal embryo development (Tzafrir et al., 2004), and mutation in the gene promoter of its respective homolog in Chinese cabbage has been found to associate with chlorophyll deficiency (Li et al., 2019). Similarly, T-DNA loss of function mutants of PT6 are embryo lethal, while milder mutants with overexpression induced gene silencing or RNAi knock-down exhibiting a chlorotic phenotype (Schock, 2014). PT6 is also a part of the RETICULATA-RELATED (RER) family. Although the precise molecular functions of members from the RER protein family remain elusive, co-expression analysis associated them with amino acid and nucleotide metabolism (Lundquist et al., 2014; Pérez-Pérez et al., 2013).

Fluorescence microscopy of protoplasts expressing GFP tagged POE1, PT2 and PT4 confirmed their localisation to the chloroplast envelope, further establishing our envelope proteomic dataset as a resource for identifying transporter candidates for future study. This will need to be repeated with all other candidates to verify their localisation to the chloroplast envelope before proceeding with further investigation. To follow up on associations with abiotic stress, knockout mutants of POE1 and PT1 can be respectively exposed to desiccation, cold or excess light/low temperature for phenotypic characterisation. Unlike the ring structures observed in POE1, PT2 and PT4 -GFP, the needle-like appearance of eGFP signals in tobacco plants expressing PT3-GFP also presents an intriguing avenue for future investigation. To investigate the potential for complex formation, assays such as co-immunoprecipitation, GFP trap, or proximity labelling with TurboID can be used. These methods can also help verify interactions between PT3 and the proteins in whose interactomes PT3 was identified as a candidate interacting partner. Overall, these candidates represent an exciting opportunity to further our understanding of metabolite transport across the chloroplast envelope, as well as the role these proteins play in plant acclimation processes.

5. Conclusion/outlook

To summarise, this work provides new insights into the chloroplast envelope landscape and highlights the role of envelope proteins in plant acclimation processes, particularly during low temperature stress. The oemiR plasmid library was an effective tool to identify OE proteins potentially implicated in cold acclimation. Contrary to previous assumptions that CLRP23 functions as an OE protein channel, evidence from *in silico* structural modelling, subfractionation analysis, and protease protection assays suggests that CLRP23 instead localises to the IE facing the IMS. Meanwhile, phenotypic and multiomic characterisations of *clrp23* under low temperature conditions further revealed severe impairments in photosynthesis and alterations in lipid composition, indicating an important role for CLRP23 in galactolipid remodelling during cold acclimation. Collectively, these findings deepen our understanding of mechanisms underlying cold acclimation at the chloroplast envelope and their broader impact on the photosynthetic function.

Extending this work, proteomic analysis of chloroplast envelope fractions in Pea uncovered seven putative transporters with currently unknown molecular function. Preliminary characterisation of four of these putative transporters with GFP microscopy successfully localised POE1, PT2 and PT4 to the chloroplast envelope. In contrast, PT3-GFP displayed needle-like structures positioned across and between the chlorophyll a autofluorescence signals of the chloroplasts, suggesting a distinct subcellular distribution. Examination of existing literature revealed connections to various environmental stress responses, including drought, salt and light/low temperature. Overall, these candidates offer a strong foundation for future research into metabolite transport across the chloroplast envelope and its role in plant acclimation. Further characterisations may therefore reveal additional mechanisms of envelope-mediated acclimation and help inform strategies for improving stress resilience in plants.

References

Afitlhile, M., Fry, M., & Workman, S. (2015). The TOC159 mutant of Arabidopsis thaliana accumulates altered levels of saturated and polyunsaturated fatty acids. *Plant Physiology and Biochemistry*, *87*, 61-72. https://doi.org/10.1016/j.plaphy.2014.12.018

Afitlhile, M., Workman, S., Duffield, K., Sprout, D., & Berhow, M. (2013). A mutant of the Arabidopsis thaliana TOC159 gene accumulates reduced levels of linolenic acid and monogalactosyldiacylglycerol. *Plant Physiology and Biochemistry*, *73*, 344-350. https://doi.org/10.1016/j.plaphy.2013.10.018

Afitlhile, M., Worthington, R., Heda, G., & Brown, L. (2021). The TOC159 null mutant of Arabidopsis thaliana is impaired in the accumulation of plastid lipids and phosphatidylcholine. *Plant Physiology and Biochemistry*, *159*, 148-159. https://doi.org/10.1016/j.plaphy.2020.12.011

Ahmad, P., Rasool, S., Gul, A., Sheikh, S. A., Akram, N. A., Ashraf, M., Kazi, A., & Gucel, S. (2016). Jasmonates: multifunctional roles in stress tolerance. *Frontiers in Plant Science*, *7*, 813. https://doi.org/10.3389/fpls.2016.00813

Alboresi, A., Dall'Osto, L., Aprile, A., Carillo, P., Roncaglia, E., Cattivelli, L., & Bassi, R. (2011). Reactive oxygen species and transcript analysis upon excess light treatment in wild-type Arabidopsis thaliana vs a photosensitive mutant lacking zeaxanthin and lutein. *BMC Plant Biology*, *11*(1), 62. https://doi.org/10.1186/1471-2229-11-62

Arora, D., Abel, N. B., Liu, C., Van Damme, P., Yperman, K., Eeckhout, D., Vu, L. D., Wang, J., Tornkvist, A., Impens, F., Korbei, B., Van Leene, J., Goossens, A., De Jaeger, G., Ott, T., Moschou, P. N., & Van Damme, D. (2020). Establishment of Proximity-Dependent Biotinylation Approaches in Different Plant Model Systems. *The Plant Cell*, *32*(11), 3388-3407. https://doi.org/10.1105/tpc.20.00235

Awai, K., Maréchal, E., Block, M. A., Brun, D., Masuda, T., Shimada, H., Takamiya, K.-i., Ohta, H., & Joyard, J. (2001). Two types of MGDG synthase genes, found widely in both 16: 3 and 18: 3 plants, differentially mediate galactolipid syntheses in photosynthetic and nonphotosynthetic tissues in Arabidopsis thaliana. *Proceedings of the National Academy of Sciences*, *98*(19), 10960-10965. https://doi.org/10.1073/pnas.181331498

Banks, J. A., Nishiyama, T., Hasebe, M., Bowman, J. L., Gribskov, M., dePamphilis, C., Albert, V. A., Aono, N., Aoyama, T., Ambrose, B. A., Ashton, N. W., Axtell, M. J., Barker, E., Barker, M. S., Bennetzen, J. L., Bonawitz, N. D., Chapple, C., Cheng, C., Correa, L. G. G., . . . Grigoriev, I. V. (2011). The Selaginella Genome Identifies Genetic Changes Associated with the Evolution of Vascular Plants. *Science*, *332*(6032), 960-963. https://doi.org/10.1126/science.1203810

Barkan, L., Vijayan, P., Carlsson, A. S., Mekhedov, S., & Browse, J. (2006). A Suppressor of fab1 Challenges Hypotheses on the Role of Thylakoid Unsaturation in Photosynthetic Function. *Plant Physiology*, *141*(3), 1012-1020. https://doi.org/10.1104/pp.106.080481

Barrero-Sicilia, C., Silvestre, S., Haslam, R. P., & Michaelson, L. V. (2017). Lipid remodelling: Unravelling the response to cold stress in Arabidopsis and its extremophile relative Eutrema salsugineum. *Plant Science*, *263*, 194-200. https://doi.org/10.1016/j.plantsci.2017.07.017

Barth, M. A., Soll, J., & Akbaş, Ş. (2022). Prokaryotic and eukaryotic traits support the biological role of the chloroplast outer envelope. *Biochimica et Biophysica Acta (BBA) - Molecular Cell Research*, *1869*(5), 119224. https://doi.org/10.1016/j.bbamcr.2022.119224

Bauer, J., Chen, K., Hiltbunner, A., Wehrli, E., Eugster, M., Schnell, D., & Kessler, F. (2000). The major protein import receptor of plastids is essential for chloroplast biogenesis. *Nature*, *403*(6766), 203-207. https://doi.org/10.1038/35003214

Becker, T., Hritz, J., Vogel, M., Caliebe, A., Bukau, B., Soll, J., & Schleiff, E. (2004). Toc12, a novel subunit of the intermembrane space preprotein translocon of chloroplasts. *Molecular biology of the cell*, *15*(11), 5130-5144. https://doi.org/10.1091/mbc.e04-05-0405

Benning, C. (2008). A role for lipid trafficking in chloroplast biogenesis. *Progress in Lipid Research*, *47*(5), 381-389. https://doi.org/10.1016/j.plipres.2008.04.001

Block, M. A., Dorne, A.-j., Joyard, J., & Douce, R. (1983). Preparation and characterization of membrane fractions enriched in outer and inner envelope membranes from spinach chloroplasts. I. Electrophoretic and immunochemical analyses. *Journal of Biological Chemistry*, *258*(21), 13273-13280. https://doi.org/10.1016/S0021-9258(17)44112-3

Block, M. A., Douce, R., Joyard, J., & Rolland, N. (2007). Chloroplast envelope membranes: a dynamic interface between plastids and the cytosol. *Photosynthesis Research*, *92*(2), 225-244. https://doi.org/10.1007/s11120-007-9195-8

Bobrovskikh, A. V., Zubairova, U. S., Bondar, E. I., Lavrekha, V. V., & Doroshkov, A. V. (2022). Transcriptomic Data Meta-Analysis Sheds Light on High Light Response in Arabidopsis thaliana L. *International Journal of Molecular Sciences*, *23*(8), 4455. https://doi.org/10.3390/ijms23084455

Bölter, B., Mitterreiter, M., Schwenkert, S., Finkemeier, I., & Kunz, H.-H. (2020). The topology of plastid inner envelope potassium cation efflux antiporter KEA1 provides new insights into its regulatory features. *Photosynthesis Research*, *145*. https://doi.org/10.1007/s11120-019-00700-2

Bölter, B., & Soll, J. (2001). Ion channels in the outer membranes of chloroplasts and mitochondria: open doors or regulated gates? *The EMBO journal*. https://doi.org/10.1093/emboj/20.5.935

Bölter, B., Soll, J., Hill, K., Hemmler, R., & Wagner, R. (1999). A rectifying ATP-regulated solute channel in the chloroplastic outer envelope from pea. *The EMBO journal*. https://doi.org/10.1093/emboj/18.20.5505

Bouchnak, I., Brugière, S., Moyet, L., Le Gall, S., Salvi, D., Kuntz, M., Tardif, M., & Rolland, N. (2019). Unraveling Hidden Components of the Chloroplast Envelope Proteome: Opportunities and Limits of Better MS Sensitivity. *Mol Cell Proteomics*, *18*(7), 1285-1306. https://doi.org/10.1074/mcp.RA118.000988

Buchanan, B. B., Gruissem, W., & Jones, R. L. (2015). *Biochemistry and molecular biology of plants*. John wiley & sons.

Castro-Bustos, S., Maruri-López, I., Ortega-Amaro, M. A., Serrano, M., Ovando-Vázquez, C., & Jiménez-Bremont, J. F. (2022). An interactome analysis reveals that Arabidopsis

thaliana GRDP2 interacts with proteins involved in post-transcriptional processes. *Cell Stress and Chaperones*, *27*(2), 165-176. https://doi.org/10.1007/s12192-022-01261-5

Chang, N., Sun, Q., Li, Y., Mu, Y., Hu, J., Feng, Y., Liu, X., & Gao, H. (2017). PDV2 has a dosage effect on chloroplast division in Arabidopsis. *Plant Cell Reports*, *36*, 471-480. https://doi.org/10.1007/s00299-016-2096-6

Cheng, J., Morin, G. B., & Chen, D. D. (2020). Bottom-up proteomics of envelope proteins extracted from spinach chloroplast via high organic content CE-MS. *Electrophoresis*, *41*(5-6), 370-378. https://doi.org/10.1002/elps.201900452

Ciccarelli, F. D., & Bork, P. (2004). The WHy domain mediates the response to desiccation in plants and bacteria. *Bioinformatics*, *21*(8), 1304-1307. https://doi.org/10.1093/bioinformatics/bti221

Clough, S. J., & Bent, A. F. (1998). Floral dip: a simplified method for Agrobacterium-mediated transformation of Arabidopsis thaliana. *The Plant Journal*, *16*(6), 735-743. https://doi.org/10.1046/j.1365-313x.1998.00343.x

Cutler, S., & McCourt, P. (2005). Dude, where's my phenotype? Dealing with redundancy in signaling networks. *Plant Physiology*, *138*(2), 558-559. https://doi.org/10.1104/pp.104.900152

Cvetkovic, J., Haferkamp, I., Rode, R., Keller, I., Pommerrenig, B., Trentmann, O., Altensell, J., Fischer-Stettler, M., Eicke, S., Zeeman, S. C., & Neuhaus, H. E. (2021). Ectopic maltase alleviates dwarf phenotype and improves plant frost tolerance of maltose transporter mutants. *Plant Physiology*, *186*(1), 315-329. https://doi.org/10.1093/plphys/kiab082

Day, P. M., & Theg, S. M. (2018). Evolution of protein transport to the chloroplast envelope membranes. *Photosynthesis Research*, *138*(3), 315-326. https://doi.org/10.1007/s11120-018-0540-x

Degenkolbe, T., Giavalisco, P., Zuther, E., Seiwert, B., Hincha, D. K., & Willmitzer, L. (2012). Differential remodeling of the lipidome during cold acclimation in natural accessions of Arabidopsis thaliana. *The Plant Journal*, *72*(6), 972-982. https://doi.org/10.1111/tpj.12007

Di Ferdinando, M., Brunetti, C., Fini, A., & Tattini, M. (2012). Flavonoids as antioxidants in plants under abiotic stresses. *Abiotic stress responses in plants: metabolism, productivity and sustainability*, 159-179. https://doi.org/10.1007/978-1-4614-0634-1_9

Dörmann, P., Hoffmann-Benning, S., Balbo, I., & Benning, C. (1995). Isolation and characterization of an Arabidopsis mutant deficient in the thylakoid lipid digalactosyl diacylglycerol. *The Plant Cell*, *7*(11), 1801-1810. https://doi.org/10.1105/tpc.7.11.1801

Dubots, E., Audry, M., Yamaryo, Y., Bastien, O., Ohta, H., Breton, C., Maréchal, E., & Block, M. A. (2010). Activation of the chloroplast monogalactosyldiacylglycerol synthase MGD1 by phosphatidic acid and phosphatidylglycerol. *Journal of Biological Chemistry*, *285*(9), 6003-6011. https://doi.org/10.1074/jbc.M109.071928

Dyall, S. D., Brown, M. T., & Johnson, P. J. (2004). Ancient Invasions: From Endosymbionts to Organelles. *Science*, *304*(5668), 253-257. https://doi.org/10.1126/science.1094884

Eberhardt, J., Santos-Martins, D., Tillack, A. F., & Forli, S. (2021). AutoDock Vina 1.2.0: New Docking Methods, Expanded Force Field, and Python Bindings. *Journal of Chemical Information and Modeling*, *61*(8), 3891-3898. https://doi.org/10.1021/acs.jcim.1c00203

Eisa, A., Malenica, K., Schwenkert, S., & Bölter, B. (2020). High Light Acclimation Induces Chloroplast Precursor Phosphorylation and Reduces Import Efficiency. *Plants*, *9*(1), 24. https://doi.org/10.3390/plants9010024

Facchinelli, F., & Weber, A. P. (2011). The metabolite transporters of the plastid envelope: an update. *Frontiers in Plant Science*, *2*, 50. https://doi.org/10.3389/fpls.2011.00050

Fan, J., Zhai, Z., Yan, C., & Xu, C. (2015). Arabidopsis TRIGALACTOSYLDIACYLGLYCEROL5 interacts with TGD1, TGD2, and TGD4 to facilitate lipid transfer from the endoplasmic reticulum to plastids. *The Plant Cell*, *27*(10), 2941-2955. https://doi.org/10.1105/tpc.15.00394

Ferro, M., Salvi, D., Brugière, S., Miras, S., Kowalski, S., Louwagie, M., Garin, J., Joyard, J., & Rolland, N. (2003). Proteomics of the chloroplast envelope membranes from Arabidopsis thaliana. *Molecular & Cellular Proteomics*, *2*(5), 325-345. https://doi.org/10.1074/mcp.M300030-MCP200

Ferro, M., Salvi, D., Rivière-Rolland, H., Vermat, T., Seigneurin-Berny, D., Grunwald, D., Garin, J., Joyard, J., & Rolland, N. (2002). Integral membrane proteins of the chloroplast envelope: identification and subcellular localization of new transporters. *Proceedings of the National Academy of Sciences*, *99*(17), 11487-11492. https://doi.org/10.1073/pnas.172390399

Fischer, K. (2011). The import and export business in plastids: transport processes across the inner envelope membrane. *Plant Physiology*, *155*(4), 1511-1519. https://doi.org/10.1104/pp.110.170241

Fischer, W. W., Hemp, J., & Johnson, J. E. (2016). Evolution of oxygenic photosynthesis. *Annual Review of Earth and Planetary Sciences*, *44*(1), 647-683. https://doi.org/10.1146/annurev-earth-060313-054810

Flügge, U.-I. (1992). Reaction mechanism and asymmetric orientation of the reconstituted chloroplast phosphate translocator. *Biochimica et Biophysica Acta (BBA) - Biomembranes*, *1110*(1), 112-118. https://doi.org/10.1016/0005-2736(92)90301-2

Flügge, U.-I. (1998). Metabolite transporters in plastids. *Current Opinion in Plant Biology*, *1*(3), 201-206. https://doi.org/10.1016/S1369-5266(98)80105-2

Fourrier, N., Bédard, J., Lopez-Juez, E., Barbrook, A., Bowyer, J., Jarvis, P., Warren, G., & Thorlby, G. (2008). A role for SENSITIVE TO FREEZING2 in protecting chloroplasts against freeze-induced damage in Arabidopsis. *The Plant Journal*, *55*(5), 734-745. https://doi.org/10.1111/j.1365-313X.2008.03549.x

Froehlich, J. (2011). Studying Arabidopsis Envelope Protein Localization and Topology Using Thermolysin and Trypsin Proteases. In R. P. Jarvis (Ed.), *Chloroplast Research in Arabidopsis: Methods and Protocols, Volume I* (pp. 351-367). Humana Press. https://doi.org/10.1007/978-1-61779-234-2_21

Froehlich, J. E., Wilkerson, C. G., Ray, W. K., McAndrew, R. S., Osteryoung, K. W., Gage, D. A., & Phinney, B. S. (2003). Proteomic study of the arabidopsis thaliana chloroplastic

envelope membrane utilizing alternatives to traditional two-dimensional electrophoresis. *Journal of Proteome Research*, *2*(4), 413-425. https://doi.org/10.1021/pr034025j

Fürtauer, L., Weiszmann, J., Weckwerth, W., & Nägele, T. (2019). Dynamics of Plant Metabolism during Cold Acclimation. *International Journal of Molecular Sciences*, *20*(21), 5411. https://doi.org/10.3390/ijms20215411

Geiger, O., López-Lara, I. M., & Sohlenkamp, C. (2013). Phosphatidylcholine biosynthesis and function in bacteria. *Biochimica et Biophysica Acta (BBA) - Molecular and Cell Biology of Lipids*, *1831*(3), 503-513. https://doi.org/10.1016/j.bbalip.2012.08.009

Goetze, T. A., Patil, M., Jeshen, I., Bölter, B., Grahl, S., & Soll, J. (2015). Oep23 forms an ion channel in the chloroplast outer envelope. *BMC Plant Biology*, *15*(1), 47. https://doi.org/10.1186/s12870-015-0445-1

Goetze, T. A., Philippar, K., Ilkavets, I., Soll, J., & Wagner, R. (2006). OEP37 is a new member of the chloroplast outer membrane ion channels. *Journal of Biological Chemistry*, *281*(26), 17989-17998. https://doi.org/10.1074/jbc.M600700200

Goodstein, D. M., Shu, S., Howson, R., Neupane, R., Hayes, R. D., Fazo, J., Mitros, T., Dirks, W., Hellsten, U., Putnam, N., & Rokhsar, D. S. (2011). Phytozome: a comparative platform for green plant genomics. *Nucleic Acids Research*, *40*(D1), D1178-D1186. https://doi.org/10.1093/nar/gkr944

Gould, S. B., Waller, R. F., & McFadden, G. I. (2008). Plastid evolution. *Annu. Rev. Plant Biol.*, *59*(1), 491-517. https://doi.org/10.1146/annurev.arplant.59.032607.092915

Gounaris, K., Mannock, D., Sen, A., Brain, A., Williams, W., & Quinn, P. (1983). Polyunsaturated fatty acyl residues of galactolipids are involved in the control of bilayer/non-bilayer lipid transitions in higher plant chloroplasts. *Biochimica et Biophysica Acta (BBA)-Biomembranes*, *732*(1), 229-242. https://doi.org/10.1016/0005-2736(83)90207-9

Gruner, S. M., Cullis, P. R., Hope, M. J., & Tilcock, C. P. (1985). Lipid polymorphism: the molecular basis of nonbilayer phases. *Annu Rev Biophys Biophys Chem*, *14*, 211-238. https://doi.org/10.1146/annurev.bb.14.060185.001235

Guan, L., Denkert, N., Eisa, A., Lehmann, M., Sjuts, I., Weiberg, A., Soll, J., Meinecke, M., & Schwenkert, S. (2019). JASSY, a chloroplast outer membrane protein required for jasmonate biosynthesis. *Proceedings of the National Academy of Sciences*, *116*(21), 10568-10575. https://doi.org/10.1073/pnas.1900482116

Gutierrez-Carbonell, E., Takahashi, D., Lattanzio, G., Rodríguez-Celma, J., Kehr, J., Soll, J. r., Philippar, K., Uemura, M., Abadía, J., & López-Millán, A. F. (2014). The distinct functional roles of the inner and outer chloroplast envelope of Pea (Pisum sativum) as revealed by proteomic approaches. *Journal of Proteome Research*, *13*(6), 2941-2953. https://doi.org/10.1021/pr500106s

Hannah, M. A., Heyer, A. G., & Hincha, D. K. (2005). A Global Survey of Gene Regulation during Cold Acclimation in Arabidopsis thaliana. *PLOS Genetics*, *1*(2), e26. https://doi.org/10.1371/journal.pgen.0010026

Harsman, A., Schock, A., Hemmis, B., Wahl, V., Jeshen, I., Bartsch, P., Schlereth, A., Pertl-Obermeyer, H., Goetze, T. A., Soll, J., Philippar, K., & Wagner, R. (2016). OEP40, a

Regulated Glucose-permeable β-Barrel Solute Channel in the Chloroplast Outer Envelope Membrane *. *Journal of Biological Chemistry*, *291*(34), 17848-17860. https://doi.org/10.1074/jbc.M115.712398

Härtel, H., Dörmann, P., & Benning, C. (2000). DGD1-independent biosynthesis of extraplastidic galactolipids after phosphate deprivation in Arabidopsis. *Proceedings of the National Academy of Sciences*, *97*(19), 10649-10654. https://doi.org/10.1073/pnas.180320497

Hauser, F., Chen, W., Deinlein, U., Chang, K., Ossowski, S., Fitz, J., Hannon, G. J., & Schroeder, J. I. (2013). A genomic-scale artificial microRNA library as a tool to investigate the functionally redundant gene space in Arabidopsis. *The Plant Cell*, *25*(8), 2848-2863. https://doi.org/10.1105/tpc.113.112805

Hemmler, R., Becker, T., Schleiff, E., Bölter, B., Stahl, T., Soll, J., Götze, T. A., Braams, S., & Wagner, R. (2006). Molecular properties of Oep21, an ATP-regulated anion-selective solute channel from the outer chloroplast membrane. *Journal of Biological Chemistry*, *281*(17), 12020-12029. https://doi.org/10.1074/jbc.M513586200

Hincha, D. K., Höfner, R., Schwab, K. B., Heber, U., & Schmitt, J. r. M. (1987). Membrane rupture is the common cause of damage to chloroplast membranes in leaves injured by freezing or excessive wilting. *Plant Physiology*, *83*(2), 251-253. https://doi.org/10.1104/pp.83.2.251

Holzinger, A., Kaplan, F., Blaas, K., Zechmann, B., Komsic-Buchmann, K., & Becker, B. (2014). Transcriptomics of Desiccation Tolerance in the Streptophyte Green Alga Klebsormidium Reveal a Land Plant-Like Defense Reaction. *PloS one*, *9*(10), e110630. https://doi.org/10.1371/journal.pone.0110630

Hölzl, G., & Dörmann, P. (2019). Chloroplast Lipids and Their Biosynthesis. *Annual Review of Plant Biology*, *70*(Volume 70, 2019), 51-81. https://doi.org/10.1146/annurev-arplant-050718-100202

Hölzl, G., & Dörmann, P. (2021). Thin-Layer Chromatography. In (Vol. 2295, pp. 29-41). https://doi.org/10.1007/978-1-0716-1362-7_3

Hosmani, P. S., Flores-Gonzalez, M., van de Geest, H., Maumus, F., Bakker, L. V., Schijlen, E., van Haarst, J., Cordewener, J., Sanchez-Perez, G., & Peters, S. (2019). An improved de novo assembly and annotation of the tomato reference genome using single-molecule sequencing, Hi-C proximity ligation and optical maps. *biorxiv*, 767764. https://doi.org/10.1101/767764

Hu, Y., Jiang, Y., Han, X., Wang, H., Pan, J., & Yu, D. (2017). Jasmonate regulates leaf senescence and tolerance to cold stress: crosstalk with other phytohormones. *Journal of Experimental Botany*, *68*(6), 1361-1369. https://doi.org/10.1093/jxb/erx004

Huang, D. W., Sherman, B. T., & Lempicki, R. A. (2009). Systematic and integrative analysis of large gene lists using DAVID bioinformatics resources. *Nat Protoc*, *4*(1), 44-57. https://doi.org/10.1038/nprot.2008.211

Hugly, S., & Somerville, C. (1992). A Role for Membrane Lipid Polyunsaturation in Chloroplast Biogenesis at Low Temperature 1. *Plant Physiology*, *99*(1), 197-202. https://doi.org/10.1104/pp.99.1.197

Hummel, J., Segu, S., Li, Y., Irgang, S., Jueppner, J., & Giavalisco, P. (2011). Ultra Performance Liquid Chromatography and High Resolution Mass Spectrometry for the Analysis of Plant Lipids [Original Research]. *Frontiers in Plant Science*, *2*. https://doi.org/10.3389/fpls.2011.00054

Hurry, V. (2017). Metabolic reprogramming in response to cold stress is like real estate, it's all about location. *Plant, cell & environment*, *40*(5), 599-601. https://doi.org/10.1111/pce.12923

Jaillon, O., Aury, J.-M., Noel, B., Policriti, A., Clepet, C., Casagrande, A., Choisne, N., Aubourg, S., Vitulo, N., Jubin, C., Vezzi, A., Legeai, F., Hugueney, P., Dasilva, C., Horner, D., Mica, E., Jublot, D., Poulain, J., Bruyère, C., . . . The French–Italian Public Consortium for Grapevine Genome, C. (2007). The grapevine genome sequence suggests ancestral hexaploidization in major angiosperm phyla. *Nature*, *449*(7161), 463-467. https://doi.org/10.1038/nature06148

Jalili, V., Afgan, E., Gu, Q., Clements, D., Blankenberg, D., Goecks, J., Taylor, J., & Nekrutenko, A. (2020). The Galaxy platform for accessible, reproducible and collaborative biomedical analyses: 2020 update. *Nucleic Acids Research*, *48*(W1), W395-W402. https://doi.org/10.1093/nar/gkaa434

Janská, A., Maršík, P., Zelenková, S., & Ovesná, J. (2010). Cold stress and acclimation–what is important for metabolic adjustment? *Plant Biology*, *12*(3), 395-405. https://doi.org/10.1111/j.1438-8677.2009.00299.x

John, A., Keller, I., Ebel, K. W., & Neuhaus, H. E. (2024). Two critical membranes: how does the chloroplast envelope affect plant acclimation properties? *Journal of Experimental Botany*, *76*(2), 214-227. https://doi.org/10.1093/jxb/erae436

John, A., Krämer, M., Lehmann, M., Kunz, H.-H., Aarabi, F., Alseekh, S., Fernie, A., Sommer, F., Schroda, M., & Zimmer, D. (2024). Degradation of FATTY ACID EXPORT PROTEIN1 by RHOMBOID-LIKE PROTEASE11 contributes to cold tolerance in Arabidopsis. *The Plant Cell*, *36*(5), 1937-1962. https://doi.org/10.1093/plcell/koae011

Jover-Gil, S., Paz-Ares, J., Micol, J. L., & Ponce, M. R. (2014). Multi-gene silencing in Arabidopsis: a collection of artificial micro RNA s targeting groups of paralogs encoding transcription factors. *The Plant Journal*, *80*(1), 149-160. https://doi.org/10.1111/tpj.12609

Jumper, J., Evans, R., Pritzel, A., Green, T., Figurnov, M., Ronneberger, O., Tunyasuvunakool, K., Bates, R., Žídek, A., Potapenko, A., Bridgland, A., Meyer, C., Kohl, S. A. A., Ballard, A. J., Cowie, A., Romera-Paredes, B., Nikolov, S., Jain, R., Adler, J., . . . Hassabis, D. (2021). Highly accurate protein structure prediction with AlphaFold. *Nature*, *596*(7873), 583-589. https://doi.org/10.1038/s41586-021-03819-2

Karimi, M., Depicker, A., & Hilson, P. (2007). Recombinational cloning with plant gateway vectors. *Plant Physiology*, *145*(4), 1144-1154. https://doi.org/10.1104/pp.107.106989

Karimi, M., Inzé, D., & Depicker, A. (2002). GATEWAY™ vectors for Agrobacterium-mediated plant transformation. *Trends in Plant Science*, *7*(5), 193-195. https://doi.org/10.1016/S1360-1385(02)02251-3

Kelly, A. A., Froehlich, J. E., & Dörmann, P. (2003). Disruption of the two digalactosyldiacylglycerol synthase genes DGD1 and DGD2 in Arabidopsis reveals the

existence of an additional enzyme of galactolipid synthesis. *The Plant Cell*, *15*(11), 2694-2706. https://doi.org/10.1105/tpc.016675

Kelly, A. A., Kalisch, B., Hölzl, G., Schulze, S., Thiele, J., Melzer, M., Roston, R. L., Benning, C., & Dörmann, P. (2016). Synthesis and transfer of galactolipids in the chloroplast envelope membranes of Arabidopsis thaliana. *Proceedings of the National Academy of Sciences*, *113*(38), 10714-10719. https://doi.org/10.1073/pnas.1609184113

Kim, J., Na, Y. J., Park, S. J., Baek, S.-H., & Kim, D. H. (2019). Biogenesis of chloroplast outer envelope membrane proteins. *Plant Cell Reports*, *38*(7), 783-792. https://doi.org/10.1007/s00299-019-02381-6

Kim, S., Chen, J., Cheng, T., Gindulyte, A., He, J., He, S., Li, Q., Shoemaker, Benjamin A., Thiessen, Paul A., Yu, B., Zaslavsky, L., Zhang, J., & Bolton, Evan E. (2025). PubChem 2025 update. *Nucleic Acids Research*, *53*(D1), D1516-D1525. https://doi.org/10.1093/nar/gkae1059

Kirchhoff, H. (2019). Chloroplast ultrastructure in plants. *New Phytologist*, *223*(2), 565-574. https://doi.org/10.1111/nph.15730

Kitajima-Koga, A., Baslam, M., Hamada, Y., Ito, N., Taniuchi, T., Takamatsu, T., Oikawa, K., Kaneko, K., & Mitsui, T. (2020). Functional analysis of rice long-chain Acyl-CoA synthetase 9 (OsLACS9) in the chloroplast envelope membrane. *International Journal of Molecular Sciences*, *21*(6), 2223. https://doi.org/10.3390/ijms21062223

Kitashova, A., Adler, S. O., Richter, A. S., Eberlein, S., Dziubek, D., Klipp, E., & Nägele, T. (2023). Limitation of sucrose biosynthesis shapes carbon partitioning during plant cold acclimation. *Plant, cell & environment*, *46*(2), 464-478. https://doi.org/10.1111/pce.14483

Kitashova, A., Lehmann, M., Schwenkert, S., Münch, M., Leister, D., & Nägele, T. (2024). Insights into physiological roles of flavonoids in plant cold acclimation. *The Plant Journal*, *120*(5), 2269-2285. https://doi.org/10.1111/tpj.17097

Kitashova, A., Schneider, K., Fürtauer, L., Schröder, L., Scheibenbogen, T., Fürtauer, S., & Nägele, T. (2021). Impaired chloroplast positioning affects photosynthetic capacity and regulation of the central carbohydrate metabolism during cold acclimation. *Photosynthesis Research*, *147*(1), 49-60. https://doi.org/10.1007/s11120-020-00795-y

Kleine, T., Nägele, T., Neuhaus, H. E., Schmitz-Linneweber, C., Fernie, A. R., Geigenberger, P., Grimm, B., Kaufmann, K., Klipp, E., Meurer, J., Möhlmann, T., Mühlhaus, T., Naranjo, B., Nickelsen, J., Richter, A., Ruwe, H., Schroda, M., Schwenkert, S., Trentmann, O., . . . Leister, D. (2021). Acclimation in plants – the Green Hub consortium. *The Plant Journal*, *106*(1), 23-40. https://doi.org/10.1111/tpj.15144

Klotke, J., Kopka, J., Gatzke, N., & Heyer, A. G. (2004). Impact of soluble sugar concentrations on the acquisition of freezing tolerance in accessions of Arabidopsis thaliana with contrasting cold adaptation – evidence for a role of raffinose in cold acclimation. *Plant, cell & environment*, *27*(11), 1395-1404. https://doi.org/10.1111/j.1365-3040.2004.01242.x

Klughammer, C., & Schreiber, U. (2008). Complementary PS II quantum yields calculated from simple fluorescence parameters measured by PAM fluorometry and the Saturation Pulse method. *PAM application notes*, *1*(2), 201-247. https://www.walz.com/files/downloads/pan/PAN078007.pdf

Kobayashi, K., Awai, K., Nakamura, M., Nagatani, A., Masuda, T., & Ohta, H. (2009). Type-B monogalactosyldiacylglycerol synthases are involved in phosphate starvation-induced lipid remodeling, and are crucial for low-phosphate adaptation. *The Plant Journal*, *57*(2), 322-331. https://doi.org/10.1111/j.1365-313X.2008.03692.x

Könnel, A., Bugaeva, W., Gügel, I. L., & Philippar, K. (2019). BANFF: bending of bilayer membranes by amphiphilic α-helices is necessary for form and function of organelles. *Biochemistry and Cell Biology*, *97*(3), 243-256. https://doi.org/10.1139/bcb-2018-0150

Koo, A. J., & Ohlrogge, J. B. (2002). The predicted candidates of Arabidopsis plastid inner envelope membrane proteins and their expression profiles. *Plant Physiol*, *130*(2), 823-836. https://doi.org/10.1104/pp.008052

Kotchoni, S. O., & Gachomo, E. W. (2009). A rapid and hazardous reagent free protocol for genomic DNA extraction suitable for genetic studies in plants. *Molecular biology reports*, *36*, 1633-1636. https://doi.org/10.1007/s11033-008-9362-9

Krause, G., Grafflage, S., Rumich-Bayer, S., & Somersalo, S. (1988). Effects of freezing on plant mesophyll cells. Symposia of the society for experimental biology,

Laemmli, U. K. (1970). Cleavage of Structural Proteins during the Assembly of the Head of Bacteriophage T4. *Nature*, *227*(5259), 680-685. https://doi.org/10.1038/227680a0

Lang, D., Ullrich, K. K., Murat, F., Fuchs, J., Jenkins, J., Haas, F. B., Piednoel, M., Gundlach, H., Van Bel, M., Meyberg, R., Vives, C., Morata, J., Symeonidi, A., Hiss, M., Muchero, W., Kamisugi, Y., Saleh, O., Blanc, G., Decker, E. L., . . . Rensing, S. A. (2018). The Physcomitrella patens chromosome-scale assembly reveals moss genome structure and evolution. *The Plant Journal*, *93*(3), 515-533. https://doi.org/10.1111/tpj.13801

Leister, D., & Kleine, T. (2008). Towards a comprehensive catalog of chloroplast proteins and their interactions. *Cell Research*, *18*(11), 1081-1083. https://doi.org/10.1038/cr.2008.297

Leonova, S., Shelenga, T., Hamberg, M., Konarev, A. V., Loskutov, I., & Carlsson, A. S. (2008). Analysis of Oil Composition in Cultivars and Wild Species of Oat (Avena sp.). *Journal of Agricultural and Food Chemistry*, *56*(17), 7983-7991. https://doi.org/10.1021/jf800761c

Levitt, J. (1980). *Responses of Plants to Environmental Stress, Volume 1: Chilling, Freezing, and High Temperature Stresses*. https://www.cabidigitallibrary.org/doi/full/10.5555/19802605739

Li, J., Liu, L.-N., Meng, Q., Fan, H., & Sui, N. (2020). The roles of chloroplast membrane lipids in abiotic stress responses. *Plant Signaling & Behavior*, *15*(11), 1807152. https://doi.org/10.1080/15592324.2020.1807152

Li, N., Gügel, I. L., Giavalisco, P., Zeisler, V., Schreiber, L., Soll, J., & Philippar, K. (2015). FAX1, a Novel Membrane Protein Mediating Plastid Fatty Acid Export. *PLOS Biology*, *13*(2), e1002053. https://doi.org/10.1371/journal.pbio.1002053

Li, X., Huang, S., Liu, Z., Hou, L., & Feng, H. (2019). Mutation in EMB1923 gene promoter is associated with chlorophyll deficiency in Chinese cabbage (Brassica campestris ssp. pekinensis). *Physiologia Plantarum*, *166*(4), 909-920. https://doi.org/10.1111/ppl.12979

Love, M. I., Huber, W., & Anders, S. (2014). Moderated estimation of fold change and dispersion for RNA-seq data with DESeq2. *Genome biology*, *15*, 1-21. https://doi.org/10.1186/s13059-014-0550-8

Lundquist, P. K., Rosar, C., Bräutigam, A., & Weber, A. P. M. (2014). Plastid Signals and the Bundle Sheath: Mesophyll Development in Reticulate Mutants. *Molecular Plant*, *7*(1), 14-29. https://doi.org/10.1093/mp/sst133

MacDonald, M. T., Lada, R. R., MacDonald, G. E., Caldwell, C. D., & Udenigwe, C. C. (2023). Changes in Polar Lipid Composition in Balsam Fir during Seasonal Cold Acclimation and Relationship to Needle Abscission. *International Journal of Molecular Sciences*, *24*(21), 15702. https://doi.org/10.3390/ijms242115702

Mair, A., Xu, S.-L., Branon, T. C., Ting, A. Y., & Bergmann, D. C. (2019). Proximity labeling of protein complexes and cell-type-specific organellar proteomes in Arabidopsis enabled by TurboID. *elife*, *8*, e47864. https://doi.org/10.7554/eLife.47864

Martin, W., Stoebe, B., Goremykin, V., Hansmann, S., Hasegawa, M., & Kowallik, K. V. (1998). Gene transfer to the nucleus and the evolution of chloroplasts. *Nature*, *393*(6681), 162-165. https://doi.org/10.1038/30234

Michaeli, S., Honig, A., Levanony, H., Peled-Zehavi, H., & Galili, G. (2014). Arabidopsis ATG8-INTERACTING PROTEIN1 Is Involved in Autophagy-Dependent Vesicular Trafficking of Plastid Proteins to the Vacuole *The Plant Cell*, *26*(10), 4084-4101. https://doi.org/10.1105/tpc.114.129999

Miura, K., & Furumoto, T. (2013). Cold signaling and cold response in plants. *Int J Mol Sci*, *14*(3), 5312-5337. https://doi.org/10.3390/ijms14035312

Miyagishima, S.-y., Froehlich, J. E., & Osteryoung, K. W. (2006). PDV1 and PDV2 mediate recruitment of the dynamin-related protein ARC5 to the plastid division site. *The Plant Cell*, *18*(10), 2517-2530. https://doi.org/10.1105/tpc.106.045484

Moellering, E. R., Muthan, B., & Benning, C. (2010). Freezing tolerance in plants requires lipid remodeling at the outer chloroplast membrane. *Science*, *330*(6001), 226-228. https://doi.org/10.1126/science.1191803

Morris, G. M., Huey, R., Lindstrom, W., Sanner, M. F., Belew, R. K., Goodsell, D. S., & Olson, A. J. (2009). AutoDock4 and AutoDockTools4: Automated docking with selective receptor flexibility. *Journal of Computational Chemistry*, *30*(16), 2785-2791. https://doi.org/10.1002/jcc.21256

Murakami, Y., Tsuyama, M., Kobayashi, Y., Kodama, H., & Iba, K. (2000). Trienoic Fatty Acids and Plant Tolerance of High Temperature. *Science*, *287*(5452), 476-479. https://doi.org/10.1126/science.287.5452.476

Nagao, M., Arakawa, K., Takezawa, D., & Fujikawa, S. (2008). Long- and short-term freezing induce different types of injury in Arabidopsis thaliana leaf cells. *Planta*, *227*(2), 477-489. https://doi.org/10.1007/s00425-007-0633-9

Neuhaus, H. E., & Wagner, R. (2000). Solute pores, ion channels, and metabolite transporters in the outer and inner envelope membranes of higher plant plastids. *Biochimica et Biophysica Acta (BBA)-Biomembranes*, *1465*(1-2), 307-323. https://doi.org/10.1016/S0005-2736(00)00146-2

Nilsson, A. K., Johansson, O. N., Fahlberg, P., Kommuri, M., Töpel, M., Bodin, L. J., Sikora, P., Modarres, M., Ekengren, S., Nguyen, C. T., Farmer, E. E., Olsson, O., Ellerström, M., & Andersson, M. X. (2015). Acylated monogalactosyl diacylglycerol: prevalence in the plant kingdom and identification of an enzyme catalyzing galactolipid head group acylation in Arabidopsis thaliana. *The Plant Journal*, *84*(6), 1152-1166. https://doi.org/10.1111/tpj.13072

O'Boyle, N. M., Banck, M., James, C. A., Morley, C., Vandermeersch, T., & Hutchison, G. R. (2011). Open Babel: An open chemical toolbox. *Journal of Cheminformatics*, *3*(1), 33. https://doi.org/10.1186/1758-2946-3-33

Ohlrogge, J. B., Kuhn, D. N., & Stumpf, P. (1979). Subcellular localization of acyl carrier protein in leaf protoplasts of Spinacia oleracea. *Proceedings of the National Academy of Sciences*, *76*(3), 1194-1198. https://doi.org/10.1073/pnas.76.3.1194

Oikawa, K., Kasahara, M., Kiyosue, T., Kagawa, T., Suetsugu, N., Takahashi, F., Kanegae, T., Niwa, Y., Kadota, A., & Wada, M. (2003). CHLOROPLAST UNUSUAL POSITIONING1 Is Essential for Proper Chloroplast Positioning. *The Plant Cell*, *15*(12), 2805-2815. https://doi.org/10.1105/tpc.016428

Oikawa, K., Yamasato, A., Kong, S.-G., Kasahara, M., Nakai, M., Takahashi, F., Ogura, Y., Kagawa, T., & Wada, M. (2008). Chloroplast outer envelope protein CHUP1 is essential for chloroplast anchorage to the plasma membrane and chloroplast movement. *Plant Physiology*, *148*(2), 829-842. https://doi.org/10.1104/pp.108.123075

Ouyang, S., Zhu, W., Hamilton, J., Lin, H., Campbell, M., Childs, K., Thibaud-Nissen, F., Malek, R. L., Lee, Y., Zheng, L., Orvis, J., Haas, B., Wortman, J., & Buell, C. R. (2006). The TIGR Rice Genome Annotation Resource: improvements and new features. *Nucleic Acids Research*, *35*(suppl_1), D883-D887. https://doi.org/10.1093/nar/gkl976

Pålsson, D., Penttinen, H., Malmberg, C., Adlercreutz, P., & Tullberg, C. (2024). Rancidity development in oat during industrial processing. *LWT*, *204*, 116448. https://doi.org/10.1016/j.lwt.2024.116448

Patzke, K., Prananingrum, P., Klemens, P. A. W., Trentmann, O., Rodrigues, C. M., Keller, I., Fernie, A. R., Geigenberger, P., Bölter, B., Lehmann, M., Schmitz-Esser, S., Pommerrenig, B., Haferkamp, I., & Neuhaus, H. E. (2018). The Plastidic Sugar Transporter pSuT Influences Flowering and Affects Cold Responses. *Plant Physiology*, *179*(2), 569-587. https://doi.org/10.1104/pp.18.01036

Pérez-Pérez, J. M., Esteve-Bruna, D., González-Bayón, R., Kangasjärvi, S., Caldana, C., Hannah, M. A., Willmitzer, L., Ponce, M. R., & Micol, J. L. (2013). Functional Redundancy and Divergence within the Arabidopsis RETICULATA-RELATED Gene Family *Plant Physiology*, *162*(2), 589-603. https://doi.org/10.1104/pp.113.217323

Petrussa, E., Braidot, E., Zancani, M., Peresson, C., Bertolini, A., Patui, S., & Vianello, A. (2013). Plant Flavonoids—Biosynthesis, Transport and Involvement in Stress Responses. *International Journal of Molecular Sciences*, *14*(7), 14950-14973. https://www.mdpi.com/1422-0067/14/7/14950

Pettersen, E. F., Goddard, T. D., Huang, C. C., Couch, G. S., Greenblatt, D. M., Meng, E. C., & Ferrin, T. E. (2004). UCSF Chimera—A visualization system for exploratory research and analysis. *Journal of Computational Chemistry*, *25*(13), 1605-1612. https://doi.org/10.1002/jcc.20084

Pohlmeyer, K., Soll, J., Steinkamp, T., Hinnah, S., & Wagner, R. (1997). Isolation and characterization of an amino acid-selective channel protein present in the chloroplastic outer envelope membrane. *Proceedings of the National Academy of Sciences*, *94*(17), 9504-9509. https://doi.org/10.1073/pnas.94.17.9504

Pommerrenig, B., Ludewig, F., Cvetkovic, J., Trentmann, O., Klemens, P. A. W., & Neuhaus, H. E. (2018). In Concert: Orchestrated Changes in Carbohydrate Homeostasis Are Critical for Plant Abiotic Stress Tolerance. *Plant and cell physiology*, *59*(7), 1290-1299. https://doi.org/10.1093/pcp/pcy037

Project, A. G., Albert, V. A., Barbazuk, W. B., dePamphilis, C. W., Der, J. P., Leebens-Mack, J., Ma, H., Palmer, J. D., Rounsley, S., Sankoff, D., Schuster, S. C., Soltis, D. E., Soltis, P. S., Wessler, S. R., Wing, R. A., Albert, V. A., Ammiraju, J. S. S., Barbazuk, W. B., Chamala, S., . . . Tomsho, L. (2013). The Amborella Genome and the Evolution of Flowering Plants. *Science*, *342*(6165), 1241089. https://doi.org/10.1126/science.1241089

Pudelski, B., Schock, A., Hoth, S., Radchuk, R., Weber, H., Hofmann, J., Sonnewald, U., Soll, J., & Philippar, K. (2012). The plastid outer envelope protein OEP16 affects metabolic fluxes during ABA-controlled seed development and germination. *Journal of Experimental Botany*, *63*(5), 1919-1936. https://doi.org/doi.org/10.1093/jxb/err375

Radauer, C., Lackner, P., & Breiteneder, H. (2008). The Bet v 1 fold: an ancient, versatile scaffold for binding of large, hydrophobic ligands. *BMC Evolutionary Biology*, *8*(1), 286. https://doi.org/10.1186/1471-2148-8-286

Rappsilber, J., Ishihama, Y., & Mann, M. (2003). Stop and go extraction tips for matrix-assisted laser desorption/ionization, nanoelectrospray, and LC/MS sample pretreatment in proteomics. *Analytical chemistry*, *75*(3), 663-670. https://doi.org/10.1021/ac026117i

Reddy, B. L., & Saier Jr, M. H. (2016). Properties and phylogeny of 76 families of bacterial and eukaryotic organellar outer membrane pore-forming proteins. *PloS one*, *11*(4), e0152733. https://doi.org/10.1371/journal.pone.0152733

Rekarte-Cowie, I., Ebshish, O. S., Mohamed, K. S., & Pearce, R. S. (2008). Sucrose helps regulate cold acclimation of Arabidopsis thaliana. *Journal of Experimental Botany*, *59*(15), 4205-4217. https://doi.org/10.1093/jxb/ern262

Richter, S., & Lamppa, G. K. (2002). Determinants for Removal and Degradation of Transit Peptides of Chloroplast Precursor Proteins *. *Journal of Biological Chemistry*, *277*(46), 43888-43894. https://doi.org/10.1074/jbc.M206020200

Röhl, T., Motzkus, M., & Soll, J. (1999). The outer envelope protein OEP24 from pea chloroplasts can functionally replace the mitochondrial VDAC in yeast. *FEBS letters*, *460*(3), 491-494. https://doi.org/10.1016/S0014-5793(99)01399-X

Routaboul, J.-M., Fischer, S. F., & Browse, J. (2000). Trienoic Fatty Acids Are Required to Maintain Chloroplast Function at Low Temperatures1. *Plant Physiology*, *124*(4), 1697-1705. https://doi.org/10.1104/pp.124.4.1697

Sánchez-Fernández, R. o., Davies, T. E., Coleman, J. O., & Rea, P. A. (2001). The Arabidopsis thaliana ABC protein superfamily, a complete inventory. *Journal of Biological Chemistry*, *276*(32), 30231-30244. https://doi.org/10.1074/jbc.M103104200

Sánchez-Baracaldo, P., & Cardona, T. (2020). On the origin of oxygenic photosynthesis and Cyanobacteria. *New Phytologist*, *225*(4), 1440-1446. https://doi.org/10.1111/nph.16249

Scherer, V., Bellin, L., Schwenkert, S., Lehmann, M., Rinne, J., Witte, C.-P., Jahnke, K., Richter, A., Pruss, T., Lau, A., Waller, L., Stein, S., Leister, D., & Möhlmann, T. (2024). Uracil phosphoribosyltransferase is required to establish a functional cytochrome b6f complex. *The Plant Journal*, *120*(3), 1064-1078. https://doi.org/10.1111/tpj.17036

Schleiff, E., Soll, J. r., Küchler, M., Kühlbrandt, W., & Harrer, R. (2003). Characterization of the translocon of the outer envelope of chloroplasts. *The Journal of cell biology*, *160*(4), 541-551. https://doi.org/10.1083/jcb.200210060

Schmutz, J., Cannon, S. B., Schlueter, J., Ma, J., Mitros, T., Nelson, W., Hyten, D. L., Song, Q., Thelen, J. J., Cheng, J., Xu, D., Hellsten, U., May, G. D., Yu, Y., Sakurai, T., Umezawa, T., Bhattacharyya, M. K., Sandhu, D., Valliyodan, B., . . . Jackson, S. A. (2010). Genome sequence of the palaeopolyploid soybean. *Nature*, *463*(7278), 178-183. https://doi.org/10.1038/nature08670

Schock, A. (2014). *Transport of metabolites in chloroplasts* LMU München: Faculty of Biology].

Schrodinger, L. (2010). The PyMOL Molecular Graphics System. *Version 3.1.1.*

Schwenkert, S., Fernie, A. R., Geigenberger, P., Leister, D., Möhlmann, T., Naranjo, B., & Neuhaus, H. E. (2022). Chloroplasts are key players to cope with light and temperature stress. *Trends in Plant Science*, *27*(6), 577-587. https://doi.org/10.1016/j.tplants.2021.12.004

Schwenkert, S., Leister, D., & Lo, W. T. (2023). Hidden keyholders – exploring metabolite transport across the outer chloroplast membrane. *Journal of Mitochondria, Plastids and Endosymbiosis*, *1*(1), 2247168. https://doi.org/10.1080/28347056.2023.2247168

Schwenkert, S., Lo, W. T., Szulc, B., Yip, C. K., Pratt, A. I., Cusack, S. A., Brandt, B., Leister, D., & Kunz, H.-H. (2023). Probing the physiological role of the plastid outer-envelope membrane using the oemiR plasmid collection. *G3: Genes, Genomes, Genetics*, *13*(10), jkad187. https://doi.org/10.1093/g3journal/jkad187

Seifert, U., & Heinz, E. (1992). Enzymatic characteristics of UDP-sulfoquinovose: diacylglycerol sulfoquinovosyltransferase from chloroplast envelopes. *Botanica acta*, *105*(3), 197-205. https://doi.org/10.1111/j.1438-8677.1992.tb00287.x

Seiwert, D., Witt, H., Janshoff, A., & Paulsen, H. (2017). The non-bilayer lipid MGDG stabilizes the major light-harvesting complex (LHCII) against unfolding. *Scientific Reports*, *7*(1), 5158. https://doi.org/10.1038/s41598-017-05328-7

Sherman, B. T., Hao, M., Qiu, J., Jiao, X., Baseler, M. W., Lane, H. C., Imamichi, T., & Chang, W. (2022). DAVID: a web server for functional enrichment analysis and functional annotation of gene lists (2021 update). *Nucleic Acids Res*, *50*(W1), W216-w221. https://doi.org/10.1093/nar/gkac194

Shimojima, M., Ohta, H., Iwamatsu, A., Masuda, T., Shioi, Y., & Takamiya, K.-i. (1997). Cloning of the gene for monogalactosyldiacylglycerol synthase and its evolutionary origin. *Proceedings of the National Academy of Sciences*, *94*(1), 333-337. https://doi.org/10.1073/pnas.94.1.333

Shomali, A., Das, S., Arif, N., Sarraf, M., Zahra, N., Yadav, V., Aliniaeifard, S., Chauhan, D. K., & Hasanuzzaman, M. (2022). Diverse physiological roles of flavonoids in plant environmental stress responses and tolerance. *Plants*, *11*(22), 3158. https://doi.org/10.3390/plants11223158

Singh, U. C., & Kollman, P. A. (1984). An approach to computing electrostatic charges for molecules. *Journal of Computational Chemistry*, *5*(2), 129-145. https://doi.org/10.1002/jcc.540050204

Soccio, R. E., & Breslow, J. L. (2003). StAR-related lipid transfer (START) proteins: mediators of intracellular lipid metabolism. *Journal of Biological Chemistry*, *278*(25), 22183-22186. https://doi.org/10.1074/jbc.R300003200

Soll, J., & Schleiff, E. (2004). Protein import into chloroplasts. *Nature Reviews Molecular Cell Biology*, *5*(3), 198-208. https://doi.org/10.1038/nrm1333

Steponkus, P. L., Dowgert, M. F., Ferguson, J. R., & Levin, R. L. (1984). Cryomicroscopy of isolated plant protoplasts. *Cryobiology*, *21*(2), 209-233. https://doi.org/10.1016/0011-2240(84)90213-X

Strittmatter, P., Soll, J., & Bölter, B. (2010). The chloroplast protein import machinery: a review. *Protein Secretion: Methods and Protocols*, 307-321. https://doi.org/10.1007/978-1-60327-412-8_18

Tang, Q., Xu, D., Lenzen, B., Brachmann, A., Yapa, M. M., Doroodian, P., Schmitz-Linneweber, C., Masuda, T., Hua, Z., & Leister, D. (2024). GENOMES UNCOUPLED PROTEIN1 binds to plastid RNAs and promotes their maturation. *Plant Communications*, *5*(12). https://doi.org/10.1016/j.xplc.2024.101069

Thorlby, G., Fourrier, N., & Warren, G. (2004). The SENSITIVE TO FREEZING2 gene, required for freezing tolerance in Arabidopsis thaliana, encodes a β-glucosidase. *The Plant Cell*, *16*(8), 2192-2203. https://doi.org/10.1105/tpc.104.024018

Tranel, P. J., Froehlich, J., Goyal, A., & Keegstra, K. (1995). A component of the chloroplastic protein import apparatus is targeted to the outer envelope membrane via a novel pathway. *The EMBO journal*, *14*(11), 2436-2446. https://doi.org/10.1002/j.1460-2075.1995.tb07241.x

Trentmann, O., Mühlhaus, T., Zimmer, D., Sommer, F., Schroda, M., Haferkamp, I., Keller, I., Pommerrenig, B., & Neuhaus, H. E. (2020). Identification of Chloroplast Envelope Proteins with Critical Importance for Cold Acclimation1 [OPEN]. *Plant Physiology*, *182*(3), 1239-1255. https://doi.org/10.1104/pp.19.00947

Trott, O., & Olson, A. J. (2010). AutoDock Vina: Improving the speed and accuracy of docking with a new scoring function, efficient optimization, and multithreading. *Journal of Computational Chemistry*, *31*(2), 455-461. https://doi.org/10.1002/jcc.21334

Tuskan, G. A., DiFazio, S., Jansson, S., Bohlmann, J., Grigoriev, I., Hellsten, U., Putnam, N., Ralph, S., Rombauts, S., Salamov, A., Schein, J., Sterck, L., Aerts, A., Bhalerao, R. R., Bhalerao, R. P., Blaudez, D., Boerjan, W., Brun, A., Brunner, A., . . . Rokhsar, D. (2006). The Genome of Black Cottonwood, Populus trichocarpa (Torr. & Gray). *Science*, *313*(5793), 1596-1604. https://doi.org/10.1126/science.1128691

Tzafrir, I., Pena-Muralla, R., Dickerman, A., Berg, M., Rogers, R., Hutchens, S., Sweeney, T. C., McElver, J., Aux, G., Patton, D., & Meinke, D. (2004). Identification of Genes

Required for Embryo Development in Arabidopsis *Plant Physiology*, *135*(3), 1206-1220. https://doi.org/10.1104/pp.104.045179

Ulrich, T., Gross, L. E., Sommer, M. S., Schleiff, E., & Rapaport, D. (2012). Chloroplast β-barrel proteins are assembled into the mitochondrial outer membrane in a process that depends on the TOM and TOB complexes. *Journal of Biological Chemistry*, *287*(33), 27467-27479. https://doi.org/10.1074/jbc.M112.382093

Varadi, M., Anyango, S., Deshpande, M., Nair, S., Natassia, C., Yordanova, G., Yuan, D., Stroe, O., Wood, G., Laydon, A., Žídek, A., Green, T., Tunyasuvunakool, K., Petersen, S., Jumper, J., Clancy, E., Green, R., Vora, A., Lutfi, M., . . . Velankar, S. (2022). AlphaFold Protein Structure Database: massively expanding the structural coverage of protein-sequence space with high-accuracy models. *Nucleic Acids Research*, *50*(D1), D439-D444. https://doi.org/10.1093/nar/gkab1061

Vicente, A. M., Manavski, N., Rohn, P. T., Schmid, L.-M., Garcia-Molina, A., Leister, D., Seydel, C., Bellin, L., Möhlmann, T., Ammann, G., Kaiser, S., & Meurer, J. (2023). The plant cytosolic m⁶A RNA methylome stabilizes photosynthesis in the cold. *Plant Communications*, *4*(6). https://doi.org/10.1016/j.xplc.2023.100634

Vojta, L., Soll, J., & Bölter, B. (2007). Protein transport in chloroplasts− targeting to the intermembrane space. *The FEBS journal*, *274*(19), 5043-5054. https://doi.org/10.1111/j.1742-4658.2007.06023.x

Waegemann, K., Eichacker, S., & Soll, J. (1992). Outer envelope membranes from chloroplasts are isolated as right-side-out vesicles. *Planta*, *187*, 89-94. https://doi.org/10.1007/BF00201628

Wang, Z., Anderson, N. S., & Benning, C. (2013). The phosphatidic acid binding site of the Arabidopsis trigalactosyldiacylglycerol 4 (TGD4) protein required for lipid import into chloroplasts. *Journal of Biological Chemistry*, *288*(7), 4763-4771. https://doi.org/10.1074/jbc.M112.438986

Webb, M. S., & Green, B. R. (1991). Biochemical and biophysical properties of thylakoid acyl lipids. *Biochimica et Biophysica Acta (BBA)-Bioenergetics*, *1060*(2), 133-158. https://doi.org/10.1016/S0005-2728(09)91002-7

Weber, A. P., & Fischer, K. (2007). Making the connections–the crucial role of metabolite transporters at the interface between chloroplast and cytosol. *FEBS letters*, *581*(12), 2215-2222. https://doi.org/10.1016/j.febslet.2007.02.010

Weber, A. P., Schwacke, R., & Flügge, U.-I. (2005). Solute transporters of the plastid envelope membrane. *Annu. Rev. Plant Bio.*, *56*(1), 133-164. https://doi.org/10.1146/annurev.arplant.56.032604.144228

Weber, A. P. M., & Fischer, K. (2009). The Role of Metabolite Transporters in Integrating Chloroplasts with the Metabolic Network of Plant Cells. In A. S. Sandelius & H. Aronsson (Eds.), *The Chloroplast: Interactions with the Environment* (pp. 159-179). Springer Berlin Heidelberg. https://doi.org/10.1007/978-3-540-68696-5_5

Wiśniewski, J. R., Zougman, A., Nagaraj, N., & Mann, M. (2009). Universal sample preparation method for proteome analysis. *Nature methods*, *6*(5), 359-362. https://doi.org/10.1038/nmeth.1322

Yamaryo, Y., Kanai, D., Awai, K., Shimojima, M., Masuda, T., Shimada, H., Takamiya, K.-i., & Ohta, H. (2003). Light and cytokinin play a co-operative role in MGDG synthesis in greening cucumber cotyledons. *Plant and cell physiology*, *44*(8), 844-855. https://doi.org/10.1093/pcp/pcg110

Yang, Y., Glynn, J. M., Olson, B. J. S. C., Schmitz, A. J., & Osteryoung, K. W. (2008). Plastid division: across time and space. *Current Opinion in Plant Biology*, *11*(6), 577-584. https://doi.org/10.1016/j.pbi.2008.10.001

Yoshihara, A., & Kobayashi, K. (2022). Lipids in photosynthetic protein complexes in the thylakoid membrane of plants, algae, and cyanobacteria. *Journal of Experimental Botany*, *73*(9), 2735-2750. https://doi.org/10.1093/jxb/erac017

Yu, C. W., Lin, Y. T., & Li, H. m. (2020). Increased ratio of galactolipid MGDG: DGDG induces jasmonic acid overproduction and changes chloroplast shape. *New Phytologist*, *228*(4), 1327-1335. https://doi.org/10.1111/nph.16766

Zheng, G., Li, L., & Li, W. (2016). Glycerolipidome responses to freezing- and chilling-induced injuries: examples in Arabidopsis and rice. *BMC Plant Biology*, *16*(1), 70. https://doi.org/10.1186/s12870-016-0758-8

Appendix

Supplementary Table 1

Targets of the oemiR plasmid collection, adapted from Schwenkert, Lo, et al. (2023). The plasmid collection was designed and generated by Philip Day and Beate Sculz prior to this work.

ID	Protein	(potential) function	Locus	amiR (sense)	Ref function	Ref loc	Structure
1	OEP24A OEP24B	Solute/ion channel Solute/ion channel	At1g45170 At5g42960	TTGAATGTAAGTCAGATTCAC	Pohlmeyer *et al.*(1998)	Simm *et al.*(2013)	β-barrel
2	OEP21A OEP21B	Solute/ion channel Solute/ion channel	At1g20816 At1g76405	TTCATCGCACAGAAGTAACTT	Bolter *et al.* (1999)	Simm *et al.*(2013)	β-barrel
3	OEP40	Glucose channel	At3g57990	TAATTCAGCGCTCATGCGCAT	Harsman *et al.*(2016)	Harsman *et al.*(2016)	β-barrel
4	OEP37	Solute/ion channel	At2g43950	TAATCTATCGCAAAGTCCCGA	Goetze *et al.* (2006)	Simm *et al.*(2013)	β-barrel
5	OEP16-1	Putative Amino Acid channel	At2g28900	TGATAGTTGCTAAATACACGT	(Philippar *et al.*2007; Pohlmeyer *et al.*1997; Pudelski *et al.*2012)	Simm *et al.*(2013)	α-helical
6	OEP16-2	Putative Amino Acid channel	At4g16160	TTCTTAGTAGACCTTTAGCGC	(Philippar *et al.*2007; Pohlmeyer *et al.*1997; Pudelski *et al.*2012)	Philippar *et al.*(2007)	α-helical
7	OEP16-4	Putative Amino Acid channel	At3g62880	TATTCGTGAATAAACTGGCCT	(Philippar *et al.*2007; Pohlmeyer *et al.*1997; Pudelski *et al.*2012)	Philippar *et al.*(2007)	α-helical
8	CLRP23	Solute/ion channel	At2g17695	TAAGACGTTATCTCATACCAA	Goetze *et al.* (2015)	Trentmann *et al.*(2020)	Other
9	WBC7	ABC transporter	At2g01320	TTCAAATTTAGCGTACAGCGA	Sanchez-Fernandez *et al.*(2001)	Simm *et al.*(2013)	α-helical
10	JASSY-1	OPDA exporter	At1g70480	TTTTCATAGAGTGATCTGCGC	Guan *et al.* (2019)	Guan *et al.*(2019)	Other
11	JASSY-2	Unknown/OPDA exporter	At1g23560	TCAATTACATTGACCTACCAG	Guan *et al.* (2019)		Other
12	MGDG2 MGDG3	Monogalactolipid synthesis	At5g20410 At2g11810	TAACATACGGCACGTTGCCTC	Kobayashi *et al.*(2009)	Awai *et al.*(2001)	α-helical
13	DGD1 DGD2	Digalactolipid synthesis	At3g11670 At4g00550	TCTTCTGCGGTTGTTGTGCAA	Kobayashi *et al.*(2009)	Kelly *et al.*(2003)	Other
14	TGD4	Lipid import	At3g06960	TATAAATGGTAACTTGGGCCA	Xu *et al.*(2008)	Bouchnak *et al.*(2019)	Other
15	SFR2	Diacylglycerol acyltransferase	At3g06510	TAATTTGAGACCTAATAGCAG	(Fourrier *et al.*2008; Thorlby *et al.*2004)	Simm *et al.*(2013)	Other
16	LACS9	Long-chainacyl-CoAsynthetase	At1g77590	TCATATTACGGTTGTGACCTA	Shockey *et al.*(2002)	Simm *et al.*(2013)	α-helical
17	OEP9-1	Unknown	At1g16000	TTAACAGTGTGCAAATGACAC		Dhanoa *et al.*(2010)	α-helical
18	OEP9-2	Unknown	At1g80890	TATGTAGTTGACTAGAGTCTA			α-helical
19	OEP7	Unknown	At3g52420	TCAAATAAACGATCATGACGC		Lee *et al.*(2001)	Tail anchored
20	CHUP1	Actin binding	At3g25690	TACTTTACAGAACTATGTCCT	Oikawa *et al.*(2003)	Oikawa *et al.*(2003)	Other
21	PDV1	Plastid division	At5g53280	TTGCTACTAAAGAATAGCCGC	Okazaki *et al.*(2015)	Miyagishima *et al.*(2006)	Other
22	PDV2	Plastid division	At2g16070	TTCTGGCTAAAATTGACCCGA	Okazaki *et al.*(2015)	Miyagishima *et al.*(2006)	Tail anchored
23	PTM	Retrograde signaling	At5g35210	TGATTATACGGCAGGAGGCAG	Sun *et al.*(2011)	Froehlich *et al.*(2003)	Other
24	HXK1	Glucose-responsive sensor hexokinase	At4g29130	TATTACCGAAAAATGGCGCTG	Jang *et al.* (1997)	Simm *et al.*(2013)	Signal anchored

ID	Protein	(potential) function	Locus	amiR (sense)	Ref function	Ref loc	Structure
25	CRL	OEP80 insertion	At5g51020	TTATAGTCGTCAAATGCGCTC	Asano *et al.*(2004), Yoshimura *e t al*(2023)	(Simm *et al.*2013)	Signal anchored
26	THF1	Sugar signaling; thylakoid formation	At2g20890	TTTATATAGAGTATCTCCCAT	Huang *et al.*(2006); (Keren *et al.* 2005)	Trentmann *et al.*(2020)	α-helical
27	TOC75-III TOC75-IV TOC75-I	Protein import	At3g46740 At4g09080 At1g35860	TACCGAGTTTCACACCCGCAC	Baldwin *et al.*(2005)	Simm *et al.*(2013)	β-barrel
28	TOC159	Protein import receptor	At4g02510	TAGAATTGCGAGTAAAGGCAG	Kubis *et al.* (2004)	Simm *et al.*(2013)	Other
29	TOC90	Protein import receptor	At5g20300	TATATTATTCTGTGACTCCCC	Hiltbrunner *et al.*(2004)	Bouchnak *et al.*(2019)	Other
30	TOC120 TOC132	Protein import receptor	At3g16620 At2g16640	TATGTTTAACCGAGCTGTCCT	Kubis *et al.* (2004)	Simm *et al.*(2013)	Other
31	TOC33 TOC34	Protein import receptor	At1g02280 At5g05000	TGTACACATCCAAACGGGCAA	Weibel *et al.* (2003)	Bouchnak *et al.*(2019)	Tail anchored
32	TOC64	Protein import	At3g17970	TTTTATCGATAAAAGCGCCGG	Qbadou *et al.*(2007)	Simm *et al.*(2013)	Signal anchored
33	OEP80	Protein insertion	At5g19620	TAACACGCACCCCTAAAGCAT	Patel *et al.* (2008)	Trentmann *et al.*(2020)	β-barrel
34	SP2 P36	Degradation of TOC complex, CHLORAD	At3g44160 At3g48620	TTTAATCGGACGCACATGCAA	Ling *et al.* (2019)	Ling *et al.*(2019)	β-barrel
35	KOC1	Tyrosine kinase	At4g32250	TTAACACCAGTAATGACGCGG	Zufferey *et al.*(2017)	Trentmann *et al.*(2020)	Tail anchored
36	PAP2 PAP9	Phosphatase	At1g13900 At2g03450	TGTACATTGGTCTATGCCCTT	Sun *et al.*(2012)	Sun *et al.*(2012)	Tail anchored

List of publications

- **Lo, W. T.**, & Leister, D. (2025). Spotlight on "A map of the rubisco biochemical landscape" by Prywes et al.(2025). *Journal of Mitochondria, Plastids and Endosymbiosis*, *3*(1), 2492069.
- Schwenkert, S., Leister, D., & **Lo, W. T.** (2023). Hidden keyholders–exploring metabolite transport across the outer chloroplast membrane. Journal of Mitochondria, Plastids and Endosymbiosis, 1(1), 2247168.
- Schwenkert, S., **Lo, W. T.**, Szulc, B., Yip, C. K., Pratt, A. I., Cusack, S. A., ... & Kunz, H. H. (2023). Probing the physiological role of the plastid outer-envelope membrane using the oemiR plasmid collection. G3: Genes, Genomes, Genetics, 13(10), jkad187.

A portion of this work has been submitted for publication:

- **Lo, W. T.**, Winkler, D., Münch, M. Lehmann, M. Steiner, K., Bölter, B., Tullberg, C., Grey, C., Kleine, T., Abdel-Salam, E., Ebel, K., Neuhaus, E.H., Büyüktas, D., Vries, S.D., Kunz, H. H., Leister, D., Schwenkert, S. (2025). Role of chloroplast lipid-remodelling protein 23 during cold acclimation in *Arabidopsis thaliana*.

Danksagung

First, I would like to thank Prof. Dr. Dario Leister, for providing a well-organised and supportive work environment in which to pursue my doctoral studies.

I am deeply grateful to my supervisor, PD Dr. Serena Schwenkert, for her mentorship throughout my doctoral journey. Her guidance extended far beyond academic supervision, and I am especially thankful for her expert advice and trust in my abilities, both of which were instrumental in the completion of this thesis. Sincere thanks are extended to the other members of my thesis advisory committee, Prof. Thomas Nägele and Dr. Thorsten Möhlmann, for their invaluable feedback and generous support.

My heartfelt thanks go to the collaborators who contributed to this work: PD Dr. Bettina Bölter, for performing the protease digest; Katharina Ebel, for conducting the freezing experiment; and Dr. Cecilia Tullberg and Dr. Carl Grey, for hosting me and whose expertise was invaluable in guiding me through the fatty acid analysis carried out at Lund University, Sweden.

I would also like to express my sincere gratitude to AG Leister for their support and for fostering a positive and stimulating research environment. Special thanks go to Tatjana for the RNAseq analysis, as well as Eslam, for performing the molecular docking simulations. I am particularly grateful to MSBioLMU, where the LC-MS experiments were conducted. Many thanks to PD Dr. Serena Schwenkert for the proteomic analysis, Dr. Martin Lehmann for the lipidomic analysis, and Kira Steiner, Yulia Davydova, and Beate Minov for their technical support.

Special thanks to Tim Lücke, who generated the *clrp23* knockout mutants and antisera against CLRP23 used in this study, as well as our bachelor's and master's students for their invaluable contributions to experimental work and data collection. Specifically: Michael Chun Kwan Yip, Emelie Otto and Sofia Larionova who contributed towards data collection and PCR genotyping for the oemiR library screens; Maximilian Münch, who performed the MTBE lipid extraction and LC-MS lipidomic quantification; Denise Winkler, who not only performed the subfractionation analysis of CLRP23 in Arabidopsis but also contributed significantly to the foundational phases of the project; and Nadia Al Thour, Laura von Winterfeld and Amira Melissa Wimmer, who performed the GFP localisation of the envelope transporter candidates for future study. Finally, I thank Dr. Jan-Ferdinand Penzler and Sophia Bagshaw for their assistance with the final edits of this thesis.

Beyond science, I am incredibly fortunate to have had the support of my family and friends. To the family I've found during over the last few years in Munich, thank you for putting the "life" in my work-life balance, and for joining me in experiencing the rich culinary, cultural and recreational life the city has to offer. To my partner Tuong Tang, thank you for your unwavering support. In addition to my family in Hong Kong, you have given me a second place to call home here in Europe, steadying me through both the highs and lows of this journey. 致我的父母，盧更裕和顧秀麗：多謝你們多年來的栽培、信任與支持。過去三年，你們每年特意來德國探望我，每星期定時與我通電話；我假期回港時，又總是陪我開開心心地吃喝玩樂。從九千多公里之外，仍能為我的博士生活帶來滿滿的溫暖，我實在感激不盡。